CE 01/36
LB/DON/23/2015
DCE 23/97

SIGNIFICANCE OF SOLAR RADIATION ON CONCRETE WATER RETAINING STRUCTURES

Annesley Erwin Barthelot

(09/8905)

LIBRARY
UNIVERSITY OF MORATUWA, SRI LANKA
MORATUWA

Thesis Submitted in Partial Fulfillment of the Requirements for the Degree
Master of Engineering

University of Moratuwa
108909

Department of Civil Engineering

University of Moratuwa
Sri Lanka

624 "15"
624 (043)

108909
+
CD-ROM

January 2015

MEng in Structural Engineering Design

108909

Declaration

I declare that this is my own work and this thesis does not incorporate without acknowledgement any material previously submitted for a Degree or Diploma in any other University or institute of higher learning to the best of my knowledge and believe it does not contain any material previously published or written by another person except where the acknowledgement is made in the text.

Also, I hereby grant University of Moratuwa the non-exclusive right to reproduce and distribute my thesis, in whole or in part in print, electronic or other medium. I retain the right to use this content in whole or part in future works (such as articles or books).

UOM Verified Signature

Signature: Date: 30/01/2015

The above candidate has carried out research for the Masters' thesis under my supervision.

UOM Verified Signature

Signature of the supervisor: Date: 05.02.2015

Abstract

According to the codes of practice for design of concrete structures, the effect of solar radiation has to be given due consideration. However, it is not specifically incorporated in the structural design. Often providing expansion or sliding joints is the common practice to accommodate the effect of solar radiation. The need to provide reinforcement bars at tensile stress regions where thermal stresses may develop within the design life of the structure is currently an undocumented fact.

Therefore the main aim of this research was to investigate the significance of solar radiation effect on concrete water retaining structures and to highlight the occurrence of high stress zones that need attention. The investigation was performed using a finite element model with gathered solar radiation data. The model was simulated with probable thermal properties of concrete and environmental conditions including solar heat flux, to identify the governing parameters.

In order to process large amounts of data and for economic reasons, a finite element method of analysis using ANSYS software was considered. This provided the robustness and contributed to focus on the sensitivity of the parameters under investigation. Further, several simplified models were verified with numerical calculations and compared with the finite element model. Characteristic points on stress response curve from the finite element analysis were compared with the numerical results. Comparisons were made with respect to the accuracy and reliability of using the finite element model for the analysis.

Based on the verified modeling approach, a typical underground water tank was investigated for sliding and fixed roof slab to wall connectivity. The temperature variation and corresponding stress variations were obtained.

It was found that significantly high tensile stresses are developed at the soffit level of the roof slab near the column heads, where normally only compressive stresses are expected. This occurs for both fixed and sliding roof slab-to-wall connections. Also at the mid spans, as the top surface of the roof slab was being compressed due to thermal expansion, the bottom surface was not being compressed due to the comparatively low temperature than the top surface (i.e. the temperature gradient). Therefore the bottom fibers developed tensile stresses, which was significantly more than the tensile stress due to selfweight only.

It is conclusive that the solar radiation is significant on concrete water retaining structures and the use of sliding or fixity conditions between the roof slab and wall is not effective in minimizing the tensile stresses due to solar heat gain;

Keywords: solar radiation, stresses in concrete, transient thermal analysis, element overlay, ANSYS

Acknowledgments

This research was performed under the supervision of Prof. S.M.A. Nanayakkara. I am extremely grateful for the guidance provided; knowledge given; understanding; motivation and numerous hours spent helping me to complete this research.

My extended thanks also go to Aruna Karunaratna and Prof. Nanayakkara for providing me with the solar radiation and the ambient temperature variation data that was used for this research.

Appreciation is also extended to the research coordinator, Dr. Baskaran for organizing review presentations from which it helped me to get a feedback on my research. Appreciation extends to the lab staff for their support too.

Finally, I am grateful to my family for their understanding and encouragement extended to me during this period.

Contents

Declaration i
Abstract ii
Acknowledgments iii
List of Figures viii
List of Tables xi
List of Abbreviations (Nomenclature) xii
1 Chapter 1 - Introduction 1
1.1 General 1
1.2 Research Objectives 2
1.3 Organization of the Thesis 2
2 Chapter 2- Literature Review 4
2.1 Introduction 4
2.2 Recommendations for Effect of Solar Radiation Given in Codes of 5
2.3 Effect of Thermal Loads in Concrete Structures 7
2.4 Temperature Rise due to Solar Radiation 9
2.5 Modes of Heat Transfer 10
2.5.1 Heat Conduction 10
2.5.2 Convection 11
2.5.3 Thermal Radiation 12
2.6 Numerical Equations for Heat Transfer 13
2.7 Numerical Equations for Thermal Stresses 14
2.8 Thermal Properties of Concrete 16
2.8.1 Specific Heat Capacity 16
2.8.2 Conductivity of Concrete 17
2.9 Uncoupled Thermal and Mechanical Analysis 18
2.10 Initial Temperature of the Structure 18
2.11 Use of ANSYS for Finite Element Analysis and Element Selection 19
2.12 Solar Radiation 20
2.12.1 Radiation Spectrum 20
2.12.2 Time and Orientation for Maximum Solar Radiation 21

2.12.3 Ground Measurements of Solar Radiation....24
2.12.4 Generalized Solar Energy Studies for Sri Lanka....26
2.13 Solar Radiation Absorption in Concrete....28
2.14 Studies on Ambient Temperature....30
2.15 Summary of Literature Review....32
3 Chapter 3 – Finite Element Analysis....34
3.1 Introduction....34
3.2 Modeling....34
3.3 Selection of Element Type....34
3.4 Degrees of Freedom....37
3.5 Material Setup....37
3.6 Real Constants....38
3.7 Surface overlaying....38
3.8 Numbering Controls....39
3.9 Physical Environments....39
3.10 Use of Arrays to Store Data....40
3.11 Load Assignment....41
3.11.1 Solar Radiation as Heat Flux....41
3.11.2 Heat Convection....42
3.12 Temperature Offset....42
3.13 Boundary Conditions....42
3.14 Analysis Setup....43
3.15 Solution Controls....43
3.15.1 Time Control....43
3.15.2 Time at End of Time Step....43
3.15.3 Transient Solution Controls....44
3.15.4 Solution Options....45
3.15.5 Nonlinear Options....46
3.15.6 Convergence Criteria....46
3.15.7 Advanced NL....47
3.16 Reference Temperature....47

4 Chapter 4 – Model Verification 48
4.1 Introduction 48
4.2 Model Verification Methodology 48
4.3 Heat Transfer by Conduction 48
4.3.1 Numerical Idealization 48
4.3.2 Numerical Solution 49
4.3.3 ANSYS Solution 50
4.3.4 Comparison Between Numerical and ANSYS Solution 51
4.4 Heat Transfer by Convection and Conduction 53
4.4.1 Numerical Solution 53
4.4.2 ANSYS Solution for Heat Transfer by Convection and Conduction 55
4.4.3 Comparison with FE model 56
4.5 Thermal Stresses 57
4.5.1 Specimen calculation for stress calculation 58
5 Chapter 5 – Sensitivity Analysis 62
5.1 Default Parameters 62
5.2 Analysis and Results 64
5.2.1 Solar Heat Flux 64
5.2.2 Sensitivity to Ambient Temperature 66
5.2.3 Effect of Initial Temperature 68
5.2.4 Effect of Convection–Radiation Coefficient 70
5.2.5 Effect of Specific Heat Capacity 72
5.2.6 Effect of Thermal Conductivity 73
5.2.7 Member Thickness 74
5.2.8 Sensitivity of Parameters 77
6 Chapter 6 – Case Study 79
6.1 Model Description 79
6.2 Idealization of the Tank for Analysis 80
6.3 Boundary Conditions 81
6.4 Inputs for Analytical Model 82
6.5 Thermal Boundary Conditions for the Model 83

6.6 Results 84
6.6.1 Slab Monolithically Cast With Walls and Column Heads (Case 1) 84
6.6.2 Sliding on Walls and Monolithic at Column Heads (Case 2) 85
7 Chapter 6 – Conclusions and Recommendations 87
8 Bibliography 88
APPENDIX A 91
APPENDIX B 98
APPENDIX C 104

List of Figures

Figure 2.1: Representation of temperature profile 6
Figure 2.2: Test model with thermal load used by Vecchio and Sato 7
Figure 2.3: Transient condition after application of thermal load [3] 8
Figure 2.4: Diurnal variation of roof panel temperature [4] 9
Figure 2.5: Cross-section of a member subjected to a rise of temperature 15
Figure 2.6: Solar radiation spectrum 20
Figure 2.7: Average solar insolation for Colombo, Sri Lanka 21
Figure 2.8: Solar declination angle 22
Figure 2.9: Variation of declination angle 23
Figure 2.10: Solar irradiance on Horizontal Plane [24] 23
Figure 2.11: Solar irradiance on Vertical Plane [24] 24
Figure 2.12: Generic spectrum for a silicon PV cell [27] 25
Figure 2.13: Total and IR radiation variation during the day [19] 26
Figure 2.14: Albedo values of Concrete [36] 29
Figure 2.15 : Ambient Temperature Variation during a day 31
Figure 3.1: 3D Couple Field Solid – SOLID5 35
Figure 3.2: Thermal Shell Element - SHELL57 35
Figure 3.3: 3-D 4-Node CONTA173 36
Figure 3.4: 3-D Target Element – TARGE170 36
Figure 3.5: Solid element overlaid with Surface element (conceptual) 39
Figure 3.6: Flow Chart - Thermal and Structural Analysis 40
Figure 3.7: Heat Flux stored in an Array 41
Figure 3.8: Solution Control – Basic 44
Figure 3.9: Solution Control - Transient 45
Figure 3.10: Solution Control – Solution Options 45
Figure 3.11: Solution Control – Nonlinear 46
Figure 3.12: Solution Control – Convergence Criteria 46
Figure 3.13: Solution Control – Advanced NL 47
Figure 4.1: Comparison of surface temperature – Convection and Conduction 57
Figure 4.1: Comparison Stress –Analytical methods and ANSYS FEA solution 61

Figure 5.1: Normalized Heat Flux variation Indented on Horizontal Plane 63
Figure 5.2: Normalized ambient temperature variation 63
Figure 5.3: Top surface temperature variation due to factored heat flux 64
Figure 5.4: surface temperature variation vs. factored heat flux 64
Figure 5.5: Temperature difference with varying heat flux 65
Figure 5.6: Surface temperature vs. solar radiation absorption factor 65
Figure 5.7: Derived factored ambient temperature variations 66
Figure 5.8: Top surface temperature variation due to factored ambient temp. 67
Figure 5.9: Surface temperature vs. factorized norm. ambient temp. 67
Figure 5.10: Temperature difference due to factorized ambient temperature 68
Figure 5.11: Top surface temperature due to initial temperature 69
Figure 5.12: Top surface temperature vs. factored initial temperature 69
Figure 5.13: Temperature difference due to factored initial temperature 70
Figure 5.14: Surface temp. variation due to coefficient of convection-radiation 71
Figure 5.15: Temp. difference due to coefficient of convection-radiation 71
Figure 5.16: Peak temperature vs. convection-radiation coefficient 72
Figure 5.17: Top surface temperature due to specific heat capacity 72
Figure 5.18: Effect of specific heat capacity on surface temperature 73
Figure 5.19: Temperature difference vs. Specific heat capacity 73
Figure 5.20: Effect of Conductivity on Top Surface Temperature 74
Figure 5.21: Effect of conductivity on temperature difference 74
Figure 5.22: Temperature vs. Depth for different member thicknesses 75
Figure 5.23: Maximum surface temperature vs. Member thickness 75
Figure 5.24: Temperature difference vs. Member thickness 76
Figure 5.25: Temperature difference vs. ratio of depth/thickness 76
Figure 5.26: Sensitivity graph for top surface temperature 77
Figure 5.27: Sensitivity graph for temperature difference 78
Figure 6.1: Underground Reservoir - Plan 79
Figure 6.2: Underground Reservoir – Section on grid 2-2 79
Figure 6.3: Underground Reservoir – Section on grid C-C 80
Figure 6.4: Idealized strip 80
Figure 6.5: Finite element model (perspective view) 81

Figure 6.6: (Continuous) monolithically cast on column heads and walls 81
Figure 6.7: (Sliding) monolithically cast over columns but sliding on walls 82
Figure 6.8: Region of Convective Surface 83
Figure 6.9: Convective surfaces indicated (Perspective view) 83
Figure 6.10: Stresses due to Selfweight + Soil pressure (Case 1) 85
Figure 6.11: Stresses due to Selfweight + Soil pressure + Thermal Load (Case 1) ...85
Figure 6.12: Stresses due to Selfweight + Soil pressure (Case 2) 86
Figure 6.13: Stresses due to Selfweight + Soil pressure + Thermal Load (Case 2) ...86

List of Tables

Table 2.1: Extract of Table 5.2 of Eurocode1- Part 5 7
Table 2.2: Typical specific heat capacity of concrete 16
Table 2.3: Conductivity of concrete 17
Table 2.4: Effect of aggregate type and dry density on conductivity 17
Table 2.5: Effect of moist density on conductivity 18
Table 2.6: Solar Radiation at Coconut Research Institute, Sri Lanka 27
Table 2.7: Comparison between reported solar energy data 27
Table 2.8: Ambient temperature variation for each zone 30
Table 2.9: Average and maximum temperature for 50 year return period 31
Table 3.10: Material Properties 37
Table 4.1: Input Parameters 49
Table 4.2: Numerical solution for heat transfer by conduction 50
Table 4.3: ANSYS solution for heat transfer by conduction 51
Table 4.4: Comparison of temp. due to heat transfer by conduction at 3600s 52
Table 4.5: Comparison of temp. due to heat transfer by conduction at 12000s 52
Table 4.6: Numerical solution for convection and conduction 55
Table 4.7 ANSYS solution due to Convection and Conduction 56
Table 4.8 Comparison of Results on Convection and Conduction 56
Table 4.9 Temperature along slab depth 58
Table 4.10 Thermal stresses using analytical methods 60
Table 4.11 Thermal Stresses from ANSYS solution 61
Table 5.1: Material and thermal Property 62
Table 5.2: FEM Arrangement 62
Table 5.3: Paired cases for convection-radiation coefficients 70
Table 6.1: Input parameters 82
Table 6.2: Stress at end of column head - Continuously Cast Slab (Case 1) 84
Table 6.3: Stress at first mid span 84
Table 6.4: Stress near column head 85
Table 6.5: Stress at first mid span 86

List of Abbreviations (Nomenclature)

3D	three dimensional
A	cross sectional area
AM1.5	Air Mass number = 1.5 atmosphere thickness, corresponding to a solar zenith angle of z=48.2°.
c	specific heat capacity, J/kg/K
DOF	Degrees of freedom
FEM	Finite element model
FEA	Finite element analysis
HFLUX, q	Solar Heat Flux, (W/m^2)
h	convective heat transfer coefficient, $W/m^2/K$
h_w	convective heat transfer coefficient, $W/m^2/K$
k	thermal conductivity, W/m/K
I_h	Solar radiation on horizontal surface , W/m^2
L	Length, heat flow path length of interest
Q	rate of heat transfer (W)
q	Surface flux (power per unit area)
T	temperature, K or °C
T_{max}	maximum shade air temperature with an annual probability of being exceeded of 0.02
T_{air}	air temperature
T_s	surface temperature
ΔT	Temperature difference, (°C, K)
t	time (s)
ρ	mass density, kg/m^3
ρc	specific heat

1 Chapter 1 - Introduction

1.1 General

Concrete Structures have frequently been associated with thermal effects. In general, investigations involved in thermal studies for immature concrete are oriented towards the heat of hydration and for the mature concrete, the main focus is towards concrete road payments and bridges where the effect of solar radiation has shown to be significant. In almost all cases, the governing effect due to solar thermal effect has resulted in structural cracks.

For matured concrete structures, there are two external thermal factors that can contribute to cracking. The first is due to seasonal variations in temperature, resulting in volume changes in the hardened concrete. When the season changes from a warm season to a cold season, thermal shrinkage occurs, and in the presence of restraints, this can result in cracking. The second factor is due to the differential temperature gradient caused by the action of the sun on the external surface of a slab or a wall, with the other surface generally not exposed to the Sun. The presence of restraints restricts the free expansion of the external surface and induces flexural tension on the inner surface, causing possible cracking. The occurrence of such cracking particularly needs to be controlled in structures such as water-tanks whose faces are exposed to water.

Solar radiation and its associated boundary conditions are highly variable. The geographical location, time of year, sunshine hours, wind conditions, etc. generally are the governing conditions and therefore investigating of these conditions are tedious. Besides the properties of concrete itself, can affect the final output. However, the analysis can be simulated numerically; the procedure can be controlled and can be consistent throughout the investigation. But the numerical equations associated with thermal analysis are of higher order partial differential equations where unique solutions are only available for specific boundary conditions. The procedure becomes more complicated due to the varying solar heat flux. Therefore a finite element model using software is considered to be a better approach.

1.2 Research Objectives

The main objective of this research is to identify the significance of solar radiation induced thermal stresses on concrete water retaining structures. In order to achieve this overall objective, supportive objectives were identified as follows:

- Development of a detailed 3D finite element model that can be used with heat flux, conduction, convection and analyze structural stresses together with structural boundary condition such as sliding and non-sliding situations.
- Verification of the validity of the modeling approach using numerical methods.
- Perform sensitivity analysis for associated parameters and identify the critical conditions.
- Carryout a case study of an underground reservoir to investigate the significance of solar radiation for different boundary conditions.

1.3 Organization of the Thesis

The introductory chapter gives an overview of the problem and the need to evaluate the significance of solar radiation effect. The research objectives of this work are also given, together with its significance to engineering practice. Next the content of this thesis is outlined.

In Chapter 2, the literature review is presented in areas such as existing codes of practice on solar radiation effects, thermal stresses in concrete, numerical methods to estimate the temperature profile and stresses, solar radiation studies and environment temperate variations. It also includes the finite element approaches and selection of element types in ANSYS software as well. Finally a summary of the literature review is presented.

Chapter 3 presents the modelling and analysis procedure in ANSYS software. Selection of suitable element type, parametrically creating the model, mesh generation, application of material properties, specifying loads and boundary condition, etc. are described. The command input and in some cases, the input using the graphical user interface (GUI) is also described.

Chapter 4 describes the model verification. Based on the available numerical formulae, samples models were verified for convection, conduction and the resultant structural stresses.

Sensitivity Analysis is presented in Chapter 5. Sensitivity on various parameters involved in boundary conditions and concrete properties are investigated.

Chapter 6 brings forth the case study of an underground reservoir. The reservoir top slab was subjected to solar radiation and the structural response for restrained and sliding conditions were investigated. Finally the conclusion of this research is presented.

2 Chapter 2- Literature Review

2.1 Introduction

This literature review covers researches related to the solar radiation effect on concrete structures. This focuses on areas such as existing codes of practice on solar radiation, heat transfer mechanisms in concrete, structural stress response due to thermal effect and the use of FEM software for analysis and simulation. The literature review is presented in the following order:

- Recommendations for Effect of Solar Radiation given in Codes of Practice for design of concrete structures
- Effect of Thermal Loads in Concrete
- Temperature Rise due to Solar Radiation
- Modes of Heat Transfer
- Numerical Equations for Heat Transfer
- Numerical Equations for Thermal Stresses
- Thermal Properties of Concrete
- Uncoupled Thermal and Mechanical Analysis
- Effect of "Hardened Temperature"
- Use of ANSYS for Finite Element Analysis and Element selection
- Solar Radiation
    - Radiation Spectrum
    - Time and Orientation for Maximum Solar Radiation
    - Ground Measurements of Solar Radiation
    - Generalized Solar Energy Studies for Sri Lanka
- Solar Radiation Absorption on Concrete
- Studies on Ambient Temperature
- Summary of Literature Review

2.2 Recommendations for Effect of Solar Radiation Given in Codes of Practice

The British Standard BS 8007 [1], provides recommendations for design and construction of water retaining structures. In clause 2.6.1 of BS 8007, under causes of cracking, the code emphasizes that direct or flexural tension in concrete arising from temperature gradients due to solar radiation may cause cracking in concrete. In defining the minimum reinforcement, in Table 5.1 of BS 8007, it is stated that, expansion joints at wide spacing may be desirable in walls and roofs that are not protected from solar heat gain. Also in calculation of crack width in Table A2 of the code, it is stated that an allowance has not been made for solar heat gain in slabs when deriving the T1, T2 values, thereby indirectly implying that solar radiation could be significant as well.

Further, BS 8007 states in an example that critical adverse loading effect occurs when thermal expansion of a roof, forces the walls of an empty structure into the surrounding backfill. The code also suggests that the passive soil pressure on the walls may be limited by use of a compressible and durable material and/or by providing a sliding joint between the top of the wall and the underside of the roof.

To summarize, the BS 8007 code indicates that solar radiation has an effect, but does not provide any sufficient guidance on the extent of this effect. However, it suggests the use of joints to minimize solar induced stresses.

The Eurocode 1 [2] has given more details on solar radiation induced thermal loading. Under thermal actions, its scope includes principles and rules for calculating thermal actions on buildings, bridges and other structures including their structural elements. Section 7 of the Eurocode 1 Part 5 considerers structures for which thermal actions are mainly a function of their use (e.g. cooling towers, silos, tanks, warm and cold storage facilities, hot and cold services etc.).

The Eurocode defines the thermal actions due to daily and seasonal changes in shade air temperature, solar radiation, re-radiation, etc., and states that these actions result in variations of the temperature distribution within individual elements of a structure. In clause 2 of section 4 the code, it is also stated that the magnitude of

the thermal effects will be dependent on local climatic conditions, together with the orientation of the structure, its overall mass, finishes etc.

The Eurocode describes the temperature distribution within an individual structural element into four essential constituent components, as illustrated in Figure 2.1 where:

a) A uniform temperature component, ΔT_u;

b) A linearly varying temperature difference component about the z-z axis, ΔT_{MY};

c) A linearly varying temperature difference component about the y-y axis, ΔT_{MZ};

d) A non-linear temperature difference component, ΔT_E. This results in a system of self-equilibrated stresses which produce no net load effect on the element.

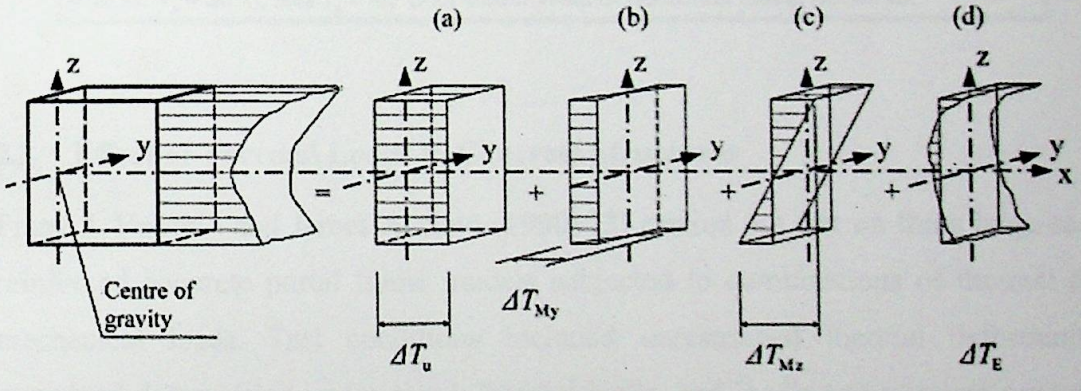

Figure 2.1: Representation of temperature profile
(extracted from Eurocode1 Part 5, BS EN 1991-1-5)

In Table 5.2 of Eurocode 1 Part 5 it is stated that values of the maximum shade air temperature T_{max} (at 0.02 annual exceedance probability), minimum shade air shade temperature T_{min}, and solar radiation effects T3, T4, and T5 which may be specified in the National Annex. It also states that if no data are available for regions between latitudes 45°N and 55°N the recommended values for T3, T4 and T5 shall be used. An extract of Table 5.2 of Eurocode 1 is shown in Table 2.1. However, since Sri Lanka is between latitudes 6°N and 9°N, these temperature values may not be applicable.

Table 2.1: Extract of Table 5.2 of Eurocode1- Part 5

(Indicative temperatures T_{out} for buildings above the ground level)

Season	Significant factor		Temperature T_{out} in °C
Summer	Relative absorptivity depending on surface colour	0,5 bright light surface	$T_{max} + T_3$
		0,7 light coloured surface	$T_{max} + T_4$
		0,9 dark surface	$T_{max} + T_5$
Winter			T_{min}
NOTE: Values of the maximum shade air temperature T_{max}, minimum shade air shade temperature T_{min}, and solar radiation effects T_3, T_4, and T_5 may be specified in the National Annex. If no data are available for regions between latitudes 45°N and 55°N the values T_3 = 0°C, T_4 = 2°C, and T_5 = 4°C are recommended, , for North-East facing elements and T_3 = 18°C, T_4 = 30°C, and T_5 = 42°C for South-West or horizontal facing elements.			

2.3 Effect of Thermal Loads in Concrete Structures

Frank J. Vecchio and James A. Sato (1990) [3] carried out test on three large-scale reinforced concrete portal frame models subjected to combinations of thermal and mechanical loads. Test conditions included unrestrained thermal deformation, restrained deformation under shock thermal loads, and loading to ultimate capacity. Figure 2.2, shows the experimental setup used by Vecchio and Sato to investigate the thermal actions.

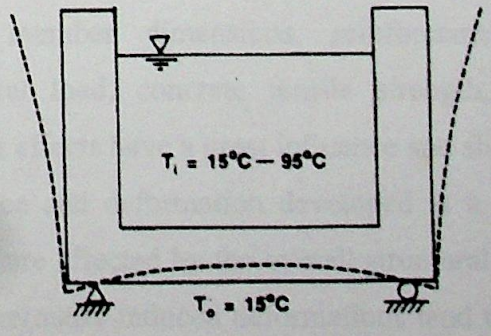

Figure 2.2: Test model with thermal load used by Vecchio and Sato

The responses were monitored in terms of resulting restraint forces, deflections, strains, cracking, and leakage. Test results had indicated that thermal loads can result in significant stressing of a structure and can lead to concentrated

damage in local regions. Based on the experimental arrangement the temperature variation, strain and stresses were given as in Figure 2.3:

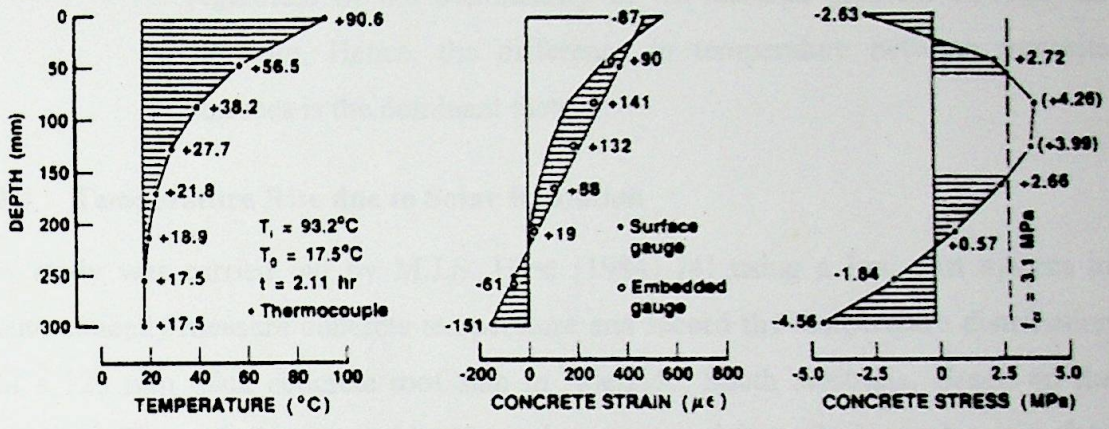

Figure 2.3: Transient condition after application of thermal load [3]
(presented by Vecchio and Sato)

Vecchio and Sato concluded the followings:

1. "Thermal loads imposed on a reinforced concrete structure can induce significant levels of deformation, stressing, and cracking. Where present, thermal loads should be expressly considered in the analysis and design of a structure."
2. "The internal forces induced in a structure by thermal loads are heavily dependent on structural stiffness. Accordingly, factors such as relative member dimensions, reinforcement details, coexisting mechanical load, concrete tensile strength, and concrete tension stiffening effects have a great influence and should be considered."
3. "The force and deformation developed at a particular location in a structure are affected by the overall structural response to the thermal loads. Thermally induced deformations tend to concentrate at weaker regions in the structure and can result in excessive cracking, yielding, and development of leakage paths."
4. "The primary thermal stresses induced in an unrestrained structure can be sufficient to cause internal cracking. This effect can subsequently influence structure stiffness or the development of leakage paths."

5. "The forces, strains, and deformations arising from thermal loads tend to be greatest shortly after the peak thermal loads are achieved, regardless of the nonlinearity of the thermal gradient through the structure. Hence, the difference in temperature between opposite surfaces is the dominant factor."

2.4 Temperature Rise due to Solar Radiation

A study was carried out by M.J.S. Hirst (1984) [4] using a low cost system to automatically measure concrete temperature and record the temperature distribution of a 125 mm thick concrete roof slab in Adelaide, South Australia. Based on the readings (Figure 2.4) presented by Hirst, the concrete slab reached a peak top surface temperature of about 66°C and a temperature difference of about 15°C for a "hot day"; where the solar radiation is generally high during the month of January in Adelaide. Based on an online solar energy calculator [5], this corresponds to a solar insolation (i.e. the amount of solar radiation energy received on a given surface area during a given time) of 24.5 MJ/m^2/day for the corresponding time of the year.

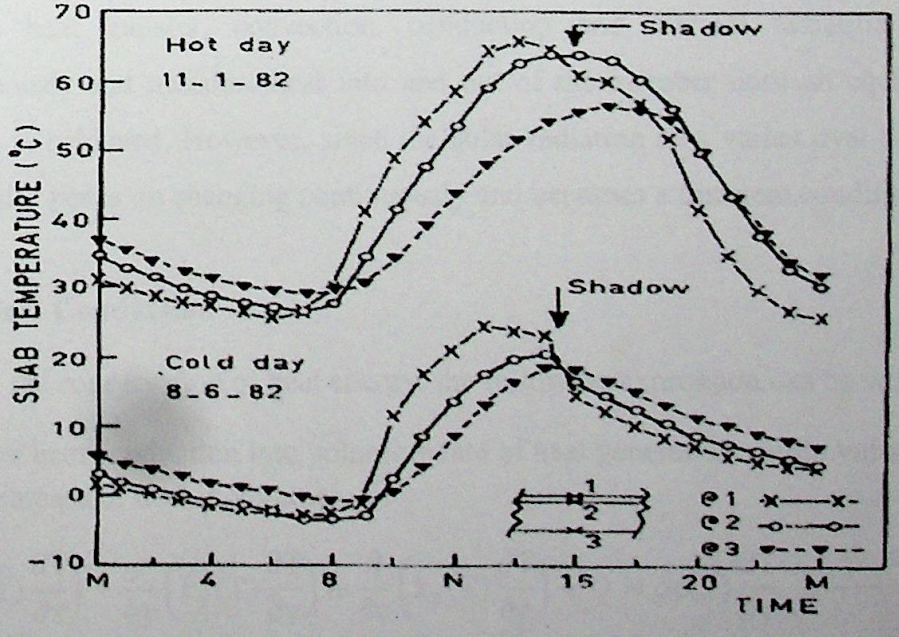

Figure 2.4: Diurnal variation of roof panel temperature [4]
(Presented by M.J.S. Hirst)

In another study on thermal loading on bridges, M.J.S. Hirst (1984) [6] concluded that thermal loading depends on climate and it is extremely variable. Further, it was stated that a calibrated computer model and meteorological data can allow a structural engineer to design bridges for thermal loading. Hirst also indicated that the probability of occurrence also should be considered.

2.5 Modes of Heat Transfer

Solar energy incident on a concrete surface is absorbed and causes the surface to increase its temperature and thereby a temperature difference is formed between the top and inner layers. This causes thermal energy to conduct into inner layers of the concrete member. Also, as the temperature of the outer surfaces is increased, a temperature difference is formed between the environment and the surface. This causes heat to dissipate from the outer surfaces towards the environment by convection and thermal radiation.

The phenomena that causes heat to dissipate from a fluid motion at the boundary layer at the heated surface is known as convection. The heat transferred by emission of electromagnetic radiation is termed as thermal radiation.

In heat transfer, convection, conduction and thermal radiation occurs simultaneously and transfers heat into and out of the member until an equilibrium condition is achieved. However, since the solar radiation also varies over time this heat transfer keeps on changing continuously and becomes a transient condition.

2.5.1 Heat Conduction

Based on the conservation of heat energy, the following expression can be written.

Rate of net heat conduction into volume + rate of heat generation within volume = Rate of increase of heat in volume

$$\frac{\partial}{\partial x}\left(k_x(T)\frac{\partial T}{\partial x}\right)+\frac{\partial}{\partial y}\left(k_y(T)\frac{\partial T}{\partial y}\right)+\frac{\partial}{\partial z}\left(k_z(T)\frac{\partial T}{\partial z}\right)+Q=\rho c(T)\frac{\partial T}{\partial \tau} \quad -- \text{ Eq. 2.1}$$

UNIVERSITY OF MORATUWA LIBRARY

Where:

Q= rate of heat generation within volume

k_x, k_y, k_z = coefficient thermal conduction in x, y, and z directions respectively

c = specific heat capacity of material

p =density of material

τ = time

Equation Eq. 2.1 can be simplified by considering:

- constant thermal conductivity in all directions and within the temperature range considered,
- constant heat capacity for the temperature range considered,
- no internal heat generation, Q=0,
- one dimensional heat flow since heat flows between outer and inner surfaces which are parallel to each other

By defining $\alpha=k/\rho c$, the heat equation can be simplified as in Eq. 2.2.

$$\frac{\partial^2 T}{\partial x^2} = \frac{1}{\alpha}\frac{\partial T}{\partial \tau} \qquad \text{---} \quad \text{Eq. 2.2}$$

To analyse this transient heat-transfer problem, one could proceed by solving the general heat-conduction equation by the separation-of-variables method, similar to the analytical treatment used for the two-dimensional steady-state condition or else using the numerical solution for specific boundary conditions.

2.5.2 Convection

The rate of heat transfer by convection q_c due to the difference between air temperature (T_{air}) and the concrete surface temperature (T_s), can be expressed by Eq. 2.3

$$q_c = h_c(T_s - T_{air}) \qquad \text{----} \quad \text{Eq. 2.3}$$

Where h_c is the convection coefficient. As per F.A Branco et al. (1993) [7] the convection heat transfer depends on various factors such as surface roughness, air velocity etc. and its correct determination is reported to be difficult. Branco et al. have suggested the relationship given in Eq. 2.4.

$$h_c = h_n + h_f \qquad \text{---- Eq. 2.4}$$

Average value of h_n for concrete surface specified by Branco et al. [7] is 6 $W/m^2/K$. The h_f depends on wind speed, V(m/sec) and is approximately expressed as in equation Eq. 2.5.

$$h_f = 3.7v \qquad \text{---- Eq. 2.5}$$

As per Faria et al (2006) [**8**], the convection coefficient can also be expressed more specifically by Eq. 2.6.

$$h_c = \begin{cases} 5.6 + 3.95v, & v \leq 5 \text{ m/s} \\ 7.6v^{0.78}, & v > 5 \text{ m/s} \end{cases} \qquad \text{---- Eq. 2.6}$$

Where, v is the velocity of wind.

2.5.3 Thermal Radiation

The thermal radiation from heated surface towards the environment is commonly known as irradiation (also known as re-radiation). The irradiation energy from the concrete surface can be determined using Stefan-Boltzmann law as in Eq. 2.7.

$$q_r = \varepsilon\sigma\left(T_s^4 - T_{air}^4\right) \qquad \text{---- Eq. 2.7}$$

Where, ε is the emissivity of concrete, which is equal to the ratio of emission from a gray concrete surface to that from perfect radiator at the same temperature, (usually within the range of 0.85-0.95) and σ is the Stefan-Boltzmann constant ($\sim 5.67 \times 10^{-8}\ Wm^{-2}K^{-4}$).

However, according to Faria et al. (2006) [**8**] the non-linearity problem of the thermal irradiation can be simplified by converting the non-linear irradiation heat transfer into a single convection–radiation coefficient as Eq. 2.8

$$h_{cr} = h_c + h_r \qquad \text{---- Eq. 2.8}$$

where;

$$h_r = \begin{Bmatrix} \varepsilon[4.8 + 0.075(T_{air} - 5)], & T_{air} \geq 5°C \\ 4.8\varepsilon, & T_{air} < 5°C \end{Bmatrix} \quad \text{---- Eq. 2.9}$$

h_{cr} =convection–radiation coefficient

h_c =convection coefficient

Then the rate of heat transfer by convection and radiation can be presented as Eq. 2.10.

$$q_{cr} = h_{cr}(T_{air} - T_s) \quad \text{---- Eq. 2.10}$$

Faria et al. stated that the simplification is valid for the usual range of temperature differences between concrete surfaces and the environment. And also, the convection–radiation coefficient is applicable under the hypothesis of direct contact between the surface of the concrete member and air.

2.6 Numerical Equations for Heat Transfer

2.6.1.1 Semi-infinite model

This type of idealization is applicable to models where the temperature change does not reach the other side or surface of the solid within the time frame under considerations.

As described by C. P. Kothandaraman [9] there are three types of boundary conditions for which solutions are available in a simple form for a body exposed to uniform heat flux. For boundary conditions defined as in equation Eq.2.11 the solution is given by equation Eq. 2.12.

The boundary condition is defined as the heat transfer due to conduction is equal to the heat flux applied to the surface. In this equation convection is not considered.

$$-k\left.\frac{\partial T}{\partial x}\right|_{x=0} = q \quad \text{---- Eq. 2.11}$$

$$(T_{x,t} - T_i) = \frac{2q(\frac{\alpha t}{\pi})^{\frac{1}{2}}}{k} \exp\left(\frac{-x^2}{4\alpha t}\right) - \frac{qx}{k}\left(1 - \text{erf}\left(\frac{x}{2\sqrt{\alpha t}}\right)\right) \quad ---- \text{Eq. 2.12}$$

Where:

q = heat flux

t = time

x = distance from surface

$T_{x,t}$ = temperature at depth x from surface at time end of time t

T_i = initial temperature

k=coefficient thermal conduction

c = specific heat capacity

p =density

α=k/ρc

2.7 Numerical Equations for Thermal Stresses

The following equations Eq. 2.13 to Eq. 2.25 are an extract from the book "Concrete Structures: Stresses and Deformations" by A. Ghali, R. Ravre [**10**].

The hypothetical strain (ε_t) that would occur at any fiber if it was free is given by;

$$\varepsilon_f = \alpha_t . T \quad ---- \text{Eq. 2.13}$$

Where, T = T(y) the temperature rise at any fiber at a distance y below a reference point O, α_t = coefficient of thermal expansion (see Figure 2.5).

If this strain is prevented, then

$$\sigma_{restrained} = -E . \varepsilon_f \quad --- \text{Eq. 2.14}$$

Where, E is the modulus of elasticity.

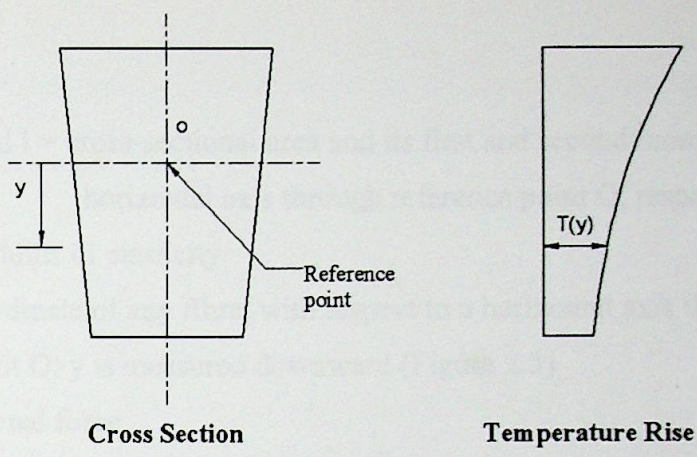

Figure 2.5: Cross-section of a member subjected to a rise of temperature

The resultant of the stress can be represented by an axial force ΔN at a reference point O and a bending moment ΔM given by

$$\Delta N = \int \sigma_{restrained} . dA \qquad \text{--- Eq. 2.15}$$

$$\Delta M = \int \sigma_{restrained} . y . dA \qquad \text{--- Eq. 2.16}$$

Substituting with strain components

$$\Delta N = -\int E . \varepsilon_f . dA \qquad \text{--- Eq. 2.17}$$

$$\Delta M = -\int E . \varepsilon_f . y . dA \qquad \text{--- Eq. 2.18}$$

By considering the basic equation for strain and stress,

$$\varepsilon = \epsilon_0 + \psi . y \qquad \text{--- Eq. 2.19}$$

$$\sigma = E(\epsilon_0 + \psi . y) \qquad \text{--- Eq. 2.20}$$

Then

$$\epsilon_0 = \frac{IN - BM}{E(AI - B^2)} \qquad \text{--- Eq. 2.21}$$

$$\psi = \frac{-BN + AM}{E(AI - B^2)} \qquad \text{--- Eq. 2.22}$$

Where:

A, B and I = cross-sectional area and its first and second moment about a horizontal axis through reference point O, respectively

E = modulus of elasticity

y = coordinate of any fibre, with respect to a horizontal axis through reference point O; y is measured downward (Figure 2.5)

N = normal force

M = bending moment about a horizontal axis through reference point O

ε and σ = strain and stress at any fibre

ε_0 and σ_0 = strain and stress at reference point O

$\psi = d\varepsilon/dy$ (the curvature)

Substituting the Moment and Axial forces from Eq. 2.17 and Eq.2.18, In matrix form,

$$\begin{Bmatrix}\Delta\varepsilon_0 \\ \Delta\psi\end{Bmatrix} = \frac{1}{E(AI - B^2)}\begin{bmatrix} I & -B \\ -B & A\end{bmatrix}\begin{Bmatrix}-\Delta N \\ -\Delta M\end{Bmatrix} \qquad --- \text{ Eq. 2.23}$$

The actual stress due to temperature is the sum of $\sigma_{restrained}$ and $\Delta\sigma$; is as follows:

$$\Delta\sigma = E[\Delta\varepsilon_0 + (\Delta\psi)y] \qquad --- \text{ Eq. 2.24}$$

$$\sigma = E[-\varepsilon_0 + \Delta\varepsilon_0 + (\Delta\psi)y] \qquad --- \text{ Eq. 2.25}$$

2.8 Thermal Properties of Concrete

2.8.1 Specific Heat Capacity

Based on the reference [11] the specific heat capacity of concrete is given in Table 2.2.

Table 2.2: Typical specific heat capacity of concrete

Temperature, °C	Specific Heat, J/kg/K
10	917
38	971
66	1038

However, according Patrick Mitchell [12], the heat capacity for concrete is given as 800 J/kg/K. [12]

2.8.2 Conductivity of Concrete

The Eurocode 1 Part 5 [2] specifies the thermal conductivity for concrete (of volume weight from 21 to 25 kN/m^3) on a range between 1.16 to 1.71 W/m/K. However as per reference [11], the thermal properties for Limestone and Quarts gravel concrete under different moisture conditions are given Table 2.3. As shown in Table 2.4 and Table 2.5 the thermal conductivity of concrete is dependent on aggregate type, moisture condition and density as well.

Table 2.3: Conductivity of concrete

Concrete Type	Moisture Condition	Thermal Conductivity W/m/K
Limestone Concrete	Moist	2.2
	50% relative humidity	1.7
	Dry	1.4
Quarts Gravel Concrete	Moist	3.3
	50% relative humidity	2.7
	Dry	2.3

Table 2.4: Effect of aggregate type and dry density on conductivity

Aggregate Type	Dry Density kg/m^3	Thermal Conductivity W/m/K
Hematite	2870	2.6
Marble	2290	1.7
Sandstone	1920	1.4
Limestone	2020	1.4
Dolerite	2180	1.2
Barite	2880	1.2
Expanded shale	1430	0.62

Table 2.5: Effect of moist density on conductivity

Aggregate Type	Moist Density kg/m^3	Thermal Conductivity W/m/K
Hematite	3040	4.1
Quartize	2400	4.1
Quartize	2440	3.5
Dolomite	2500	3.3
Granite	2420	2.6
Marble	2440	2.2
Limestone	2440	2.6

2.9 Uncoupled Thermal and Mechanical Analysis

For applications of solid mechanics, strains induced in a solid body due to mechanical loading and/or temperature change were reported not to introduce a significant change in the temperature distribution within that body (Kavalenko [**13**] ; Boley and Weiner [**14**]). This assumption was also adopted by Anna Saetta et al. (1993) [**15**] to investigate the stress due to variable thermal loads of a concrete Dam and a typical bridge box girder section. They neglected the variation of the thermal characteristics with the stress-strain state of the material and had studied the problem in a simplified uncoupled manner. After the thermal transient was solved, the mechanical problem was solved.

2.10 Initial Temperature of the Structure

As per Eurocode 1 – part 5 [**2**], the initial temperature of the structure (defined as T_0), should be taken as the temperature of a structural element at the relevant stage of its restraint (completion). If it is not predictable the average temperature during the construction period should be taken.

LIBRARY
UNIVERSITY OF MORATUWA, SRI LANKA
MORATUWA

2.11 Use of ANSYS for Finite Element Analysis and Element Selection

ANSYS provides many element types from which one has to choose the most suitable element to analyze the model under investigation. ANSYS user manual [16] specifically defines an element type named SOLID65 that can be used for the 3-D modeling of solids with or without reinforcing bars (rebar). The solid is capable of cracking in tension and crushing in compression. In concrete applications, for example, the solid capability of the element may be used to model the concrete while the rebar capability is available for modeling reinforcement behavior. The element has special features such as modeling of reinforcement (as smeared reinforcement), plasticity, creep, cracking, crushing, and stress stiffening etc. Therefore SOLID65 has been the common selection when modeling reinforced concrete members. However, it is noted that SOLID65 element cannot be used for transient thermal analysis since it does not have the temperature degrees of freedom (DOF).

In a study by L. Dahmani, at al. [17] had used SOLID65 for the analytical model. In another investigation carried out by L. Dahmani, at al. [18] to investigate the thermal stresses induced by high temperature gradient in the concrete beam, Dahmani at al. had performed a sequential, nonlinear, transient thermal-structural analysis, while taking into account the thermal conductivity and specific heat. The analysis was initially performed using SOLID70 elements to get the temperature profile across the beam. SOLID70 is an element in ANSYS with 3-D thermal conduction capability. The element has eight nodes with a single degree of freedom, temperature, at each node. The element is applicable to a 3-D, steady-state or transient thermal analysis.

Next, Dahmani at al. switched the elements from SOLID70 to SOLID65 structural elements to perform a reinforced concrete analysis using smeared reinforcement layer to evaluate the structural response due to the temperature profile.

As shown in the ANSYS verification example VM33, (Transient Thermal Stress in a Cylinder) [16], SOLID5 elements have been used to carry out a transient thermal stress analysis. The SOLID5 is 3-D magnetic, thermal, electric, piezoelectric, and structural field capability with limited coupling between the fields. It also provides features to limit the DOF when required. Aruna et al. [19] had used

108909

108909

SOLID5 elements to simulate both thermal and structural behavior of concrete slab without the need to switch the element types during analysis. In this analysis, a concrete slab subjected to solar radiation was analyzed. Input heat flux and the convection heat loss to the surrounding were set as time dependent boundary conditions. The temperature variation in the slab was compared with experimental results and had shown to give a good correlation.

Therefore, it is conclusive that if the investigations are not concerned with reinforcement nor cracking or other specific brittle behavior, SOLID5 elements can be used for thermal and structural stress analysis of concrete members.

2.12 Solar Radiation

2.12.1 Radiation Spectrum

Solar radiation incident outside the earth's atmosphere, which is known as the extraterrestrial radiation, amounts to about 1367W/m^2. This is also referred to the Solar Constant [**20**], [**21**], Solar radiation includes visible light (typically 43% of solar energy), near infrared light (52%), and ultraviolet light (5%). The solar radiation reaching the Earth is partly absorbed, scattered and reflected by molecules, aerosols, water vapor and clouds as it passes through the atmosphere. Therefore the amount of solar radiation reaching the ground level varies [**22**].

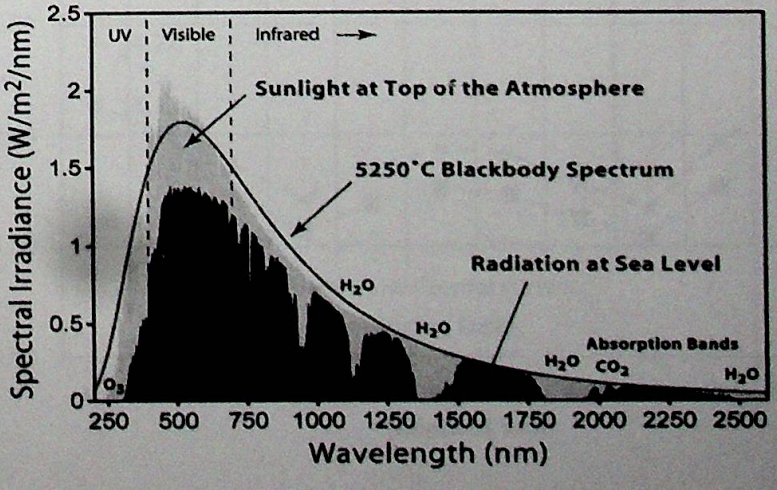

Figure 2.6: Solar radiation spectrum

(From Wikipedia: http://en.wikipedia.org/wiki/File:Solar_Spectrum.png)

The radiation at ground level can be divided into direct and indirect (diffused) components. The direct component is the direct solar radiation that is directly incident on a surface while the indirect radiation refers to the solar radiation resulting from multiple scattering by the environment. The total amount of solar radiation falling on a horizontal surface (i.e. the direct solar beam plus the indirect solar radiation on a horizontal surface) is referred as global solar radiation [**23**].

2.12.2 Time and Orientation for Maximum Solar Radiation

The amount of solar energy and its incident angle on a plane depends on the time of the year, the geometrical position (Latitude) and the direction of the plane. Based on the Solar Electricity Handbook, where it hoists a website for solar energy calculator [**5**], by entering the geographical location for Colombo, the average Solar Insolation was extracted and is presented in Figure 2.7. Solar Insolation is a measure of solar irradiance over of period of time - typically over the period of a single day. Solar Irradiance is a measure of how much solar power is received for a particular location.

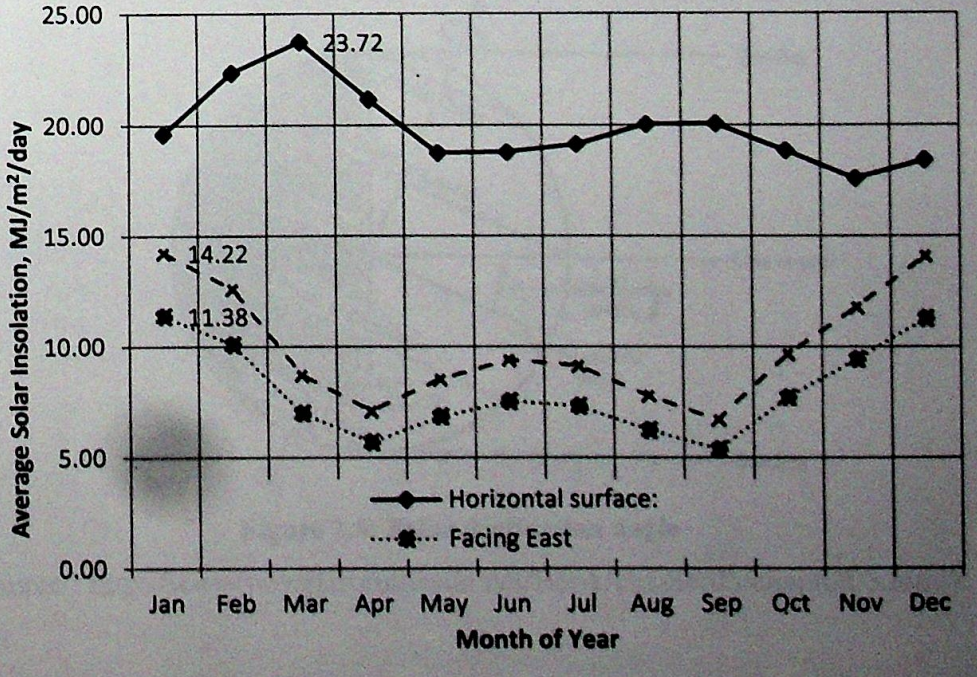

Figure 2.7: Average solar insolation for Colombo, Sri Lanka

(Data from solar energy calculator, [5] . The website does not provide details for plane facing North nor West since it is combined to South and East directions)

As per Figure 2.7, it indicates that during the mid of March and early September the solar insolation is high on a horizontal surface; the month of March reports the highest of the two. Also a plane facing the East or South receives the maximum solar insolation during the month of December and January. For a plane facing South this is about 60% of the maximum insolation received on a horizontal plane.

This implies that the maximum solar energy is received by a horizontal plane. Among the other planes, the plane facing South is the next to receive the maximum solar energy during the month of December to January, which is only about 60% of the energy received by the horizontal surface. Therefore for a structure in Colombo, the most critical surface is the top horizontal surface during a clear day in the month of March.

As given in Figure 2.9, the maximum solar energy reaching a horizontal surface can be considered when the sun passes directly on top on a clear day. For Sri Lanka it would be around 7th April and 4th September when the declination is 7°N corresponding to the geographical location of Sri Lanka.

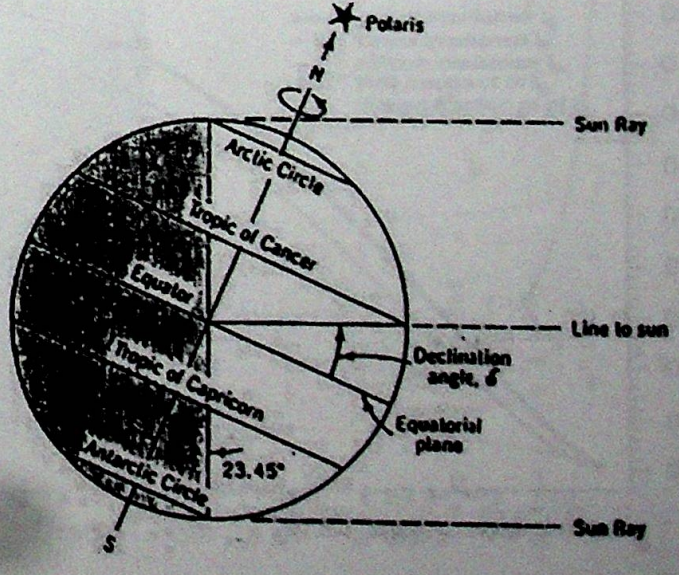

Figure 2.8: Solar declination angle

(Source : http://www.powerfromthesun.net/Book/chapter03/chapter03.html)

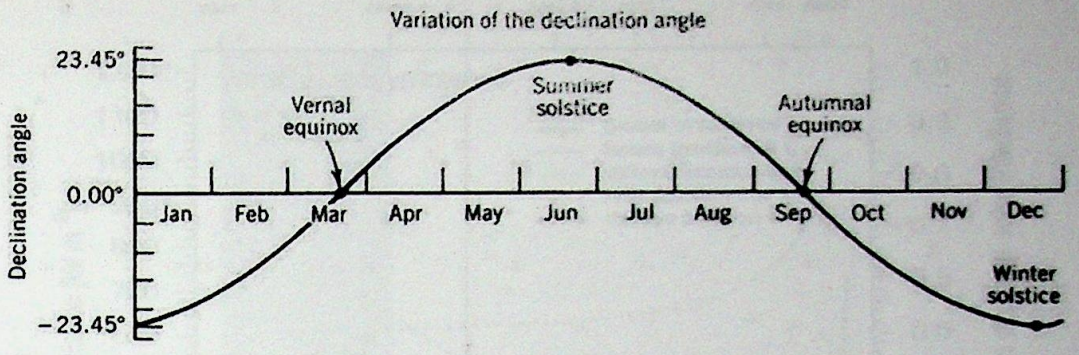

Figure 2.9: Variation of declination angle

(Source : http://www.powerfromthesun.net/Book/chapter03/chapter03.html)

According to an investigation by Ronnen Levinson et al. [24], the solar irradiance on a horizontal surface and vertical surface was presented as in Figure 2.10 and Figure 2.11 respectively.

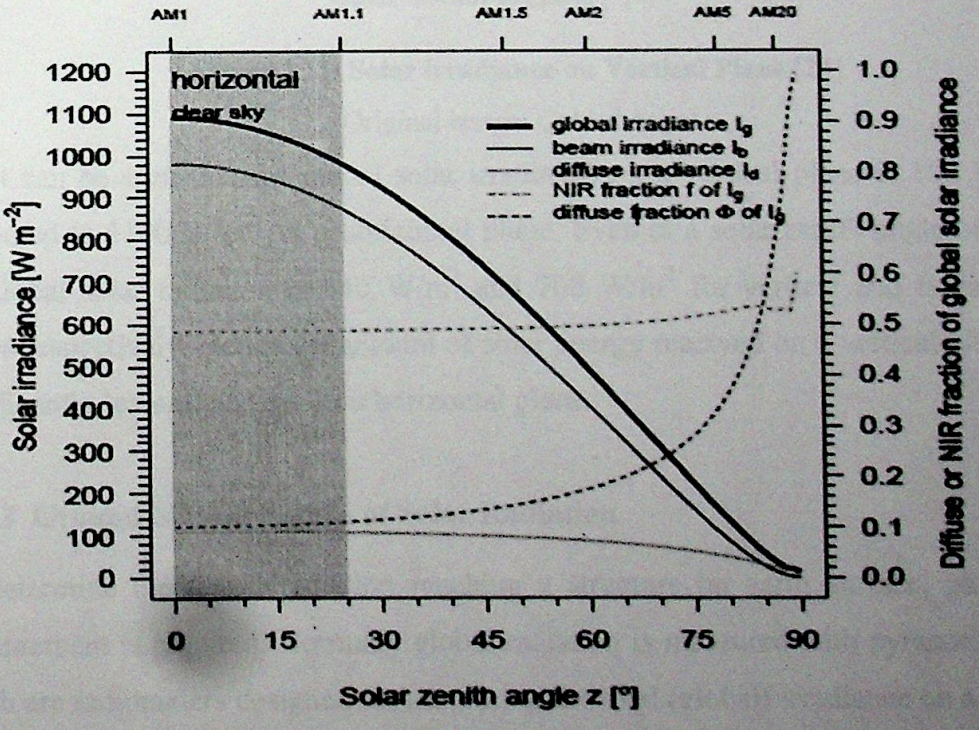

Figure 2.10: Solar irradiance on Horizontal Plane [24]

(Original image: Color Image)

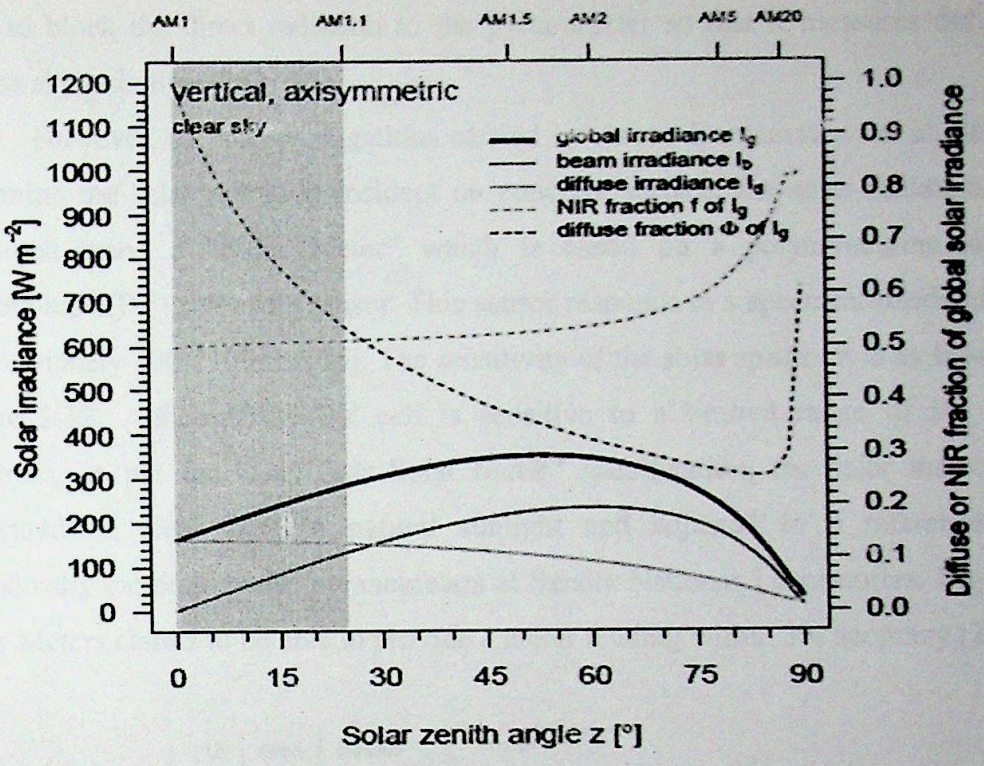

Figure 2.11: Solar irradiance on Vertical Plane [24]

(Original image: Color Image)

It can be seen that the global solar irradiance on a vertical plane is 160 W/m^2 compared to 1100 W/m^2 for a horizontal plane. Even at a solar zenith angle of 45^0, the global solar radiation is 340 W/m^2 and 700 W/m^2 for vertical and horizontal planes respectively. Hence the amount of solar energy received on a vertical plane is significantly lower than that for a horizontal plane.

2.12.3 Ground Measurements of Solar Radiation

To determine the actual radiation reaching a structure on earth surface, physical measurement is required. Normally global radiation is measured with pyranometers, which are radiometers designed for measuring the total (global) irradiance on a plane surface. Direct radiation is measured with a pyrheliometer that has a slightly larger view than the sun and its aureole and does not see the rest of the sky. To make measurements, the pyrheliometer must point precisely at the sun and this is achieved by using an automatic two-axis sun tracker. A shading assembly on the sun tracker is

used to block the direct radiation to the pyranometer so that it measures only the diffuse sky radiation [25], [23].

However, as per investigations carried by Aruna Karunarathne et al. [19] to determine the solar radiation incident on concrete surface, the solar radiation was measured using a "Solar Meter" which is based on a polycrystalline silicon photovoltaic (PV) cell as its sensor. This sensor responds to a spectrum bandwidth of approximately 300-1100nm [26]. The sensitivity of the solar spectrum is as shown in Figure 2.12. Although the PV cell is sensitive to a limited range of the solar spectrum, as per the "Day Star Solar Meter" specification, the solar meters are calibrated on clear days in natural sunlight and adjusted to a reference cell periodically calibrated with pyranometers at Sandia National Laboratories. Day Star Solar Meters claims to be able to provide a meter reading within 3% accuracy [26].

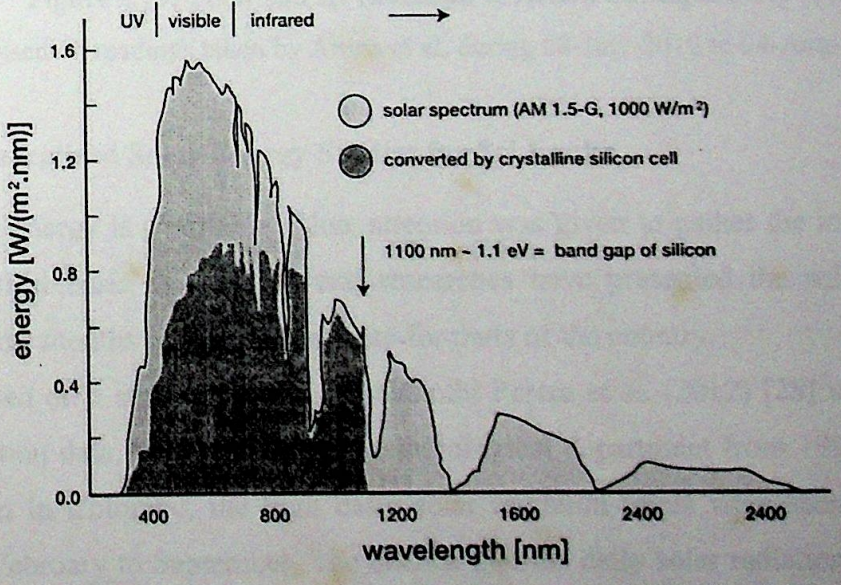

Figure 2.12: Generic spectrum for a silicon PV cell [27]

(Original Image: colour image)

As per Aruna et al. [19] on road pavement slabs to investigate the effect of solar induced cracking, the average daily solar radiation variation from 08-July-2010 to 04-Aug-2010 were recorded using a solar meter. Figure 2.13 shows the solar radiation variation gathered by Aruna et al.

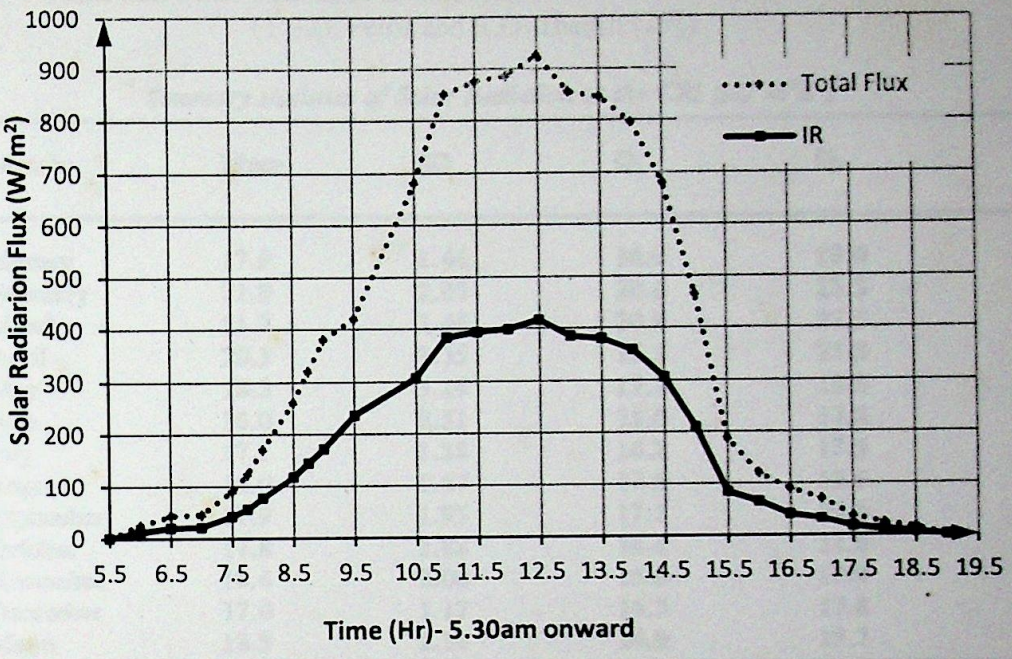

Figure 2.13: Total and IR radiation variation during the day [19]

(Based on readings taken by Aruna et al. during 08-July-2010 to 04-Aug-2010)

2.12.4 Generalized Solar Energy Studies for Sri Lanka

Since solar energy is a variable value, attention was given to gather the information in a statistical basis as well. Several researches have presented the solar energy values for the months of the year and also for parts of the country.

Based on a study carried out by Kanthi Perera et al. (2012) **[28]** using daily solar radiation data, collected by the Meteorological department from 1997 to 2007 at a station in Colombo, the high daily solar radiation totals were seen from the month of February to September. The chance that the daily solar radiation above 16 MJ/m^2 was more than 87% for the months from February to September.

T.S.G. Peiris and R.O. Thattill (1995) **[29]** proposed an 'alternative' model to estimate solar radiation based on sunshine hours by processing mean-monthly solar radiation at the Coconut Research Institute (CRI), Lunuwila, Sri Lanka.

Table **2.6** shows the statistical information presented by Peiris and Thattill based on 17 years (1976-1992) of data.

Table 2.6: Solar Radiation at Coconut Research Institute, Sri Lanka
(T.S.G. Peiris and R.O. Thattill [29])

Summary statistics of Solar Radiation at the CRI (MJ $m^{-2}d^{-1}$)

Month	Mean	SD	Q_1	Q_3
January	17.9	1.44	16.9	19.0
February	21.0	2.89	20.6	23.3
March	21.7	1.46	20.9	22.5
April	20.3	1.35	19.5	21.3
May	18.3	1.19	17.7	18.8
June	16.0	2.51	15.0	17.8
July	17.3	1.38	16.2	17.5
August	18.0	1.47	17.5	18.5
September	17.9	1.95	17.1	19.6
October	17.8	1.82	16.4	18.6
November	16.4	2.04	15.6	17.9
December	17.0	1.17	16.5	17.8
Mean	18.3	2.34	16.9	19.7

(based on estimated values from 1976 to 1992.
SD: Standard deviation; Q_1: 25% percentile; Q3: 75% percentile)

In a report on solar resource assessment for Sri Lanka and the Maldives prepared by Dave Renné et al [30], revealed that the annual solar energy for Sri Lanka ranges from 4.5 to 6.0 kWh/m^2/day, are consistent with, and slightly higher than earlier studies using sunshine recorders, which gave results of 4.2 to 5.6 kWh/m^2/day. (For comparison, 4.2 kWh/m^2/day and 5.6 kWh/m^2/day convert to 15.12 MJ/m^2/day and 20.16 MJ/m^2/day respectively.)

Table 2.7: Comparison between reported solar energy data

Source	Solar Energy Value
Kanthi Perera et al. [28]	Chance of getting solar radiation above 16 MJ/m2/day is more than 87% for the months from February to September .
T.S.G. Peiris and R.O. Thattill [29]	mean-monthly solar radiation is 18.3 MJ/m^2/day
Dave Renné et al. [30]	Annual solar energy is between 16.2 to 21.6 MJ/m^2/day

2.13 Solar Radiation Absorption in Concrete

As pointed out by Dennis A. Morian [31], "there are several factors which influence the solar radiation absorption into a given slab surface. These include the time of the day and year, the latitude, and cloudiness, and so on" (Chapman A.J. [32]; Taljaston 1987 [33]; Branco et al. 1992 [7]).

Branco et al. [7] had showed that the total solar radiation that reaches the surface of a concrete slab is the sum of direct and indirect contributions and presented in an equation as given in Eq. 2.26 extracted from the report by Dennis A. Morian [31].

$$q_s = \alpha \left[I_d Sin\,\theta + I_r \left(\frac{1 + \text{Cos}\,\gamma}{2} \right) \right] \qquad \text{--- Eq. 2.26}$$

Where

q_s = solar radiation (W/m^2)

α = surface heat absorptivity of concrete (= 0.6) (Chapman, 1982)

I_d = direct solar radiation (W/m^2)

I_i = indirect solar radiation (W/m^2)

θ = incident angle of solar radiation against the slab surface (degree)

γ = inclination angle (degree) of slab surface w.r.t horizontal.

According to Aruna et al. [19], the Infra-red component of solar radiation has the main contribution to thermal heat on concrete and its component is about 45% of the measured reading by a Solar Flux meter.

However in other researches on solar radiation on concrete, details more about the thermal effect on concrete. The solar energy absorption is shown to be dependent on the color and texture of concrete. In this context, the term Albedo is commonly used. Albedo is the ratio of reflected solar radiation to the total amount that falls on a surface, known as incident solar radiation (ACPA, 2002 [34]) and is measured on a scale of 0 to 1. An albedo value of 0 indicates a "black" body that does not reflect any light whereas an albedo value of 1 indicates a "white" perfectly reflective surface

(Boriboonsomsin and Reza, 2007 [35]). By considering the Albedo value, the solar absorption value can be derived.

Investigations on effects of composition and exposure on the solar reflectance of Portland cement concrete by Ronnen Levinson and Hashem Akbari (2002) [36] concluded the following.

> "Concrete albedo grew as the cement hydration reaction progressed (mean increase 0.08), but stabilized within six weeks of casting. The mature albedos of the eight properly-made, "smooth" concrete mixes ranged from 0.41 to 0.77 (mean 0.59). Simulated weathering, soiling, and abrasion each reduced average concrete albedo (mean decreases 0.06, 0.05, and 0.19, respectively), though some samples became slightly more reflective through weathering or soiling. Simulated rain (wetting) strongly depressed the albedos of concretes (mean decrease 0.23) until their surfaces were dried. Exposure similarly affected the albedos of the improperly-made, "rough" concretes."

The findings of Levinson and Akbari is shown in Figure 2.14.

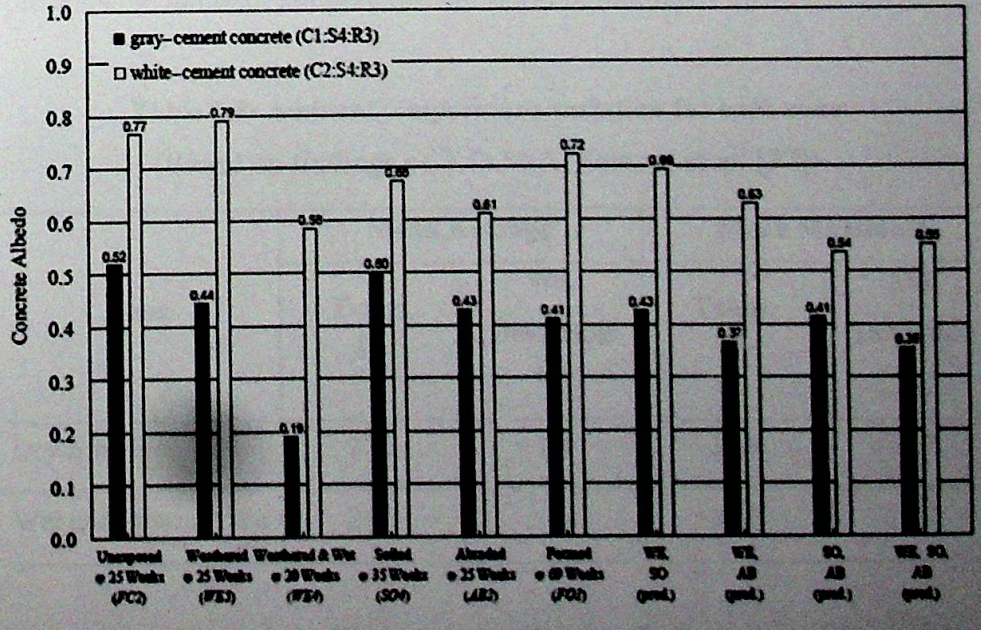

Measured and predicted mature albedos of the most-reflective white-cement and gray-cement smooth concretes. Shown from left to right are reflectances measured in six states (unexposed, weathered, weathered and wet, soiled, abraded, and farmed), and reflectances predicted for four geometrically combined exposures (weathered & soiled, weathered & abraded, soiled & abraded, and weathered & soiled & abraded).

Figure 2.14: Albedo values of Concrete [36]

UNIVERSITY OF MORATUWA LIBRARY

Since the solar absorption factor is the difference between unity and albedo, based on the information presented by Levinson and Akbari [36], it can be generalized that the solar absorption factor is in the range of 0.55 to 0.65 for grey concrete and 0.3 to 0.45 for white concrete.

2.14 Studies on Ambient Temperature

T.D.M.A. Samuel and R. Srikanthan (1982) [37] presented an estimate for the solar radiation for Sri Lanka using data from 26 meteorological stations of the country. They concluded that the "Dry Zone" had a mean average temperature of 27.5°C with a standard deviation of 1.4°C and a mean maximum temperature of 30.9°C with a standard deviation of 1.7°C. The Wet and Intermediate zones together was indicated to have a mean average temperature of 24.7°C with a standard deviation of 4°C and a mean maximum temperature of 28.5°C with a standard deviation of 3.7°C. Samuel and Srikanthan further stated that the air was nearly always moist through the country with a mean relative humidity of 77.0% and standard deviation of 2.5. Table 2.8 represents the ambient temperature variation in tabulated form.

Table 2.8: Ambient temperature variation for each zone

(Based on findings of T.D.M.A. Samuel et al. [37])

Zone	Mean Average		Mean Maximum	
	Temp. °C	Std. Deviation °C	Temp. °C	Std. Deviation °C
Dry zone	27.5	1.4	30.9	1.7
Wet and intermediate	24.7	4	28.5	3.7

Based on the statistical information, the distribution on ambient temperature variation, for a probability of 0.02, (equivalent to 50 year return period), the average and maximum temperature for Sri Lanka is presented in Table 2.9 (The calculation were based on statistical equation for normal distribution).

Table 2.9: Average and maximum temperature for 50 year return period

(Based on findings of T.D.M.A. Samuel et al. [37])

Zone	Temperature, ^{0}C	
	Average	Maximum
Dry zone	30.4	34.4
Wet and intermediate	32.9	36.1

As part of the research done by Aruna et al. [19], the ambient temperature variation in Moratuwa area was recorded and presented as a normalized function as shown in Figure 2.15.

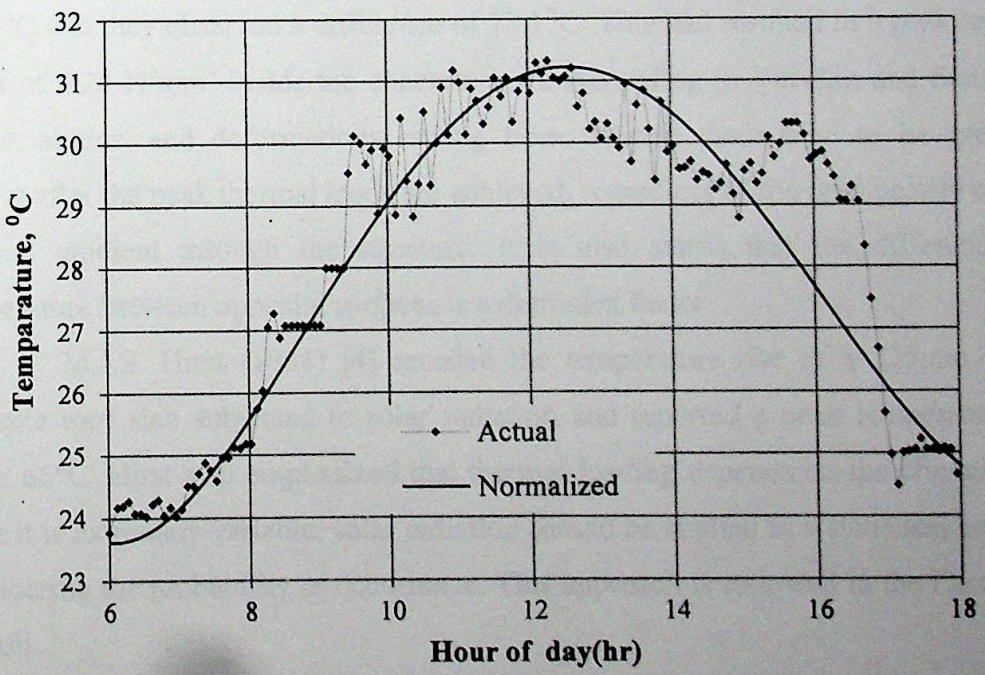

Figure 2.15 : Ambient Temperature Variation during a day

(Recorded by Aruna et al. on 3rd August 2010)

From Figure 2.15 it is noted that the maximum temperature is about 31.3^{0}C which is just below the mean maximum value (32.2^{0}C) that was presented by T.D.M.A. Samuel et al. for wet and intermediate zones.

2.15 Summary of Literature Review

The British code BS 8007 has emphasized the need to consider the effect of solar radiation for which it has not specifically incorporated into its equations. However, the Eurocode 1 part 5 has given more details on how to incorporate the solar radiation effect on structures. Nevertheless, it has only suggested generalized temperature ranges applicable to the European region. Specific thermal actions and critical locations of the structures that are subjected to solar radiation has not been detailed in the Eurocode 1.

Investigations have shown the importance of thermal loading, solar radiation and its temperature peaks on concrete structures. Vecchio and Sato (1990) [3] studied the thermal gradient caused by heated water inside a tank. The outer surface temperature was kept at 15^0C and the inner water temperature was heated up to 95^0C and they observed a difference of 73.1^0C. This had resulted in a peak tensile stress of 4.26 N/mm^2 inside the concrete wall. According to Vecchio and Sato, the forces, strains, and deformations arising from thermal loads tend to be greatest shortly after the peak thermal loads are achieved, regardless of the nonlinearity of the thermal gradient through the structure. It is also stated that the difference in temperature between opposite surfaces is a dominant factor.

M.J.S. Hirst (1984) [4] recoded the temperature rise of a 125mm thick concrete roof slab subjected to solar radiation and reported a peak temperature of about 66°C. Hirst also emphasized that thermal loading depends on the climate and since it is extremely variable, solar radiation should be studied in a statistical context considering the probability of occurrence. This approach is followed in the Eurocode as well.

Based on a solar energy calculator [5] the maximum solar radiation is to be received during the month of March on a horizontal plane. During the months of December to January the peak solar radiation on South and North faces is about 60% of that received by a Horizontal Plane. Ronnen Levinson et al. [24] presented peak solar irradiation variations and showed that the horizontal plane is more susceptible to solar radiation energy.

There are many researches done to investigate the effect due to solar radiation on concrete road pavements. The amount of solar radiation reaching the concrete member and the amount of energy absorbed are shown as important parameters. Also as investigated by Aruna et al. [19], a photovoltaic handheld solar meter can also be used to measure the solar radiation.

With regards to the solar radiation absorbed by the concrete surface, the albedo, defined as the ratio of reflected radiation from the surface to incident radiation upon it is important. Many investigations have been carried out to show the importance of the albedo value and how it depends on the surface color and the texture as well.

ANSYS does not provide a specific element to simulate heat flux, conduction and convection simultaneously. This is due to the fact that ANSYS considers the heat flux (solar radiation input) and the convection as mutually exclusive and only allows to apply only one load type [16]. However, a method by overlaying of element has been suggested in ANSYS user guide [16].

As shown by Anna Saetta et al. (1993) [15] transient thermal-structural problems can be solved by solving transient thermal problem first and next the structural problem can be solved as a static problem.

There are many researches done to investigate the effect due to solar radiation on concrete road pavements. The amount of solar radiation reaching the concrete member and the amount of energy absorbed are shown as important parameters. Also as investigated by Aruna et al. [**19**], a photovoltaic handheld solar meter can also be used to measure the solar radiation.

With regards to the solar radiation absorbed by the concrete surface, the albedo, defined as the ratio of reflected radiation from the surface to incident radiation upon it is important. Many investigations have been carried out to show the importance of the albedo value and how it depends on the surface color and the texture as well.

ANSYS does not provide a specific element to simulate heat flux, conduction and convection simultaneously. This is due to the fact that ANSYS considers the heat flux (solar radiation input) and the convection as mutually exclusive and only allows to apply only one load type [**16**]. However, a method by overlaying of element has been suggested in ANSYS user guide [**16**].

As shown by Anna Saetta et al. (1993) [**15**] transient thermal-structural problems can be solved by solving transient thermal problem first and next the structural problem can be solved as a static problem.

3 Chapter 3 – Finite Element Analysis

3.1 Introduction

ANSYS Multiphysics 12 was used to perform the finite element analysis. In ANSYS, finite element models can be created using command line input or using the graphical user interface (GUI). For this research, the command line input method was used since it simplifies the parametric study of the model. Further it provides consistency and reusability of the command code. This was useful when sensitivity analysis was done where only specific parameters needed to be modified.

This chapter describes the methodology and commands used to perform the analysis using ANSYS software. Command line input code is also indicated and described where appropriate.

It would be useful to note that ANSYS command input provides the facility to add comments to the command list so that the code is more meaningful. Comment proceeds with the exclamation mark. Therefore any text following an exclamation mark within a line is considered as a comment.

3.2 Modeling

The members were modeled as individual volumes. The volumes were generated using the "BLOCK" command by providing the x, y and z coordinates across its diagonal. When parametric models were required, variables were associated to the input values of the command.

3.3 Selection of Element Type

As the main element, SOLID5, a 3D Coupled-Field Solid element (see Figure 3.1) was selected.

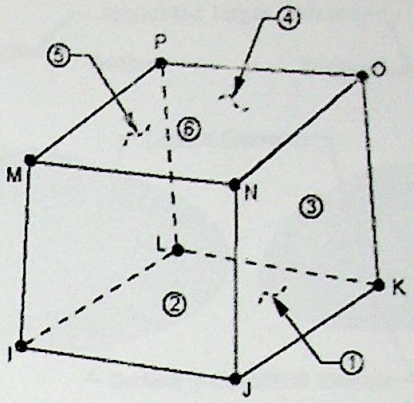

Figure 3.1: 3D Couple Field Solid – SOLID5

To apply the convection boundary condition, SHELL57 element type was selected (see Figure 3.2). SHELL57 is a 3-D element having in-plane thermal conduction capability. The element has four nodes with a single degree of freedom, temperature, at each node. The conducting shell element is applicable to a 3-D, steady-state or transient thermal analysis.

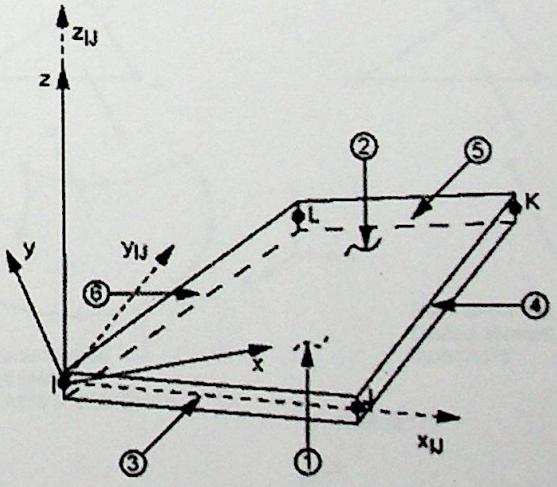

Figure 3.2: Thermal Shell Element - SHELL57

In the structural analysis, in order to perform a sliding action (only for selected cases) a contact element pair was used. In order to form a contact face, the contact interface was formed with a "target" and a "contact" element. As the Target element TARGE170 and as the contact element CONTA173 was chosen.

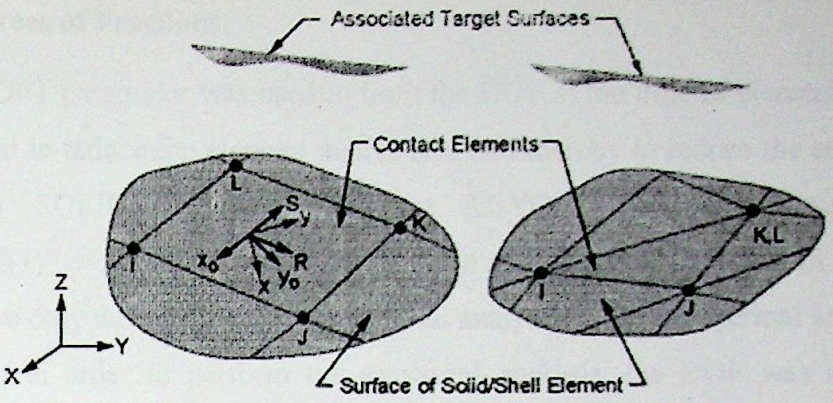

Figure 3.3: 3-D 4-Node CONTA173

TARGE170 elements are used to represent various 3-D "target" surfaces for the associated contact elements CONTA173. ANSYS states that this element supports translational or rotational displacement, temperature, forces and moments on this target elements.

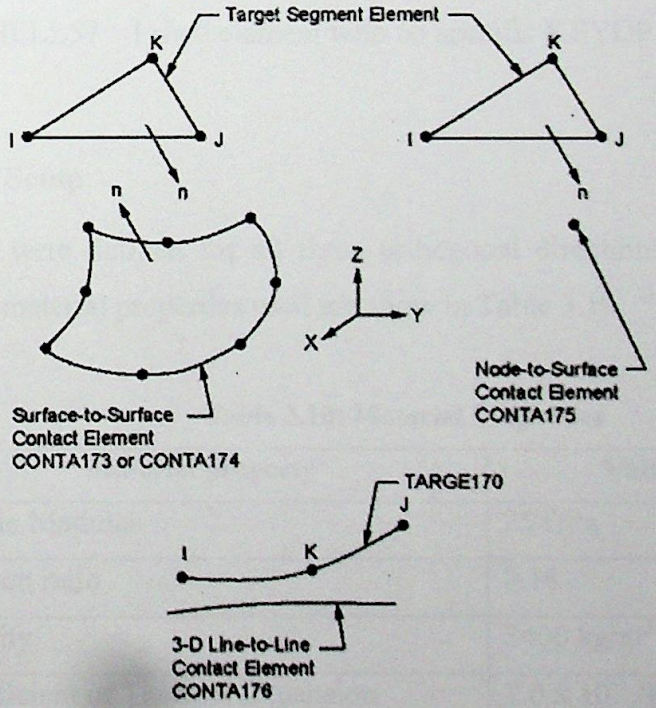

Figure 3.4: 3-D Target Element – TARGE170

3.4 Degrees of Freedom

The KEYOPT parameter was used to limit the DOF at the time of element selection. This helped to reduce the element matrix size and thereby to reduce the computation time. For SOLID5 element, the first KEYOPT parameter designated as "KEYOPT(1)" was set to value 8, to limit the degrees of freedom (DOF) to temperature only during the transient thermal analysis. After the thermal analysis was completed, in order to perform the structural analysis, the DOF was reset to its default condition.

For SHELL57, the only DOF is the Temperature hence no specific restriction of DOF was required. In case of sliding analysis for element CONTA173, the KEYOPT was set to 0 to limit the DOF to UX, UY, UZ only.

Command:

```
ET,1,SOLID5,8  ! Degrees of Freedom limited to temperature only.
ET,2,SHELL57   ! shell element with no specific KEYOPTs.
```

3.5 Material Setup

The properties were defined for all three orthogonal directions, i.e. X, Y and Z directions. The material properties used are show in Table 3.10.

Table 3.10: Material Properties

Material property	Value
Elastic Modulus	25 GPa
Poisson ratio	0.18
Density	2400 kg/m^3
Coefficient of Thermal Expansion	1.0 x 10^{-5} /K
Specific Heat Capacity	800 J/kg/K

Command:

MP,EX,1, 25000000000

MP,EY,1, 25000000000

MP, EZ,1,25000000000

MP,NUXY,1, 0.18

MP,NUYZ,1,0.18

MP,NUXZ,1,0.18

MP,ALPX,1, 1.0e-5

MP,ALPY,1, 1.0e-5

MP,ALPZ,1,1.0e-5

MP,DENS,1,2400

MP,KXX,1,1.6

MP,KYY,1,1.6

MP,KZZ,1,1.6

MP,C,1,800

3.6 Real Constants

The real constants are required to define the SHELL57 elements. This command sets the surface element thickness and links the material property to the surface element.

Command:

R,1,.0001,.0001,.0001,.0001,0

The above command defines a real constant of 0.1mm thick surface element. The real constant is not applicable for SOLID5 element

3.7 Surface overlaying

Surface overlaying involves adding SHELL57 elements on to the external faces of the member (modeled with SOLID5 Elements) where convection is required. The surface overlaying was done by selecting the Nodes of surfaces where convection was required and then SHELL57 surface elements were created on the selected nodes using the ESURF command.

UNIVERSITY OF MORATUWA LIBRARY

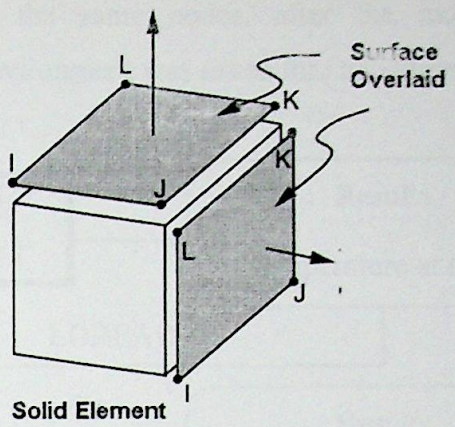

Figure 3.5: Solid element overlaid with Surface element (conceptual)

The command listing is as follows:

Command:

NSEL, S,LOC, Y, 0.2, 0.21 ! Select the nodes based on location

ESURF,0 ! Create surface on nodes

3.8 Numbering Controls

Because, the model was created with separate volume blocks, after it was meshed into elements, it results in coinciding but unconnected nodes. In order for the adjacent elements belonging to two different volumes to be connected, the nodes had to be merged into a common node. The command NUMMRG was used to merge the nodes that were at the same location and also to remove the extra nodes.

Command:

NUMMRG,ALL

3.9 Physical Environments

Physical environment in ANSYS provides a facility to save the model environment so that it can be retrieved later. This feature helped to use the same physical model but change or redefine elements, apply loads and change the type of analysis etc.

Initially the SOLID5 element was restricted to only thermal behaviour by limiting the degrees of freedom to thermal only. However, since both the thermal and

structural analysis share the same nodes, after the modelling, meshing and overlaying, the physical environment was saved into an external file.

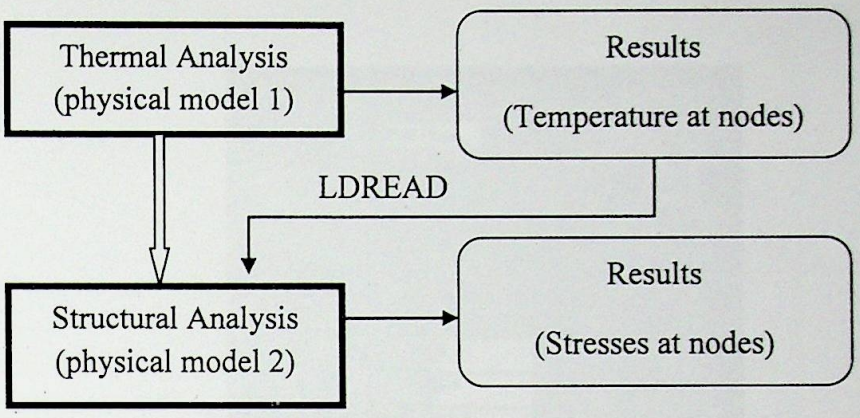

Figure 3.6: Flow Chart - Thermal and Structural Analysis

Next the model was preceded into the thermal analysis. Then based on the selected time where the temperature value was of interest, the temperature values were loaded to the physical mode using the LDREAD command.

3.10 Use of Arrays to Store Data

The varying heat flux values were stored with respect to the time value in a two dimensional array. Time step was taken as 1800s interval. The *DIM command was used to define the array.

Command:

*DIM, HFH, TABLE , 25

HFH(1,0)=0,1800,3600,5400,7200,9000,10800,12600,14400,16200

HFH(11,0)=18000,19800,21600,23400,25200,27000,28800,30600,32400,34200,360

00,37800,39600,41400,43200

HFH(1,1)=0,6.8,26.8,58.6,100,148.2,200,251.8,300,341.4

HFH(11,1)=373.2,393.2,400,393.2,373.2,341.4,300,251.8,200,148.2,100,58.6,26.8,6

.8,0

Since the array does not take more than 10 entries for the initial entry, the values were set at 2 stages. The array entry can be verified under:

Parameters> array Parameters> Define /Edit. (See Figure 3.7)

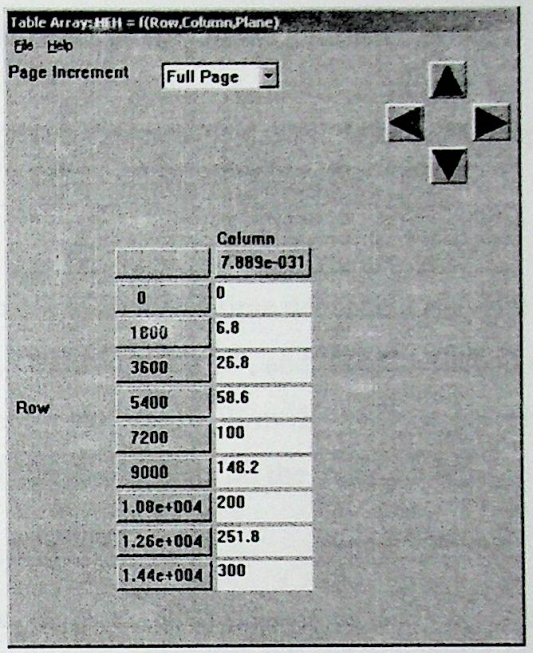

Figure 3.7: Heat Flux stored in an Array

3.11 Load Assignment

3.11.1 Solar Radiation as Heat Flux

The solar radiation was applied as heat flux to the surface of the SOLID5 elements. A positive value was applied to indicate that heat flows into the element. Since the solar radiation variation was stored in an array, the heat flux was assigned with the name of the array enclosed with "%" symbols.

Command:

SFA,10,1,HFLUX,%HFH%

The above command applies the heat flux as a surface load on area number 10. HFH is the name of the array containing the heat flux variation.

3.11.2 Heat Convection

The convection load was applied to the SHELL57 elements. The convection load requires two parameters; the ambient temperature and the convection coefficient. The two input parameters cannot be applied within the same command and therefore the parameters were defined using two command inputs.

Command:

SFE,SURF_OUTER,1,CONV,2,%AM%,%AM%,%AM%,%AM%

SFE,SURF_OUTER,1,CONV,1,10,10,10,10

The first command line applies a time dependent ambient temperature variation that is stored in an array defined as "AM", and then the second command line defines the convection heat coefficient, of 10 $W/m^2/K$. "SURF_OUTER" is the component named given to the SHELL57 elements on the outer surface.

3.12 Temperature Offset

Since the temperature units in ANSYS are in Kelvin, temperature offset from absolute zero to zero Celsius was set using the TOFFSET command considering values of 273 as the offset value.

Command

TOFFST,273 ! temperature offset from absolute zero to zero Celsius

3.13 Boundary Conditions

Boundary conditions are needed to constrain the model to get a unique solution. For the case of thermal analysis model, the boundary condition was set by defining an initial temperature to all elements in the model using the TUNIF command.

Command:

TUNIF, 23.6 ! to set the initial temperature of all elements to 23.6^0C.

For the Structural analysis case, the boundary conditions were applied to the edge faces of the model by setting the displacement DX, DY and DZ to 0.

Command:

DA, 39, UX,0

The above command applies '0' displacement in Global X direction on area number 39 which is the column base area number.

3.14 Analysis Setup

Transient analysis type was used for thermal analysis and static analysis was used for structural stress calculation.

Command

```
ANTYPE,4        !To perform a transient analysis
ANTYPE,0        !To perform a static structural analysis
```

3.15 Solution Controls

In general, the values were set to ANSYS defaults except for the following settings.

3.15.1 Time Control

Automatic time stepping was turned on to ensure that the appropriate heat flux values were taken at the relevant time step during the transient analysis.

Command:

```
AUTOTS,ON
```

Next, the time step incremental settings were defined. For the sake of solution efficiency, ANSYS recommends specifying values for all fields of the time step command.

Command:

```
DELTIM, 1, 1,1800, ON
```

3.15.2 Time at End of Time Step

The end time was set to the number of seconds to perform the transient analysis. In general this was set to 43200s, to run the transient analysis for 12hours. In some cases this was extended as well.

Command

```
FTIME,42300
```

The output results were requested for nodal solution of all load steps so that time distributed temperature variation results were available for post processing.

Command:

OUTRES,NSOL,ALL

Time graphical user interface input for time control and result request are as shown in Figure 3.8.

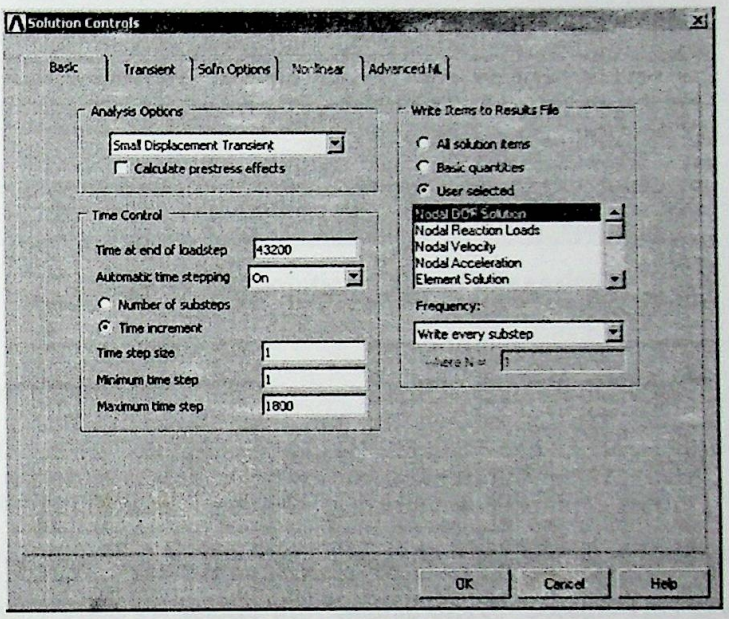

Figure 3.8: Solution Control – Basic

However, when contact elements were used, the analysis option was set to large displacement Transient.

Command:

NLGEOM, ON

3.15.3 Transient Solution Controls

Transient effects were enabled with stepped loading. This means that the heat flux remained constant for the time period considered. Heat flux values were entered in 1800 second intervals. This setting helped to converge the solution effectively. See Figure 3.9.

Command

KBC, 1 ! Stepped loading on

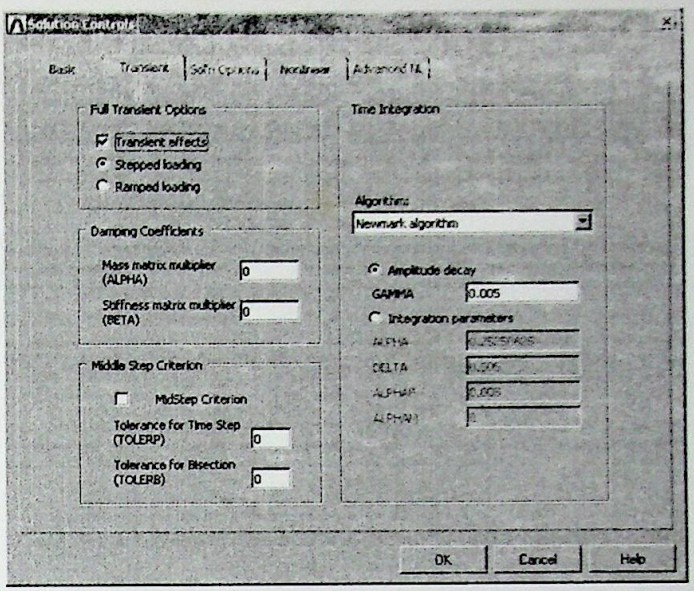

Figure 3.9: Solution Control - Transient

3.15.4 Solution Options

Equation Solvers were not specifically specified so that ANSYS selects the suitable solver based on the physics of the problem. During solution phase, ANSYS indicates the solver used; it was observed that for both the transient thermal analysis and structural analysis, ANSYS selects the "Sparse direct" solver. This is also the default solver used by ANSYS for linear and nonlinear, static and full transient analyses.

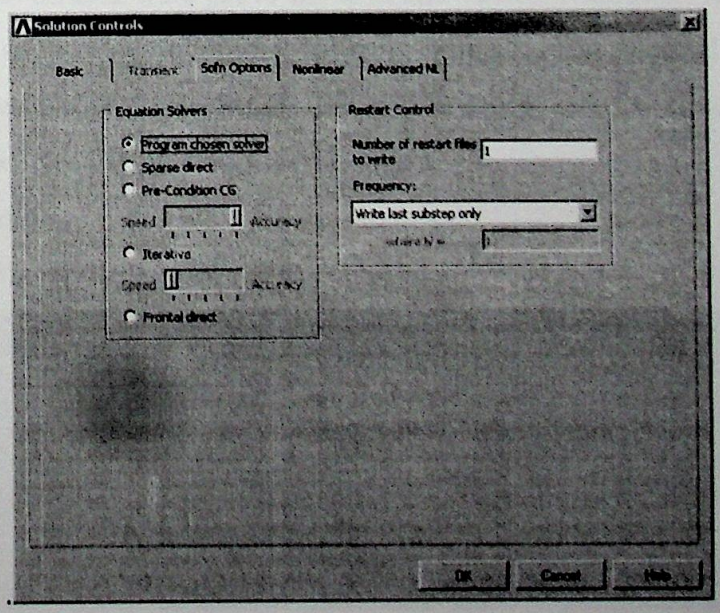

Figure 3.10: Solution Control – Solution Options

3.15.5 Nonlinear Options

The nonlinear options (Figure 3.11) were set to defaults so that ANSYS choses the best value based on the model complexity. As specified by ANSYS, automatic solution control will toggle line search on and off as needed. When contact elements are present in the model, Linear Search is enabled.

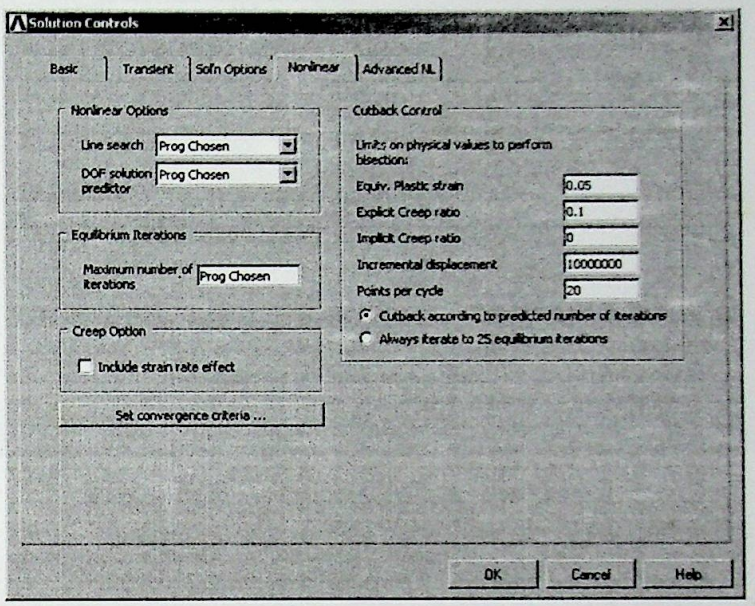

Figure 3.11: Solution Control – Nonlinear

3.15.6 Convergence Criteria

The convergence criteria were set to 0.1% of the values. Minimum reference value was set to -1 so that no minimum value is imposed. For thermal analysis, the "temperature" was used to determine the convergence and for structural analysis "force" was used. See Figure 3.12 for GUI input.

Command:

CNVTOL, TEMP,, 0.001, 2,-1

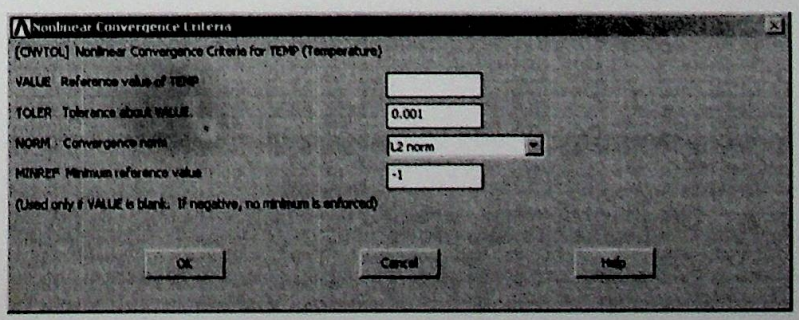

Figure 3.12: Solution Control – Convergence Criteria

UNIVERSITY OF MORATUWA LIBRARY

3.15.7 Advanced NL

The advance nonlinear options were set to ANSYS defaults. See Figure 3.13

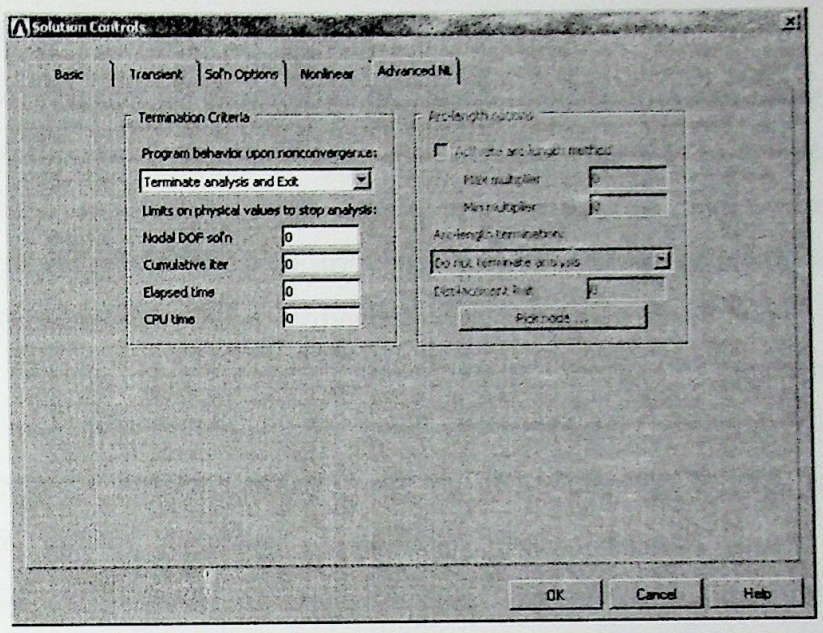

Figure 3.13: Solution Control – Advanced NL

3.16 Reference Temperature

The thermal stresses are dependent on the reference temperature. Hence it is important to define this value for the stress response. It is the temperature of a structural element at the relevant stage of its restraint (completion). To define this temperature value, TREF command was used.

Command:

```
TREF, 25    ! reference temperature for the thermal strain calculations.
```

4 Chapter 4 – Model Verification

4.1 Introduction

This chapter presents the verification of the finite element model using numerical methods. Verification was required since a modeling approach to analyze heat flux and convection simultaneously was introduced in the ANSYS model. Also in case of structural response the stress distribution due to thermal behavior and sliding behavior was also needed to be verified.

The calculations were based on standard formula for heat transfer and structural stress analysis. Initially the model was verified for temperature distribution and the next stage structural stresses were verified. Numerical solution and ANSYS results for various parametric conditions were compared. Based on these comparisons the FE model was adjusted to give reasonable accurate results within appreciable computational time.

4.2 Model Verification Methodology

For verification purpose a concrete slab was considered. Initially the model was verified only for conduction with constant heat flux. After calibrating the suitable element size, next the model was verified for both conduction and convection under a constant heat flux.

Next, the model was analyzed and peak temperature values within the time frame considered were extracted. Since the structural response can be considered not to influence the temperature values, the structural response was verified for the peak temperature situation only. The structural analysis was performed for a simply support boundary condition; the slab was considered to be supported on two opposite edges (one way spanning).

4.3 Heat Transfer by Conduction

4.3.1 Numerical Idealization

The transient thermal model was idealized to a semi-infinite solid model. To ensure this condition, the specimen slab was sized to 1mx1mx0.4m. The 0.4 m thickness was selected so that during the time considered the temperature on the bottom of the

slab remained unchanged, i.e. the heat does not penetrate the slab depth. Then considering the slab is a semi-infinite mode, the formula [9] given in Eq. 4.1 was used.

$$(T_{x,t} - T_i) = \frac{2q\left(\frac{\alpha t}{\pi}\right)^{\frac{1}{2}}}{k} \exp\left(\frac{-x^2}{4\alpha t}\right) - \frac{qx}{k}\left(1 - \text{erf}\left(\frac{x}{2\sqrt{\alpha t}}\right)\right) \quad \text{---} \quad \text{Eq. 4.1}$$

where

q= heat flux

α = thermal diffusivity, k/pc

k = coefficient thermal conduction

c = specific heat capacity

p =density

t = time

Model verification was performed considering the material and thermal parameters as given in Table 4.1.

Table 4.1: Input Parameters

Parameters	Value	Unit
Heat flux (constant), q	100	W/m^2
Initial temperature, T_i	25	^0C
Conduction coefficient, k	1.6	W/m
Specific heat capacity, C	800	J/kg/K
Density, p	2400	kg/m^3
Elastic modulus, E	25	GPa
Thermal diffusivity, k/pc	8.333×10^{-7}	m^2/s

4.3.2 Numerical Solution

Specimen calculation at time, t=900s, at depth 0.05m is given below.

$$(T_{x,t} - T_i) = \frac{2q\left(\frac{\alpha t}{\pi}\right)^{\frac{1}{2}}}{k} \exp\left(\frac{-x^2}{4\alpha t}\right) - \frac{qx}{k}\left(1 - \text{erf}\left(\frac{x}{2\sqrt{\alpha t}}\right)\right)$$

$$(T_{0.05,900} - 25) = \frac{2x100x(\frac{8.33x10^{-7}x900}{\pi})^{\frac{1}{2}}}{1.6} \exp\left(\frac{-0.05^2}{4x8.33x10^{-7}x900}\right)$$

$$-\frac{100x0.05}{1.6}\left(1 - \text{erf}\left(\frac{0.05}{2\sqrt{8.33x10^{-7}x900}}\right)\right)$$

$T_{0.05,900} = 25.225°C$

Similarly calculations were performed for time t, at depths of x. Results from numerical equations are given in Table 4.2.

Table 4.2: Numerical solution for heat transfer by conduction

Time (s)	Temperature at distance 'x' from surface, °C				
	x=0 m	x=0.05 m	x=0.1 m	x=0.15 m	x=0.2 m
900	26.932	25.225	25.008	25.000	25.000
1800	27.732	25.672	25.092	25.006	25.000
2700	28.346	26.109	25.251	25.037	25.003
3600	28.863	26.516	25.449	25.097	25.015
4500	29.319	26.894	25.666	25.183	25.039
5400	29.731	27.249	25.891	25.288	25.075
6300	30.110	27.582	26.117	25.408	25.124
7200	30.463	27.898	26.343	25.537	25.183
8100	30.795	28.198	26.567	25.674	25.252
9000	31.108	28.485	26.788	25.816	25.329
9900	31.406	28.760	27.005	25.962	25.413
10800	31.691	29.025	27.218	26.111	25.502
11700	31.964	29.281	27.427	26.261	25.596
12000	32.053	29.364	27.496	26.311	25.628
12600	32.227	29.528	27.633	26.411	25.694

4.3.3 ANSYS Solution

With the same parameters as used for the numerical calculation, the analysis was performed in ANSYS. The results are as given in Table 4.3.

Table 4.3: ANSYS solution for heat transfer by conduction

Time (s)	Temperature at distance 'x' from surface, °C		
	X=0 m	X=0.1 m	X=0.2 m
5	25.0232	25	25
14	25.0684	25	25
41	25.1947	25	25
122	25.5088	25	25
293.72	25.9745	25.0001	25
609.23	26.5155	25.0026	25
1380.2	27.3566	25.0425	25.0002
3154.8	28.6075	25.3264	25.0115
4954.8	29.5179	25.7623	25.0566
6754.8	30.2769	26.2177	25.15
8554.8	30.9406	26.6661	25.2863
10355	31.5374	27.1008	25.4527
11477	31.8833	27.3638	25.5677
12600	32.2128	27.6208	25.6892

4.3.4 Comparison Between Numerical and ANSYS Solution

Surface temperature at end of time 3600s and 12000s, was considered. The error percentage was calculated as the change in temperature with respect to a reference temperature. This is because the structural stresses are evaluated with respect to a reference temperature. For verification calculation purpose the reference temperature (T_{ref}) is taken as 25^0C.

Let T_{ANSYS} = Temperature from ANSYS,

And let $T_{Numerical}$ = Temperature from Numerical solution,

Then the temperature increase with respect to the reference temperature can be written as:

$$\Delta T_{ANSYS} = T_{ANSYS} - T_{ref}$$

$$\Delta T_{Numerical} = T_{Numerical} - T_{ref}$$

Hence:

$$\text{Error } \% = [(\Delta T_{ANSYS} - \Delta T_{Numerical}) / \Delta T_{Numerical}] \times 100\%$$

UNIVERSITY OF NAIROBI LIBRARY

Therefore the Error % can be written as in Eq. 4.2

Error %= $[(T_{ANSYS} - T_{Numerical})/ (T_{Numerical} - T_{ref})] \times 100\%$ ---- Eq. 4.2

Table 4.4: Comparison of temp. due to heat transfer by conduction at 3600s

Element Size	Time Step Setting in ANSYS	ANSYS	Numerical	Error %
0.040	DELTIM, 15, 15,1800,	28.738	28.863	3.236%
0.040	DELTIM, 15, 15,300,	28.723	28.863	3.624%
0.040	DELTIM, 60, 15,300,	28.710	28.863	3.961%
0.040	DELTIM, 1, 1,300,	28.727	28.863	3.521%
0.040	DELTIM, 1, 1,1800,	28.734	28.863	3.339%
0.040	DELTIM, 0.1, 0.1,1800,	28.752	28.863	2.873%
0.200	DELTIM, 1, 1,1800,	26.745	28.863	54.828%
0.100	DELTIM, 1, 1,1800,	27.902	28.863	24.877%
0.050	DELTIM, 1, 1,1800,	28.655	28.863	5.384%
0.040	DELTIM, 1, 1,1800,	28.734	28.863	3.339%
0.030	DELTIM, 1, 1,1800,	28.802	28.863	1.579%
0.020	DELTIM, 1, 1,1800,	28.849	28.863	0.362%

Table 4.5: Comparison of temp. due to heat transfer by conduction at 12000s

Element size	Time Step Setting in ANSYS	ANSYS	Numerical	Error %
0.020	DELTIM, 60, 60,600,	32.026	32.053	0.383%
0.020	DELTIM, 1, 1,900,	32.036	32.053	0.241%
0.020	DELTIM, 1, 1,1800,	32.039	32.053	0.198%
0.025	DELTIM, 60, 60,600,	32.016	32.053	0.525%
0.040	DELTIM, 60, 60,600,	31.972	32.053	1.148%
0.100	DELTIM, 1, 1,1800,	31.549	32.053	7.146%
0.040	DELTIM, 15, 15,1800,	31.982	32.053	1.007%
0.040	DELTIM, 60, 60,1800,	31.976	32.053	1.092%
0.040	DELTIM, 120, 120,1800,	31.967	32.053	1.219%
0.040	DELTIM, 300, 300,1800,	31.94	32.053	1.602%

0.040	DELTIM, 1, 1,1800,	31.985	32.053	0.964%
0.040	DELTIM, 0.1, 0.1,1800,	31.985	32.053	0.964%
0.040	DELTIM, 0.1, 0.1,900,	31.982	32.053	1.007%

From Table 4.5 and Table 4.4 it is observed that the element size 0.1m has an error of about 25% at the end of 3600s but reduces to about 7% and the end of 12000s. However, element size of 0.02m gives minimum error on conduction. At end of 3600s the error is 0.36% and reduces to 0.2% at end of 12000s. The DELTIM parameter of ANSYS indicates that the error reduces when the DELTIM is set to higher values of about of 1800s.

4.4 Heat Transfer by Convection and Conduction

4.4.1 Numerical Solution

The numerical solution with convection and conduction was solved using equation Eq. 4.1. The heat dissipated due to convection (q_c) was calculated at every step based on the surface temperature(T_s) and ambient temperature (T_{amb}) with a constant convection coefficient (h_c) of 10 W/m^2/°C. This heat energy was reduced from the applied heat flux and used for the next step. Specimen calculation is given below:

From Eq. 4.1:

$$(T_{x,t} - T_i) = \frac{2q\left(\frac{\alpha t}{\pi}\right)^{\frac{1}{2}}}{k}\exp\left(\frac{-x^2}{4\alpha t}\right) - \frac{qx}{k}\left(1 - \text{erf}\left(\frac{x}{2\sqrt{\alpha t}}\right)\right)$$

For temperature at surface, x=0, then

$$\exp\left(\frac{-x^2}{4\alpha t}\right) = 1$$

$$\frac{qx}{k}\left(1 - \text{erf}\left(\frac{x}{2\sqrt{\alpha t}}\right)\right) = 0$$

Hence equation reduces to:

$$(T_{x,t} - T_i) = \frac{2q\left(\frac{\alpha t}{\pi}\right)^{\frac{1}{2}}}{k}$$

Surface Temperature at the end of 30s,

$$(T_{0.0,30} - 25) = \frac{2x100x\left(\frac{8.33x10^{-7}x30}{\pi}\right)^{\frac{1}{2}}}{1.6}$$

$$T_{0.0,30} = 25.353°C$$

Average heat loss due to convection from 0 to 30s = $[0+h_c(T_s-T_{amb})]/2$

$= 10x(25.353-25)/2 = 1.763\ W/m^2$

Therefore, effective heat flux for the next time step = 100-1.763 =98.237 W/m^2.

Surface Temperature at the end of 60s,

$$(T_{0.0,60} - 25) = \frac{2x98.237x\left(\frac{8.33x10^{-7}x60}{\pi}\right)^{\frac{1}{2}}}{1.6}$$

$$T_{0.0,60} = 25.49°C$$

Average heat loss due to convection from 30s to 60s = $1.763 + h_c(T_s-T_{amb})/2$

$=1.763 + 10x(25.49-25)/2 = 4.213\ W/m^2$

Therefore effective heat flux for the next time step = 100-4.213 =95.787 W/m^2.

Similarly numerical results with time step of 30s up to 1800s are shown in Table 4.6; surface temperature and the convection heat energy as q_c. Extended calculation with time step 120s until 10800s duration is shown in appendix A.2.

It should be noted that due to the fact that the diffusivity of concrete is relatively low, sufficient time was provided for heat to conduct into the middle elements of the ANSYS model, so that heat will not concentrate at the surface only. Also to ensure that heat does not penetrate the opposite face of the model (this is a limitation of the numerical method) the heat flux was also kept at a low value. Hence the time duration was extended to 10800s (3 hours) with a constant heat flux of 100 W/m^2. However this results in a low surface temperature rage for comparison.

Table 4.6: Numerical solution for convection and conduction

Time (s)	Surface Temp. °C	q_c W/m2	540	26.308	12.917	1200	26.829	18.193
			570	26.338	13.231	1230	26.847	18.379
			600	26.368	13.534	1260	26.865	18.562
			630	26.397	13.828	1290	26.883	18.742
0	25	0	660	26.425	14.112	1320	26.901	18.919
30	25.353	1.763	690	26.452	14.388	1350	26.918	19.093
60	25.49	4.213	720	26.479	14.657	1380	26.935	19.264
90	25.585	5.375	750	26.505	14.918	1410	26.952	19.433
120	25.667	6.262	780	26.53	15.172	1440	26.968	19.6
150	25.739	7.032	810	26.554	15.42	1470	26.985	19.764
180	25.803	7.711	840	26.578	15.662	1500	27.001	19.926
210	25.861	8.32	870	26.601	15.898	1530	27.016	20.085
240	25.914	8.877	900	26.624	16.129	1560	27.032	20.242
270	25.964	9.392	930	26.647	16.355	1590	27.047	20.398
300	26.01	9.872	960	26.668	16.576	1620	27.063	20.551
330	26.054	10.322	990	26.69	16.792	1650	27.078	20.702
360	26.095	10.747	1020	26.711	17.004	1680	27.092	20.851
390	26.135	11.151	1050	26.731	17.211	1710	27.107	20.998
420	26.172	11.535	1080	26.752	17.415	1740	27.122	21.143
450	26.208	11.902	1110	26.771	17.615	1770	27.136	21.287
480	26.243	12.254	1140	26.791	17.811	1800	27.15	21.429
510	26.276	12.592	1170	26.81	18.003			

4.4.2 ANSYS Solution for Heat Transfer by Convection and Conduction

Analysis with 0.02m element size with SOLID5 and SHELL57 elements were overlaid. The thickness of the overlay surface was set to 0.00001m. Convergence tolerance was set to 0.1%. Table 4.7 shows the results from ANSYS.

Table 4.7 ANSYS solution due to Convection and Conduction

Time (s)	Surface Temp. (^{0}C)
41	25.1928
122	25.4948
269.5	25.8685
521.2	26.2625
1055	26.7702
2108	27.3825
3908	28.0346
5708	28.4764
7508	28.8179
9308	29.0957
10800	29.2926

4.4.3 Comparison with FE model

Table 4.8 shows the surface temperature comparison between the ANSYS and Numerical solutions together with the deviation error based on Eq. 4.2. The error is high at the start but gradually reduces to about 2.5% at end of 3600s and again increases. The deviation is due to the invalidity of the numerical formula since the heat conducted tends to penetrate to the opposite surface on the ANSYS model and whereas the numerical solution assumes an infinite depth.

However, it can be considered that the ANSYS model is valid for conduction and convection at constant heat flux.

Table 4.8 Comparison of Results on Convection and Conduction

Time, s	ANSYS, °C	Numerical, °C	Error %
270	25.869	25.986	-11.917
522	26.263	26.338	-5.643
1055	26.770	26.820	-2.736
2108	27.383	27.435	-2.156

3908	28.035	28.122	-2.799
5708	28.476	28.597	-3.353
7508	28.818	28.965	-3.710
9308	29.096	29.266	-3.992
10800	29.293	29.483	-4.247

The comparison is graphically shown in Figure 4.1.

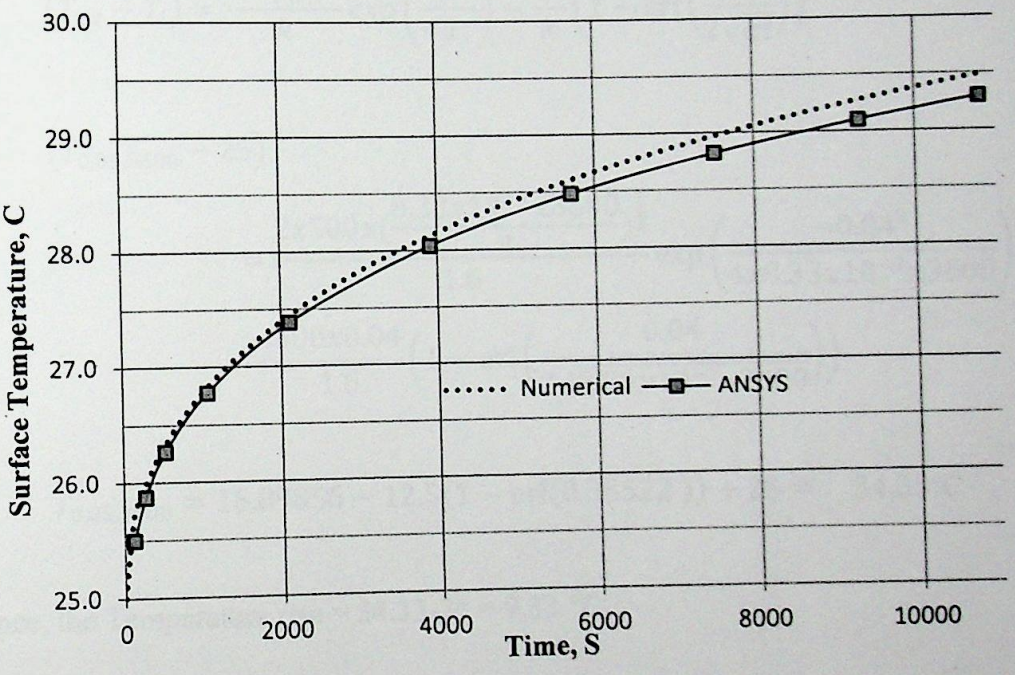

Figure 4.1: Comparison of surface temperature – Convection and Conduction

4.5 Thermal Stresses

For a constant heat flux of 500 W/m^2 temperature profile was evaluated for conduction only. The structural stresses were calculated considering freely supported boundary conditions. These conditions were considered since simplified numerical solutions were not available to validate other boundary conditions.

The dimension of the slab considered was 3m x 1m in plan and 0.28m in thickness. The time frame was limited to 3600s to be consistent with the formula of

the semi-infinite model used to calculate the temperature profile. The stresses were calculated at the end of 3600s with reference to 25°C temperature.

4.5.1 Specimen calculation for stress calculation

In order to calculate the stresses, the temperature profile across the depth of the slab was calculated using equation Eq. 2.22.

Specimen calculation of temperature at time, t=3600s, at depth 0.04m is given below.

$$(T_{x,t} - T_i) = \frac{2q\left(\frac{\alpha t}{\pi}\right)^{\frac{1}{2}}}{k}\exp\left(\frac{-x^2}{4\alpha t}\right) - \frac{qx}{k}\left(1 - \text{erf}\left(\frac{x}{2\sqrt{\alpha t}}\right)\right)$$

$$(T_{0.05,3600} - 25)$$

$$= \frac{2x500x\left(\frac{8.33x10^{-7}x3600}{\pi}\right)^{\frac{1}{2}}}{1.6}\exp\left(\frac{-0.04^2}{4x8.33x10^{-7}x3600}\right)$$

$$- \frac{500x0.04}{1.6}\left(1 - \text{erf}\left(\frac{0.04}{2\sqrt{8.33x10^{-7}x3600}}\right)\right)$$

$$T_{0.05,3600} = 16.89856 - 12.5(1 - \text{erf}(0.36522)) + 25 = \quad 34.33°C$$

Hence, the Temperature rise = 34.33-25 = 9.33 °C

Similarly calculations were performed at 0.01m intervals. Temperature values at 0.04 depths are shown in Table 4.9.

Table 4.9 Temperature along slab depth

Depth from surface (m)	0	0.04	0.08	0.120	0.160	0.20	0.24	0.28
Temperature (°C)	44.32	34.34	28.79	26.27	25.34	25.08	25.01	25.00
Temperature rise (°C)	19.32	9.33	3.79	1.27	0.34	0.08	0.01	0.00

Next the stresses were calculated as described in section 2.7 of this report. Hence equations from Eq. 2.13 to Eq. 2.25 are used.

The specimen calculation for thermal stress at a location 0.04m below the slab top is given below:

Cross sectional area, $A = 1 \times 0.28 = 0.28\ m^2$

First moment or area about a horizontal axis through the top face= B

$= 1 \times 0.28 \times 0.28/2 = 0.0392\ m^3$

First moment of area about a horizontal axis through top face, I

$= 1/12 \times 1 \times 0.28^3 + 1 \times 0.28 \times (0.28/2)^2$

$= 7.3173 \times 10^{-3}$

Modulus of elasticity, $E = 25 \times 10^6\ kN/m^2$

y = coordinate of any fibre, from top face. The reference point is taken as the top of the slab surface.

Consider a depth 0.04 from surface, depth increment is taken as 0.01m.

For a Temperature rise of 9.33 °C the hypothetical strain (ε_t) that would occur at any fiber if it was free, $\varepsilon_f = \alpha_t . T$

$= 1 \times 10^{-5} \times 9.33$

$= 9.33 \times 10^{-5}$

If it is restrained, then,

$$\sigma_{restrained} = -E . \varepsilon_f = -25 \times 10^9 \times 9.33 \times 10^{-5}$$

The resultant of the stress represented by axial force ΔN, at the reference point is given by:

$$\Delta N = \int \sigma_{restrained} . dA$$

The depth increase was taken as 0.01m. Hence $dA = 0.01 \times 1$

Hence,

$$\Delta N = \int \sigma_{restrained} . dA = \Sigma (\ldots + -25 \times 10^9 \times 9.33 \times 10^{-5} \times 0.01 \times 1 + \ldots)$$

$$= -235.062\ kN$$

The resultant of the stress represented by a bending moment ΔM, at the reference point is given by:

$$\Delta M = \int \sigma_{restrained} \cdot y \cdot dA$$

For element at depth 0.04m, y=0.04 m

$\Delta M = \int \sigma_{restrained} \cdot y \cdot dA = \Sigma$ (…+- $25x10^9$ x 9.33×10^{-5} x 0.04 0.01 x 1 + …)

= -9.677 kNm

Substituting the Moment and Axial forces

$$\begin{Bmatrix} \Delta\varepsilon_0 \\ \Delta\psi \end{Bmatrix} = \frac{1}{E(AI - B^2)} \begin{bmatrix} I & -B \\ -B & A \end{bmatrix} \begin{Bmatrix} -\Delta N \\ -\Delta M \end{Bmatrix}$$

$$\begin{Bmatrix} \Delta\varepsilon_0 \\ \Delta\psi \end{Bmatrix} = \frac{1}{12805.33} \begin{bmatrix} 7.3173 \times 10^{-3} & -0.0392 \\ -0.0392 & 0.28 \end{bmatrix} \begin{Bmatrix} -(-235.062) \\ -(-9.677) \end{Bmatrix}$$

Hence;

$$\begin{Bmatrix} \Delta\varepsilon_0 \\ \Delta\psi \end{Bmatrix} = \begin{Bmatrix} 1.047x10^{-4} \\ -5.08x10^{-4} \end{Bmatrix}$$

The actual stress due to temperature at depth y is given by

$$\Delta\sigma = E[\Delta\varepsilon_0 + (\Delta\psi)y]$$

$$\Delta\sigma = 25x10^6[1.047x10^{-4} + (-5.08x10^{-4})yx0.04] = 2092\ kN/m^2$$

$$\sigma = E[-\varepsilon_0 + \Delta\varepsilon_0 + (\Delta\psi)y]$$

$$\sigma = E[-9.33 \times 10^{-5} + 1.047x10^{-4} + (-5.08x10^{-4})yx0.04]$$

= -240.5 kN/m^2 = 0.24 N/mm^2

The stresses along the depth of the sab is given in Table 4.10. More details are given in Appendix A.4.

Table 4.10 Thermal stresses using analytical methods

Depth from surface (m)	0	0.04	0.08	0.120	0.160	0.20	0.24	0.28
Temperature rise (°C)	-2.27	-0.22	0.65	0.78	0.50	0.06	-0.43	-0.94

Table 4.11 Thermal Stresses from ANSYS solution

Depth, m	Temperature °C	Stress N/mm^2
0.000	44.243	-2.680
0.020	38.627	-1.272
0.040	34.237	-0.240
0.060	30.973	0.446
0.080	28.676	0.837
0.100	27.155	0.991
0.120	26.21	0.969
0.140	25.656	0.830

Depth, m	Temperature °C	Stress N/mm^2
0.160	25.346	0.616
0.180	25.178	0.360
0.200	25.091	0.080
0.220	25.046	-0.213
0.240	25.024	-0.514
0.260	25.014	-0.820
0.280	25.011	-1.130

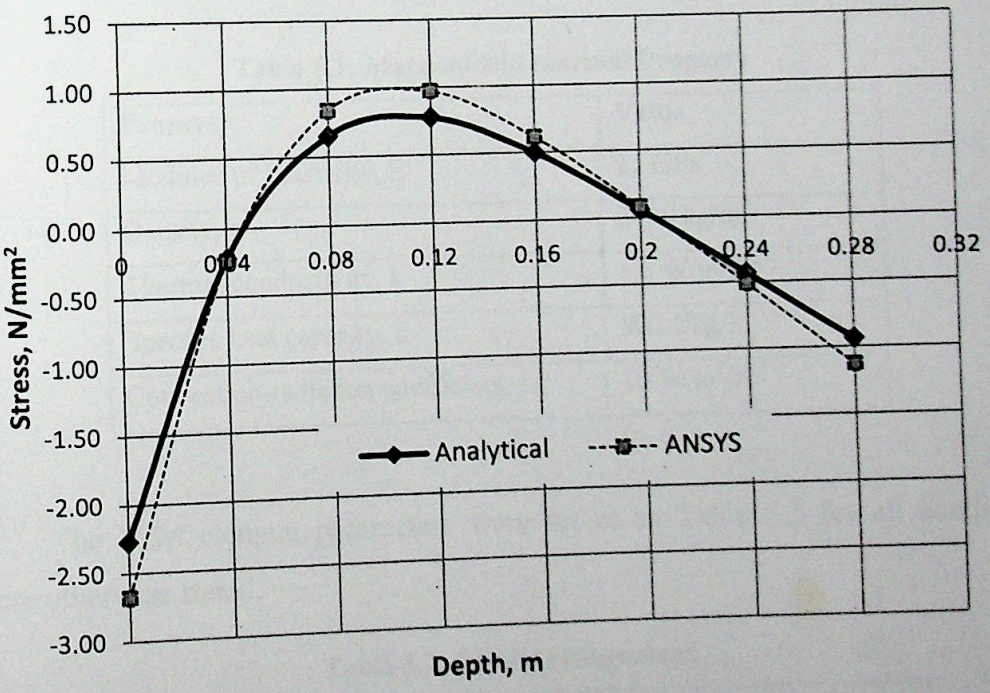

Figure 4.1: Comparison Stress –Analytical methods and ANSYS FEA solution

It can be concluded that the solutions given by analytical methods and ANSYS are comparable.

5 Chapter 5 – Sensitivity Analysis

In order to determine the sensitivity towards the temperature and resulting stresses, concrete thermal properties and thermal and structural boundary conditions were considered. Since the thermal stresses are primarily dependent on the thermal gradient and the peak temperature [3], [7], the temperature results were gathered for the surface temperature and the maximum temperature difference between the top and bottom surfaces.

5.1 Default Parameters

The sensitivity analysis was performed by establishing a set of parameters (default parameters) as given in Table 5.1 and then each parameter was varied to determine its sensitivity while the rest were kept to the default values.

Table 5.1: Material and thermal Property

Property	Value
Modulus of Elasticity, E	25 GPa
Density, ρ	2400 kg/m^3
Thermal conductivity, k	1.6 W/m/K
Specific heat capacity, c	800 J/kg/K
Convection-radiation coefficient, h_{cr}	10 W/m^2/K

The FEM element parameters were set as in Table 5.2 for all conditions unless otherwise stated.

Table 5.2: FEM Arrangement

Property	Value
Specimen size	3000mm x 500mm x 200mm
Element size	20 mm
Overlaid surface thickness	0.01mm

The normalized heat flux was taken by considering 45% of the total solar radiation as used by Aruna et al. [19].

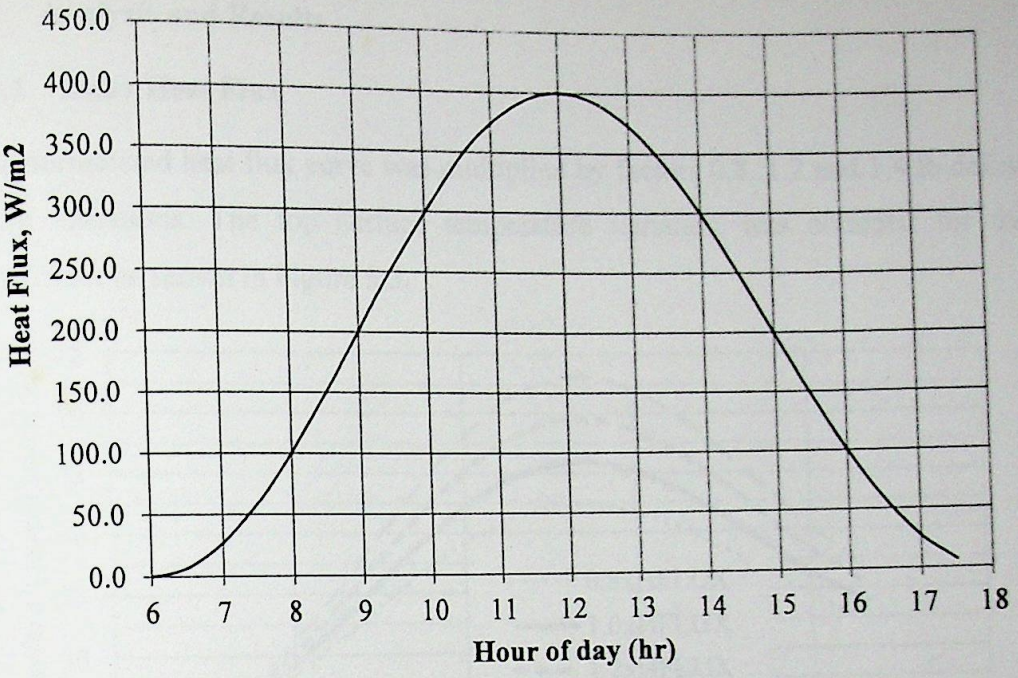

Figure 5.1: Normalized Heat Flux variation Indented on Horizontal Plane

(based on reading from Aruna et al [19])

For the purpose of the analysis, 6 am of the day was set to 0 hours.

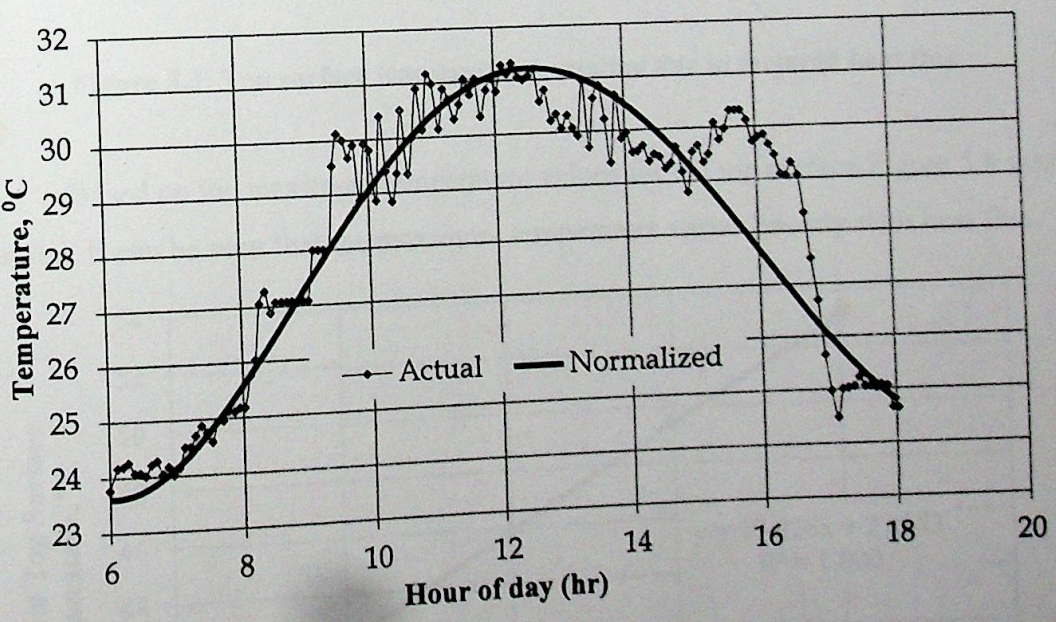

Figure 5.2: Normalized ambient temperature variation

(values were extracted from readings taken by Aruna et al on 3rd August 2010)

For the purpose of the analysis, 6 am of the day was set to 0 hours.

5.2 Analysis and Results

5.2.1 Solar Heat Flux

The normalized heat flux curve was multiplied by factors 0.8, 1.2 and 1.4 to define 3 more variations. The top surface temperature variation was obtained for these conditions as shown in Figure 5.3.

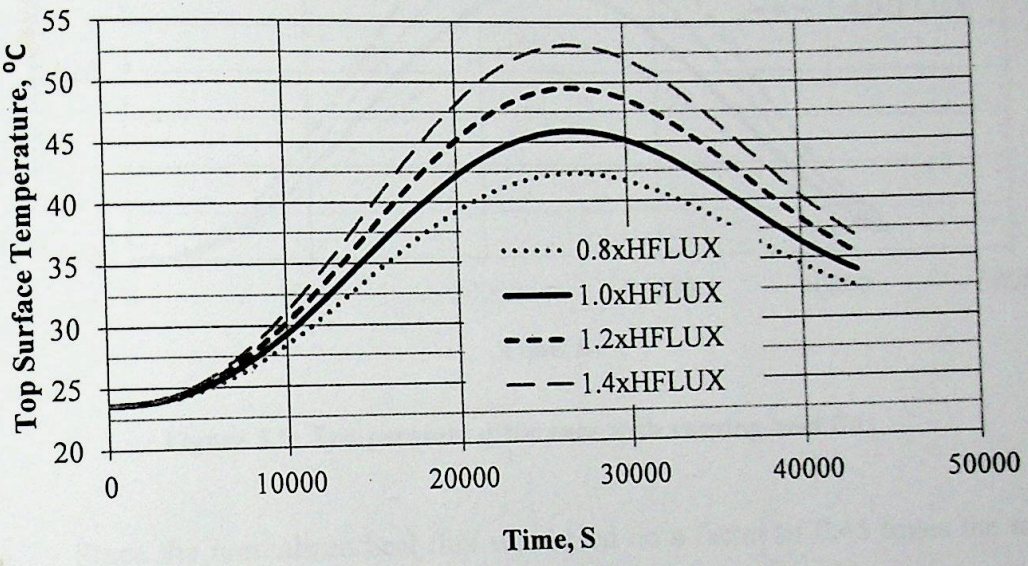

Figure 5.3: Top surface temperature variation due to factored heat flux

Based on the maximum temperature values for the top surface Figure 5.4 was derived. It can be seen that the maximum temperature varies linearly with heat flux.

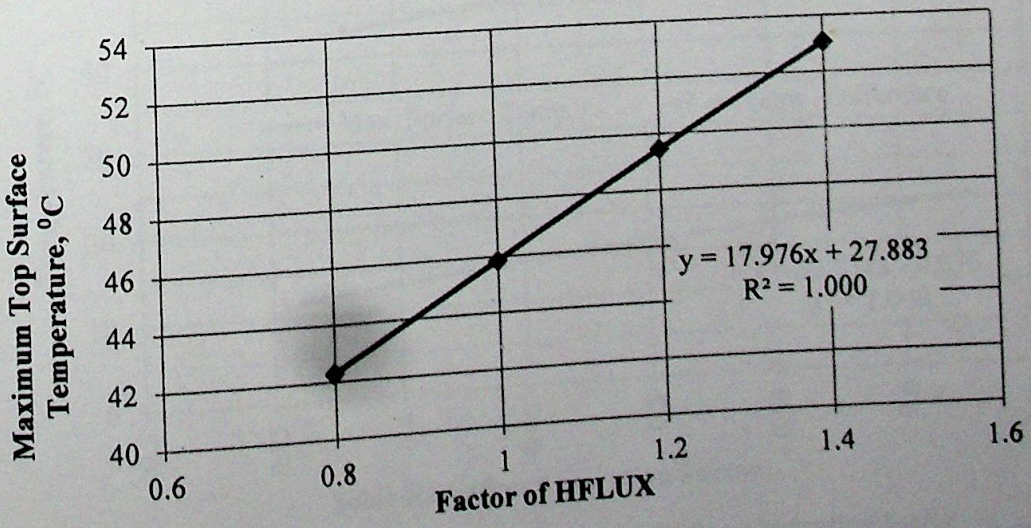

Figure 5.4: surface temperature variation vs. factored heat flux

The temperature difference between the top and bottom surfaces is as shown in Figure 5.5.

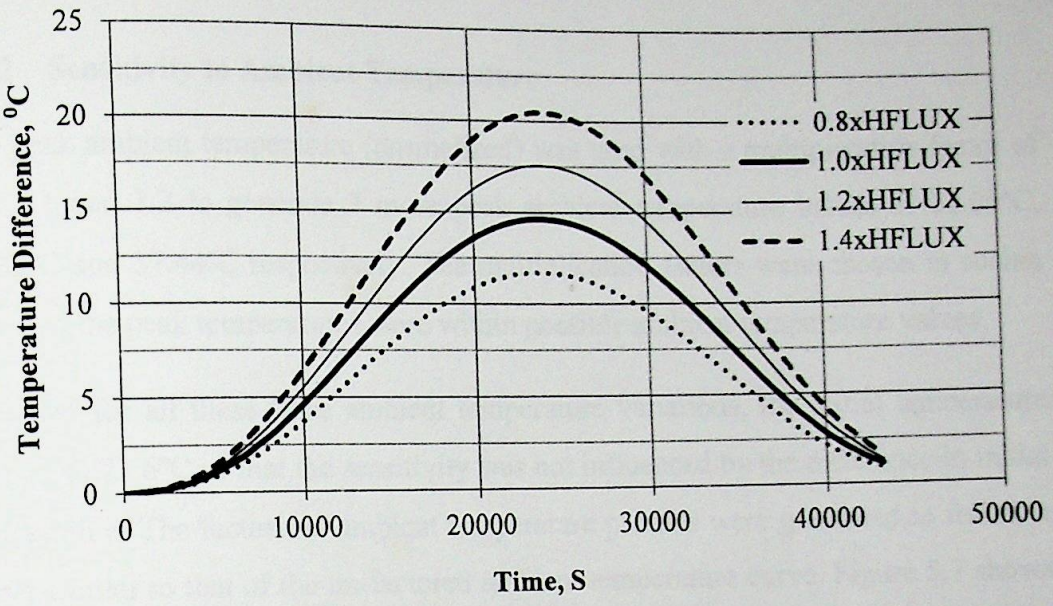

Figure 5.5: Temperature difference with varying heat flux

Since the normalized heat flux was based on a factor of 0.45 times the total solar radiation, this can be represented by the overall factor as "solar radiation absorption factor" as in Figure 5.6.

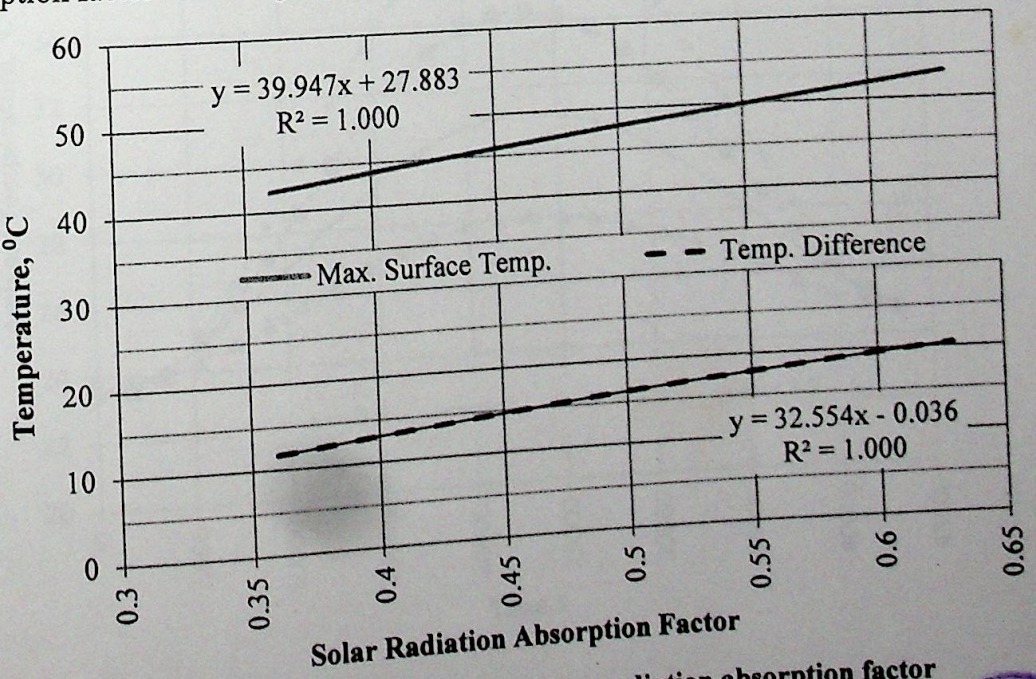

Figure 5.6: Surface temperature vs. solar radiation absorption factor

UNIVERSITY OF MORATUWA LIBRARY

It can be seen that the maximum top surface temperature varies lineally with the absorption factor for the range considered.

5.2.2 Sensitivity to Ambient Temperature

The peak ambient temperature (normalized) was used with a multiplication factor of 0.9, 1.1 and 1.2 to generate 3 more peak ambient temperature values of 28.08°C, 34.32°C and 37.44°C respectively. The multiplication factors were chosen in such a way that the peak temperatures were within possible ambient temperature values.

However for all these three ambient temperature variations, the initial temperature was set to 23.6°C so that the sensitivity was not influenced by the difference in initial temperature. The factorized ambient temperature profiles were generated to follow a curve similar to that of the un-factored ambient temperature curve. Figure 5.7 shows the temperature profiles used for the analysis.

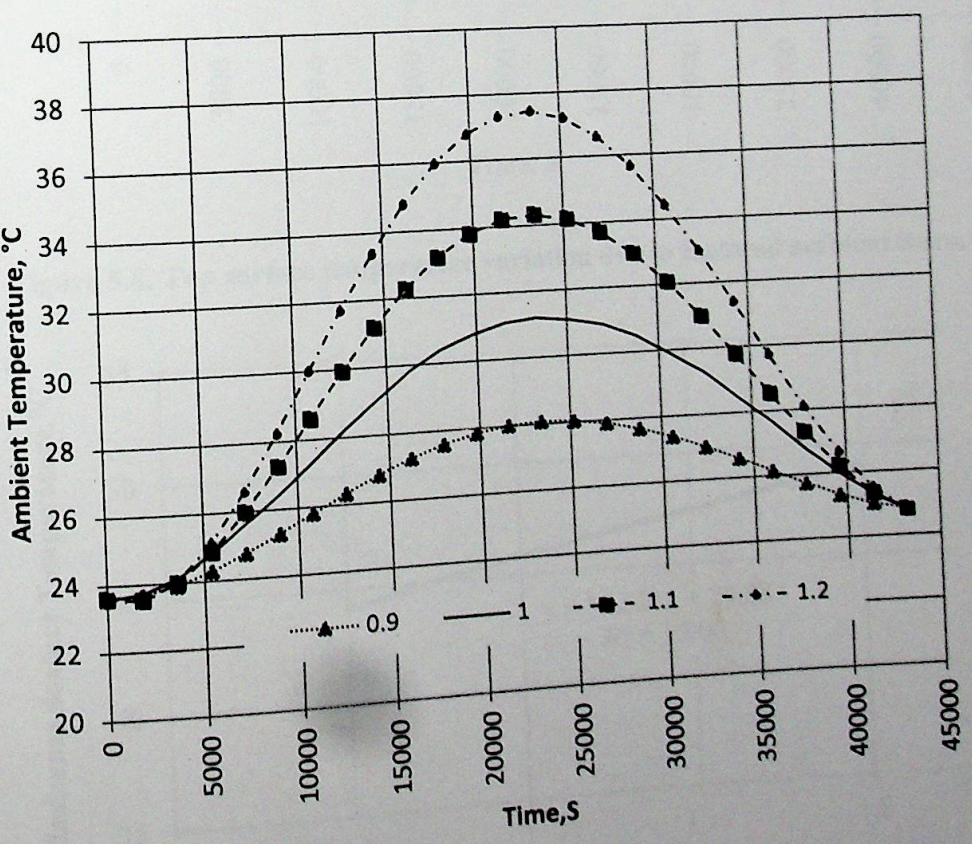

Figure 5.7: Derived factored ambient temperature variations

The resulted top surface temperature variation is shown in Figure 5.10. Together with Figure 5.9 it is seen that the top surface is sensitive to the ambient temperature, resulting in a temperature variation from 44.1°C to 49.3°C for an ambient temperature variation factor of 0.9 to 1.2.

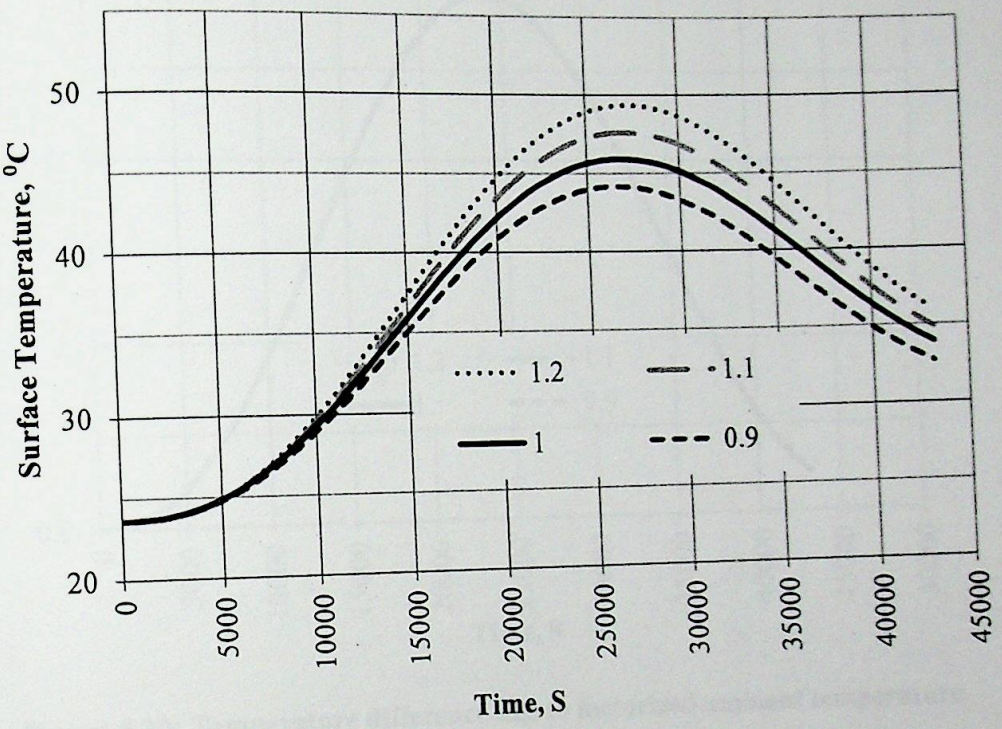

Figure 5.8: Top surface temperature variation due to factored ambient temp.

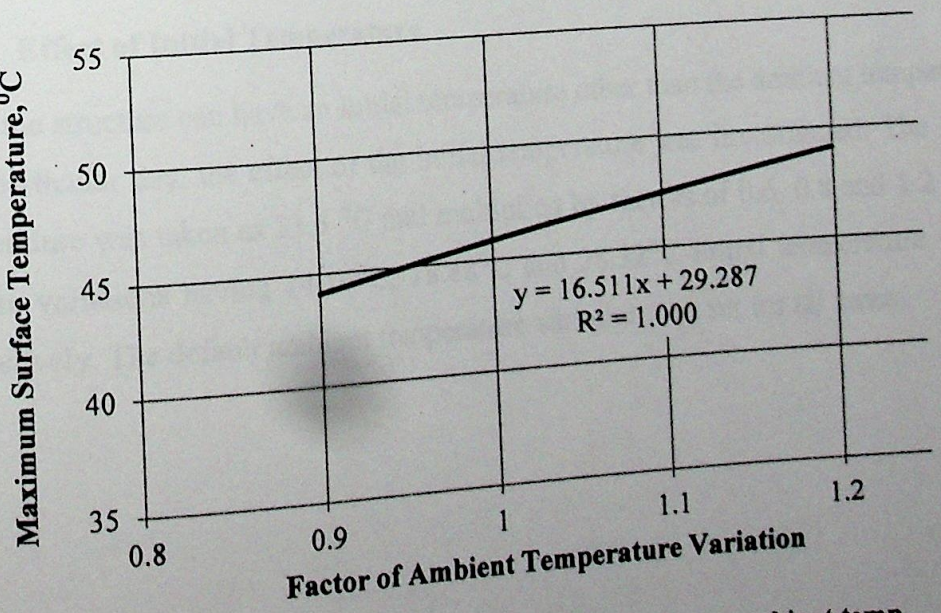

Figure 5.9: Surface temperature vs. factorized norm. ambient temp.

Figure 5.11 shows that the temperature difference between top and bottom surface is not dependant on the peak ambient temperature variation.

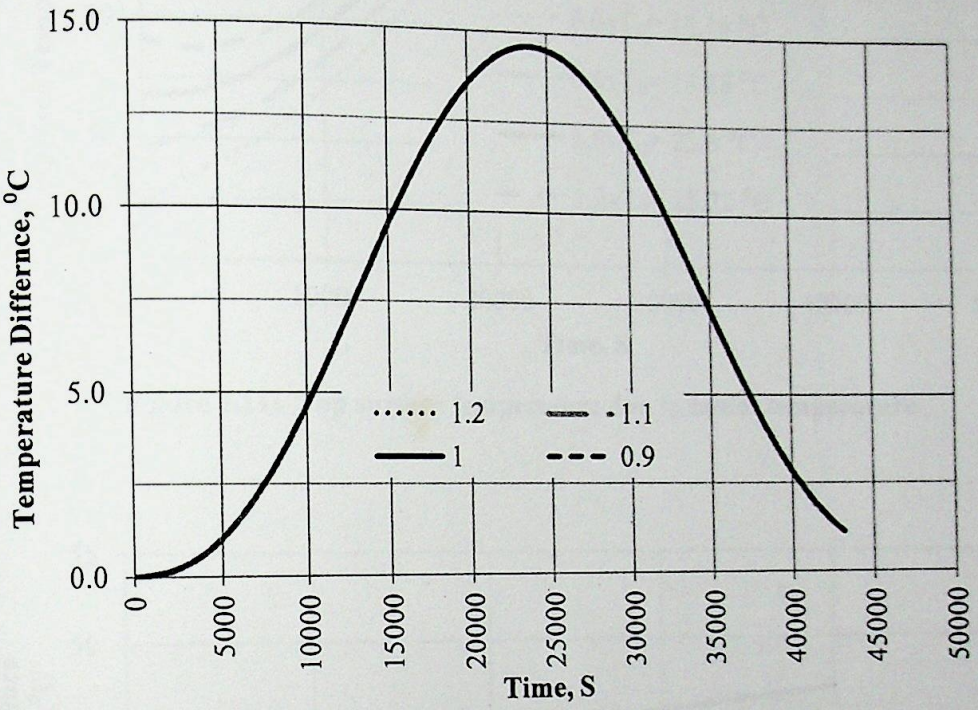

Figure 5.10: Temperature difference due to factorized ambient temperature

5.2.3 Effect of Initial Temperature

Since the structure can have an initial temperature other than the ambient temperature on a particular day, the effect of the initial temperature was investigated. The initial temperature was taken as 23.6 ^{0}C and multiplied by factors of 0.6, 0.8 and 1.2 to get 3 more variations having 14.16^{0}C, 18.88^{0}C and 28.32^{0}C initial temperature values respectively. The default ambient temperature variation was set for all cases.

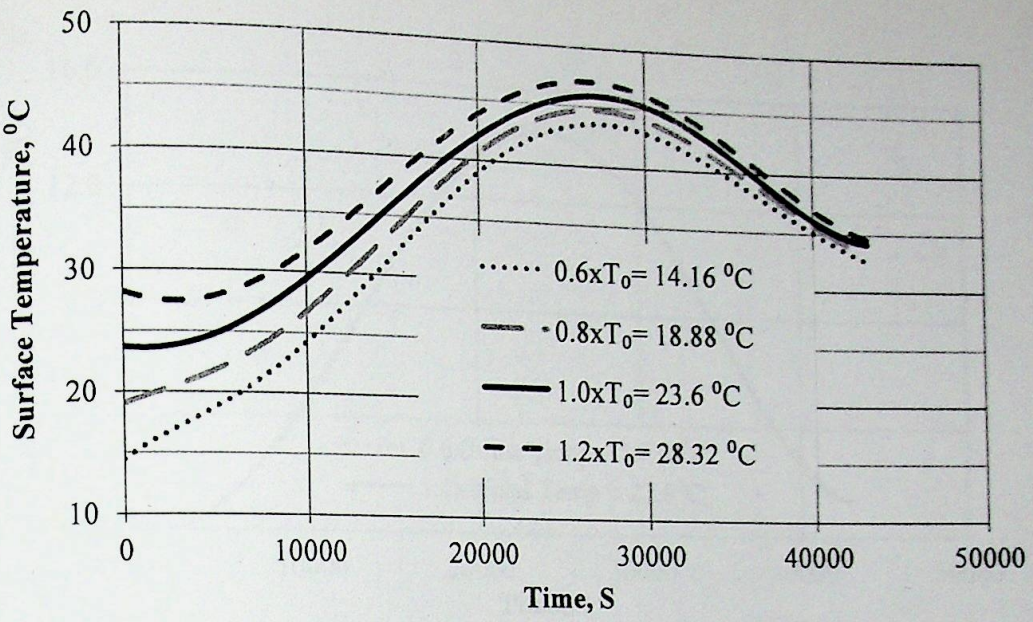

Figure 5.11: Top surface temperature due to initial temperature

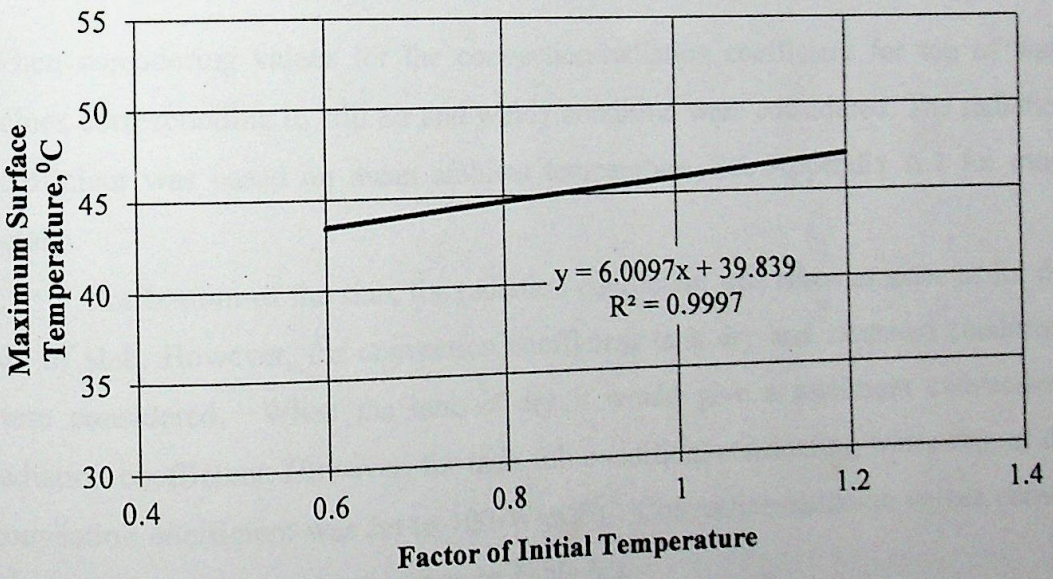

Figure 5.12: Top surface temperature vs. factored initial temperature

The maximum surface temperatures of 43.55°C, 44.7°C, 45.86°C and 47.07°C corresponds to the initial temperatures of 14.16°C, 18.88°C, 23.6°C and 28.32°C respectively. It can also be seen that, for 20% increase in initial temperature, the surface temperature increases by only about 1.2°C. Also as shown in Figure 5.13, the temperature different between the top and bottom surface is not significant on the initial temperature.

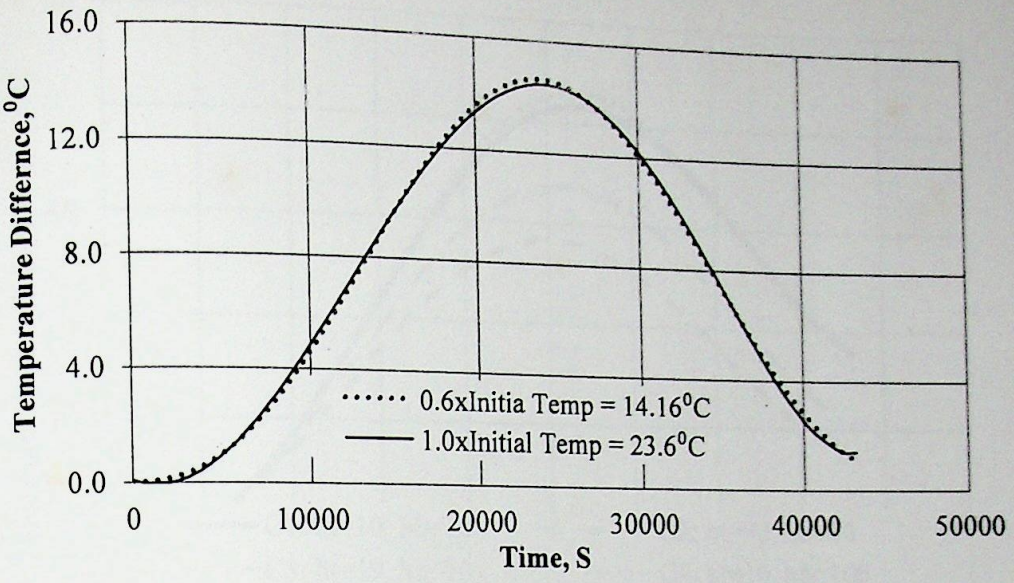

Figure 5.13: Temperature difference due to factored initial temperature

5.2.4 Effect of Convection–Radiation Coefficient

When considering values for the convection-radiation coefficient for top of slab, values corresponding to still air and windy condition were considered. The radiation coefficient was based on mean ambient temperature. See Appendix A.1 for more details.

For bottom of the slab, the radiation coefficient was taken as same as for the top of slab. However, for convection coefficient tank dry and saturated conditions were considered. When the tank is dry it would give a minimum convection–radiation coefficient. However, for tank full condition, considering water vapour the convection coefficient was set to 100 $W/m^2/°C$. Convection-radiation values chosen for slab top and bottom are as given in Table 5.3.

Table 5.3: Paired cases for convection-radiation coefficients

Case	Coefficient, $W/m^2/^0C$	
	Top Surface	Bottom Surface
C1	10	10
C2	30	10
C3	19	100
C4	10	

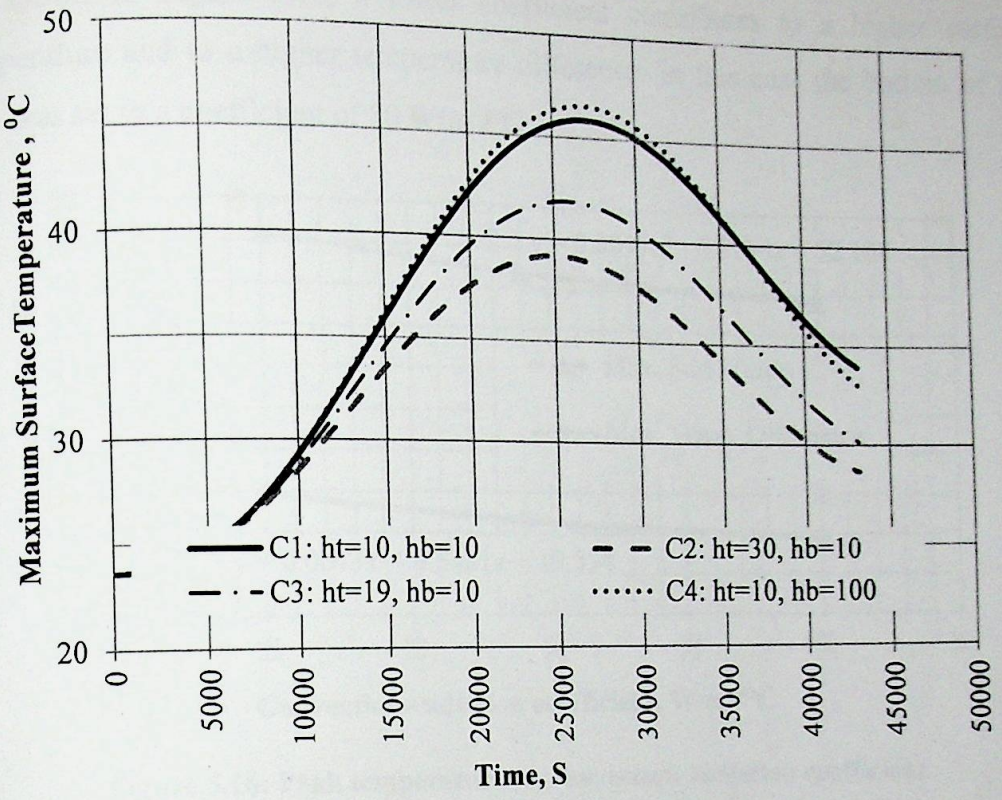

Figure 5.14: Surface temp. variation due to coefficient of convection-radiation

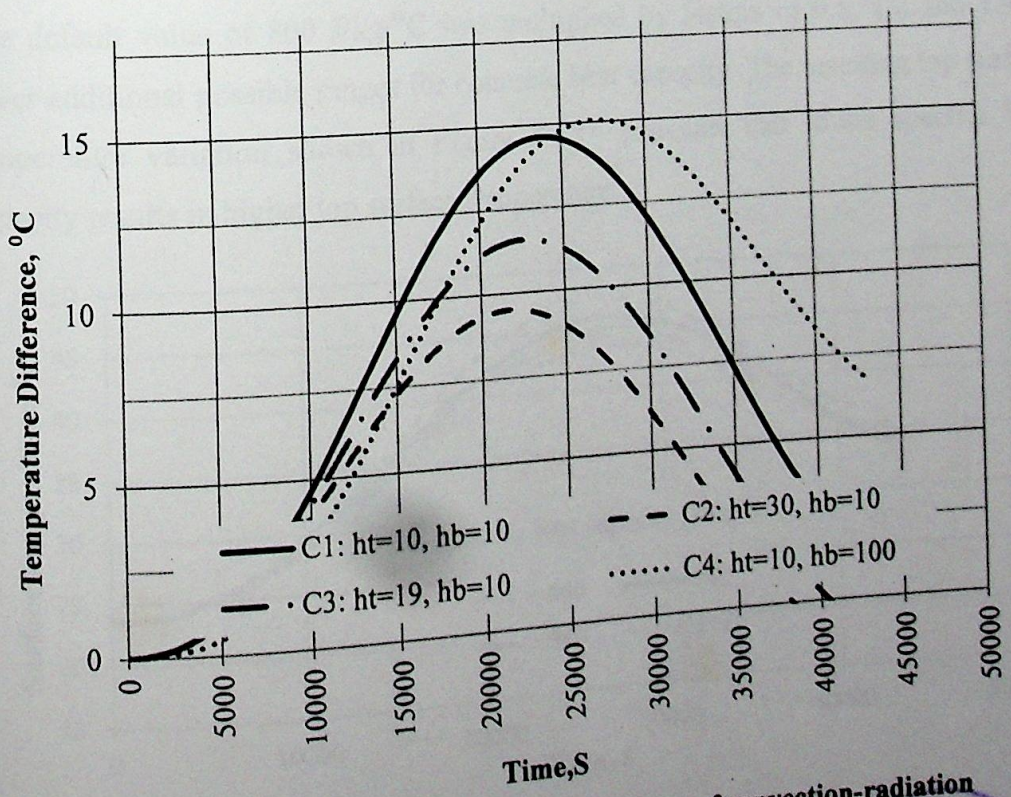

Figure 5.15: Temp. difference due to coefficient of convection-radiation

As shown in Figure 5.16, a lower coefficient contributes to a higher surface temperature and to a higher temperature difference. In this case the bottom of the slab was set to a coefficient of 10 W/m^2/°C.

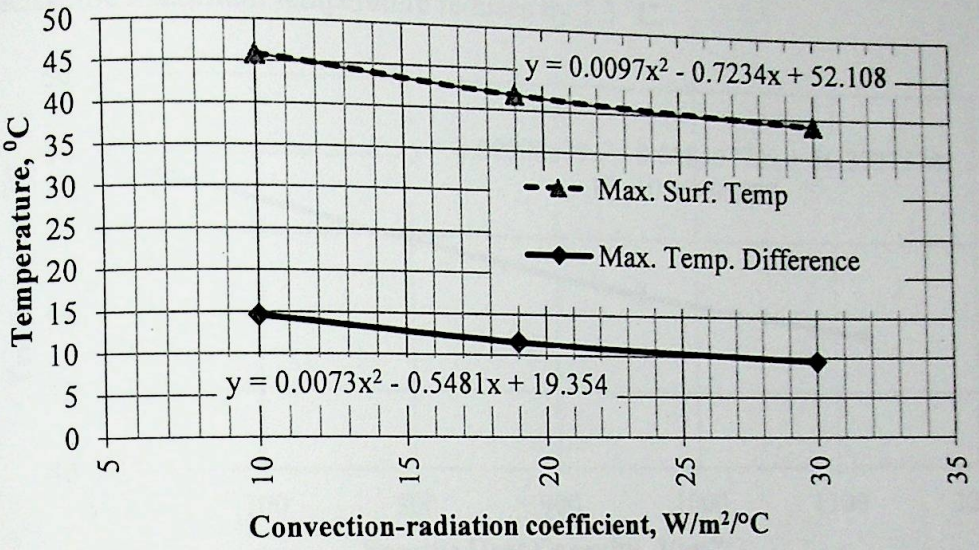

Figure 5.16: Peak temperature vs. convection-radiation coefficient

5.2.5 Effect of Specific Heat Capacity

The default value of 800 J/kg/°C was multiplied by factors of 0.8, 1.2 and 1.4 to cover additional possible ranges for concrete heat capacity. The resulting top surface temperature variation shown in Figure 5.17 indicates that lower specific heat capacity results in higher top surface temperature.

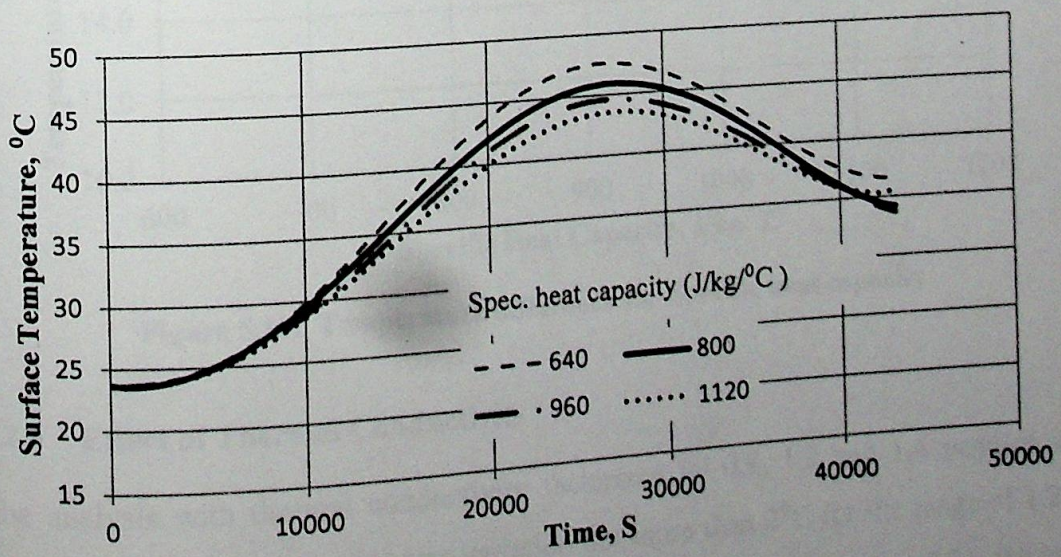

Figure 5.17: Top surface temperature due to specific heat capacity

The maximum surface temperature presented against the specific heat capacity is shown in Figure 5.18. Accordingly, for a 20% increase in specific heat capacity, the maximum temperature reduces by 1.3 °C.

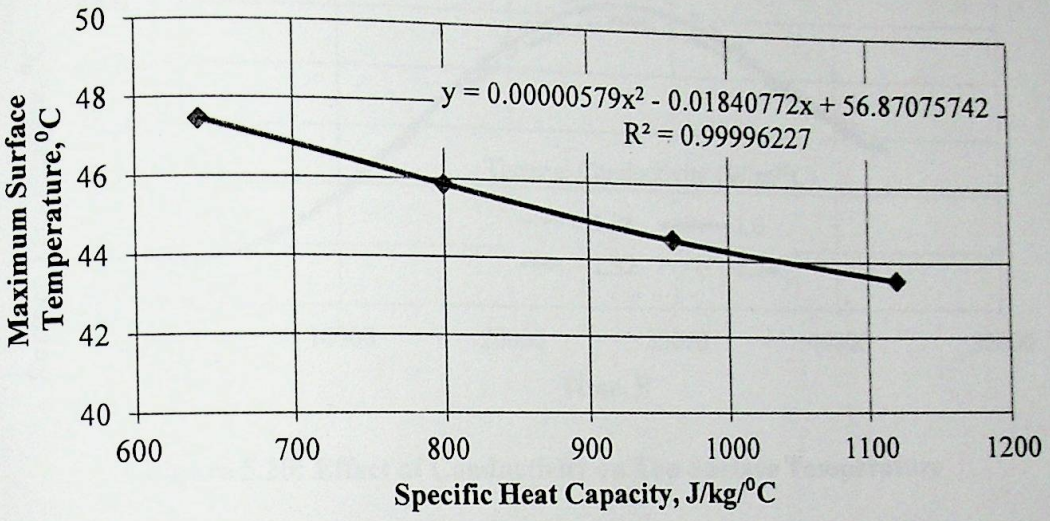

Figure 5.18: Effect of specific heat capacity on surface temperature

The temperature difference between surfaces drops by about 0.9% with reference to 25°C, for a 20% increase in specific heat capacity. See Figure 5.19.

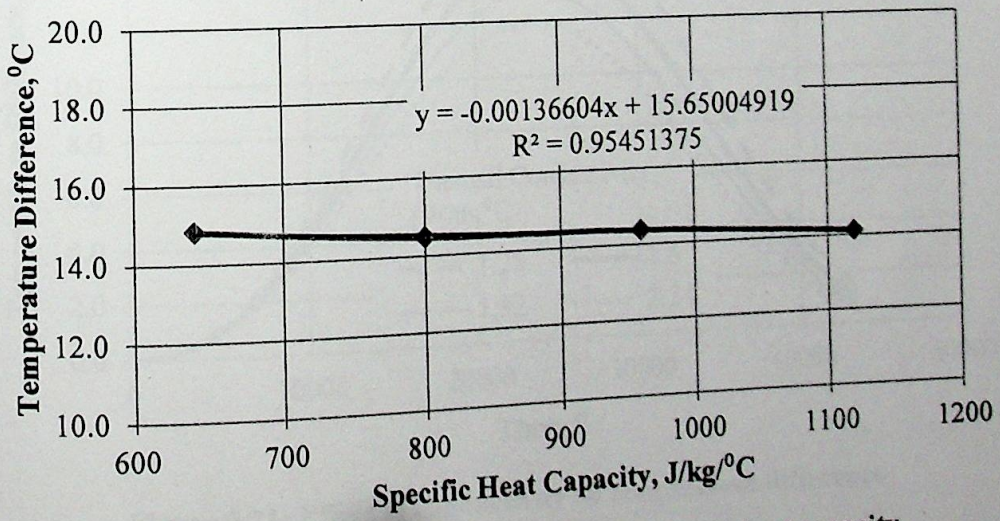

Figure 5.19: Temperature difference vs. Specific heat capacity

5.2.6 Effect of Thermal Conductivity

The analysis with thermal conductivity factorized by 0.8, 1.2 and 1.4 resulted in maximum top surface temperature variation not more than 2°C for the range of 1.28 W/m/°C to 2.24 W/m/°C as shown in Figure 5.20. However as in Figure 5.21, the top

and bottom surface temperature difference varies by 4.5°C for the range of thermal conductivity values. For a 20% variation in in thermal conductivity, the top surface temperature varies by 4%.

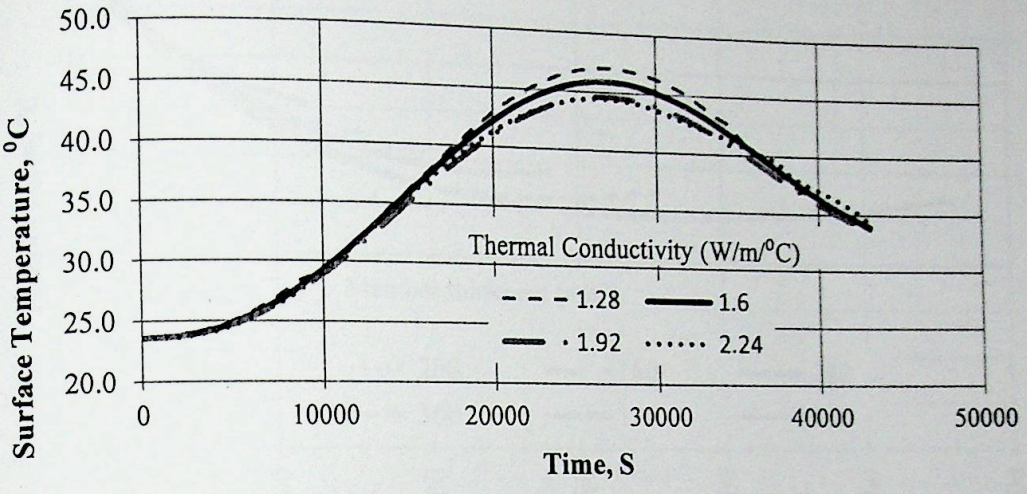

Figure 5.20: Effect of Conductivity on Top Surface Temperature

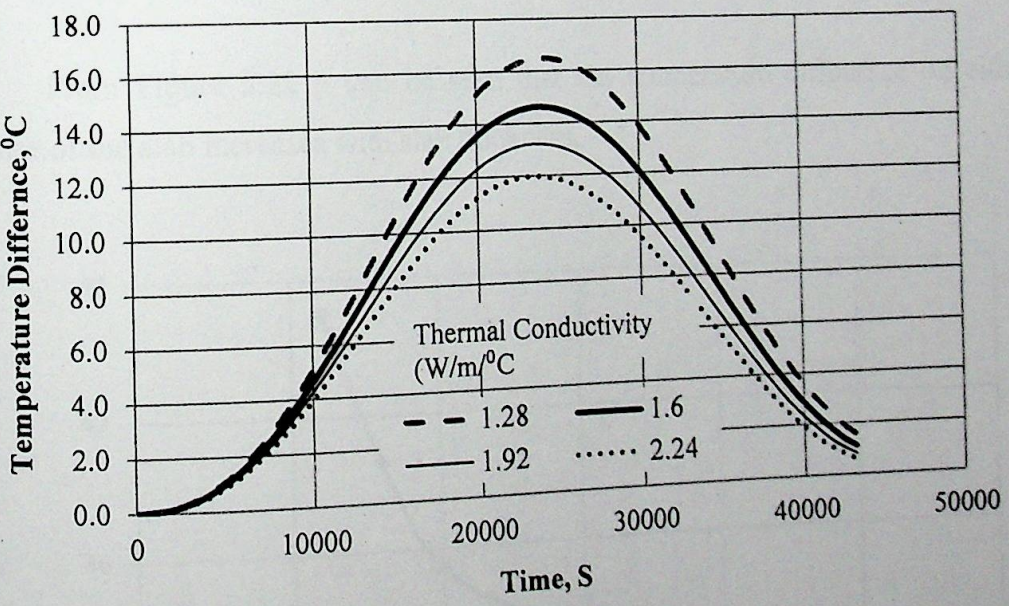

Figure 5.21: Effect of conductivity on temperature difference

5.2.7 Member Thickness

Member thickness varied in multiple of 40mm. This was to ensure that for all conditions, the element sizes were 20mm cubes and also since the temperature variation was checked at 40mm depths. This also ensured that the model was

consistent for all cases. The selected thicknesses were 120 mm, 160 mm, 200 mm, 280mm 360 mm and 560 mm.

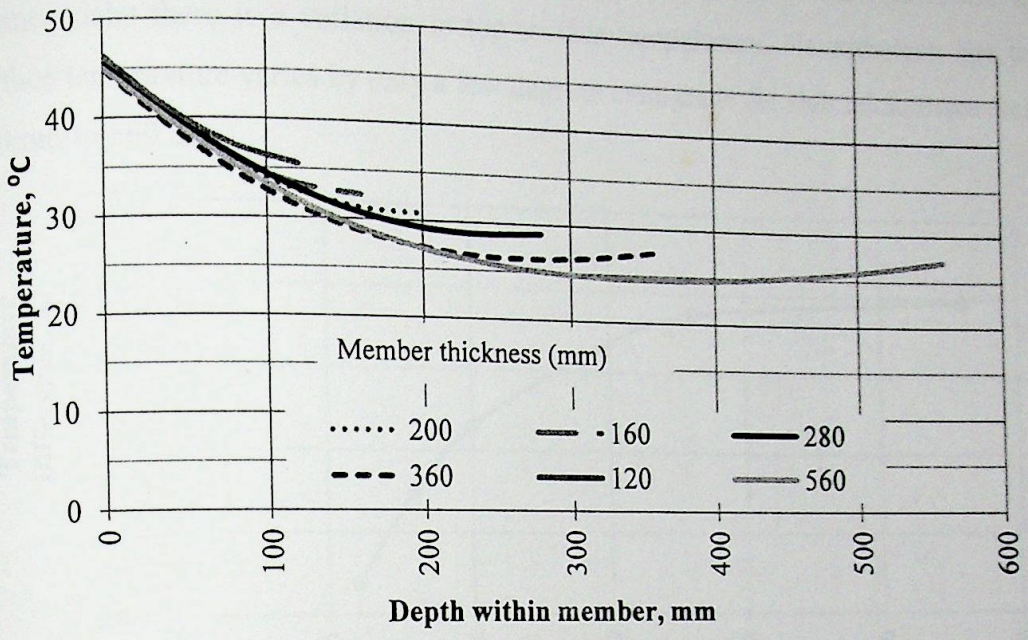

Figure 5.22: Temperature vs. Depth for different member thicknesses

From Figure 5.22 it can be seen that the temperature difference on either surface of the slab increases with slab thickness.

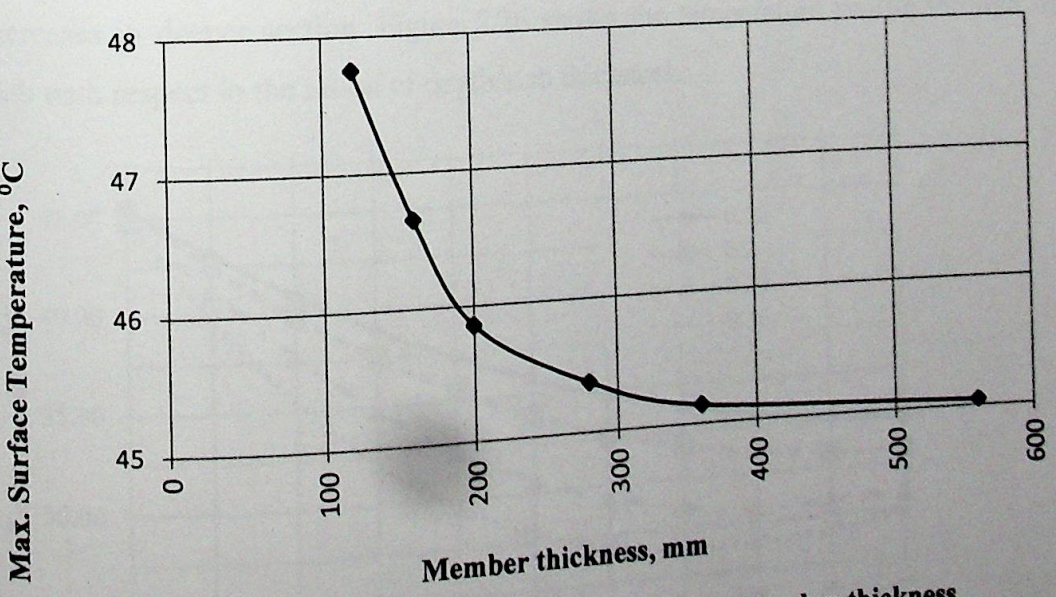

Figure 5.23: Maximum surface temperature vs. Member thickness

The asymptote in Figure 5.2 indicates that the top surface temperature is almost constant for slab depths exceeding about 300mm thickness. However, for thinner slabs there is a variation in top surface temperature. Nevertheless, the top surface temperature varies by only a few degrees centigrade for slab thicknesses from 120mm to 560 mm.

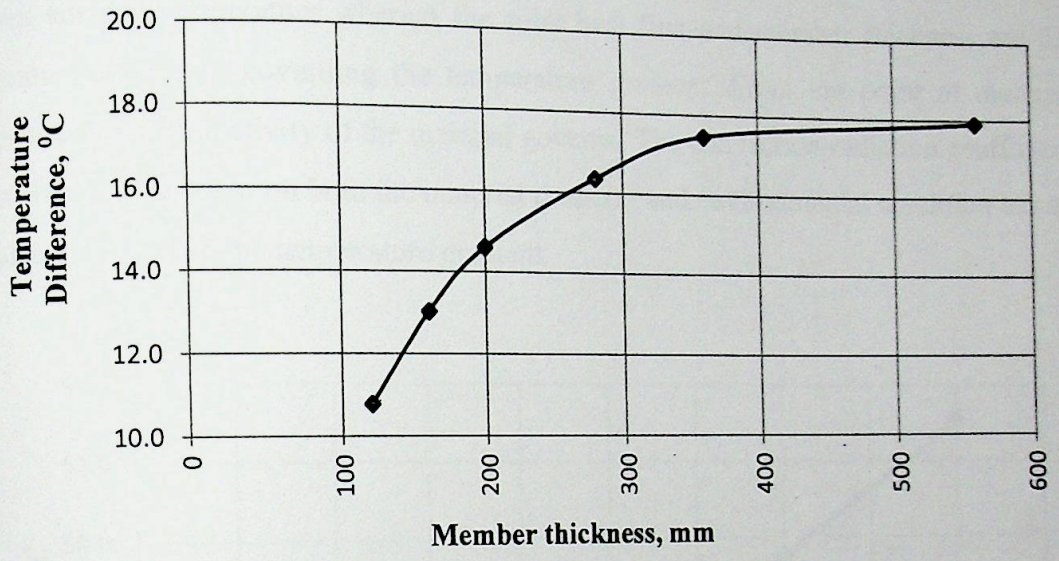

Figure 5.24: Temperature difference vs. Member thickness

As shown in Figure 5.25 the non-linearity of the temperature gradient increases in deeper section. Figure 5.26 shows the temperature profile through the slab with respect to the ration of depth/slab thickness.

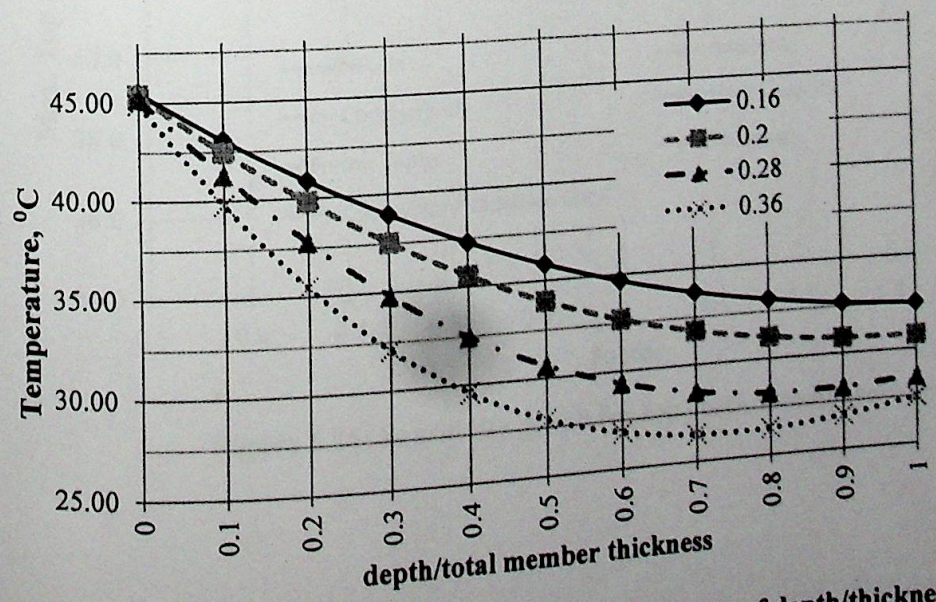

Figure 5.25: Temperature difference vs. ratio of depth/thickness

5.2.8 Sensitivity of Parameters

Based on the parameters considered, variation of maximum top surface temperature is shown in Figure 5.26 and temperature difference is shown in Figure 5.27. It can be seen that, among the environmental conditions, the solar heat flux and the initial and ambient temperature variation are the main governing parameter in for the maximum top surface temperature whereas the solar heat flux and member thickness are the main parameters governing the temperature gradient. From the point of material properties, conductivity of the material governs. The convection-radiation coefficient which is dependent on both the material property and environmental condition has an effect mainly on the temperature gradient.

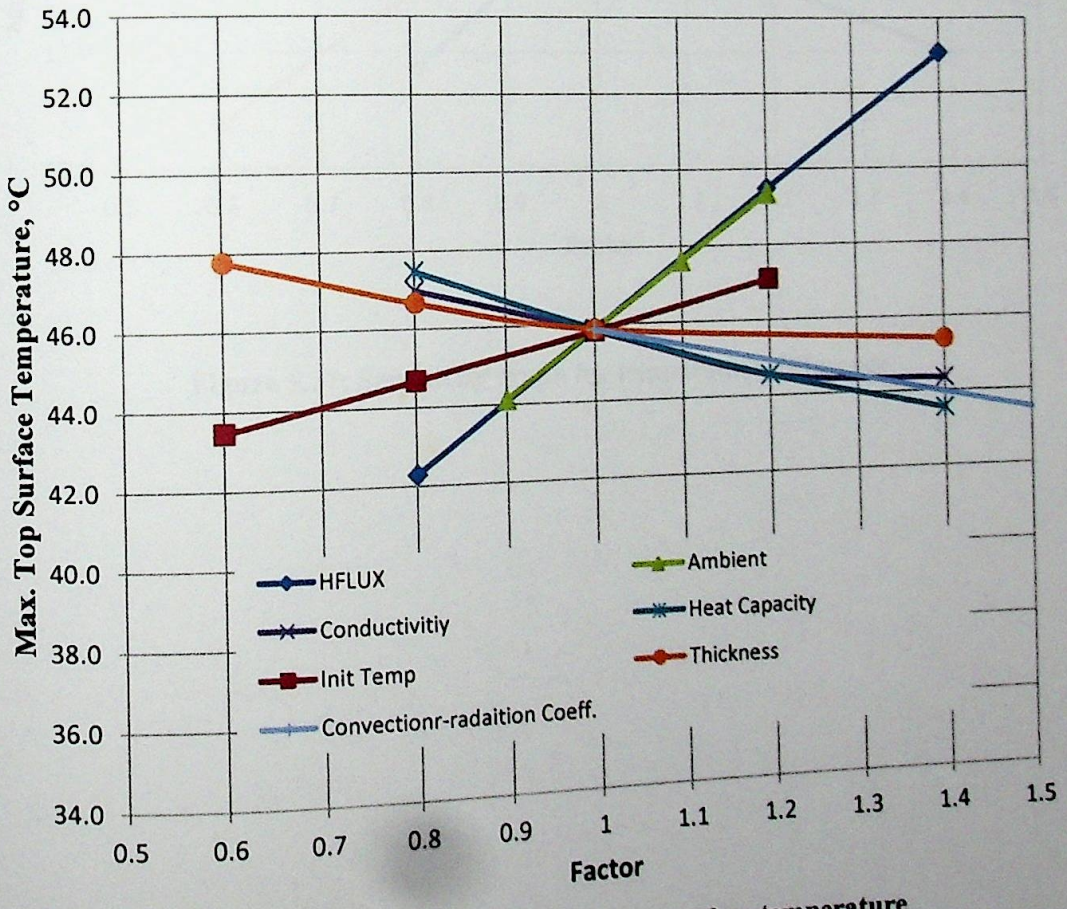

Figure 5.26: Sensitivity graph for top surface temperature

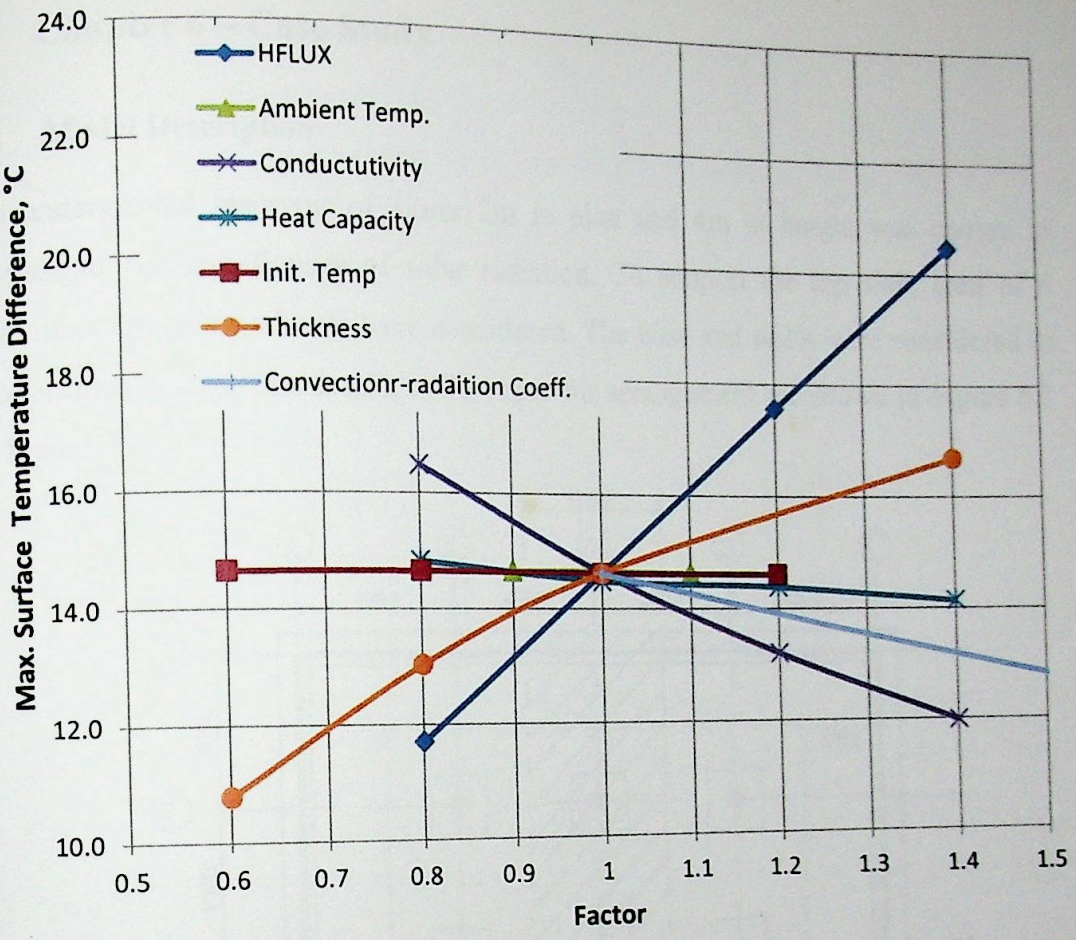

Figure 5.27: Sensitivity graph for temperature difference

6 Chapter 6 – Case Study

6.1 Model Description

An underground reservoir of 12mx12m in plan and 4m in height was chosen to investigate the significance of solar radiation. To support the top slab, total of 6 columns with column heads were considered. The base and walls were considered as monolithically cast. The details of the reservoir arrangement are shown in Figure 6.1 to Figure 6.3.

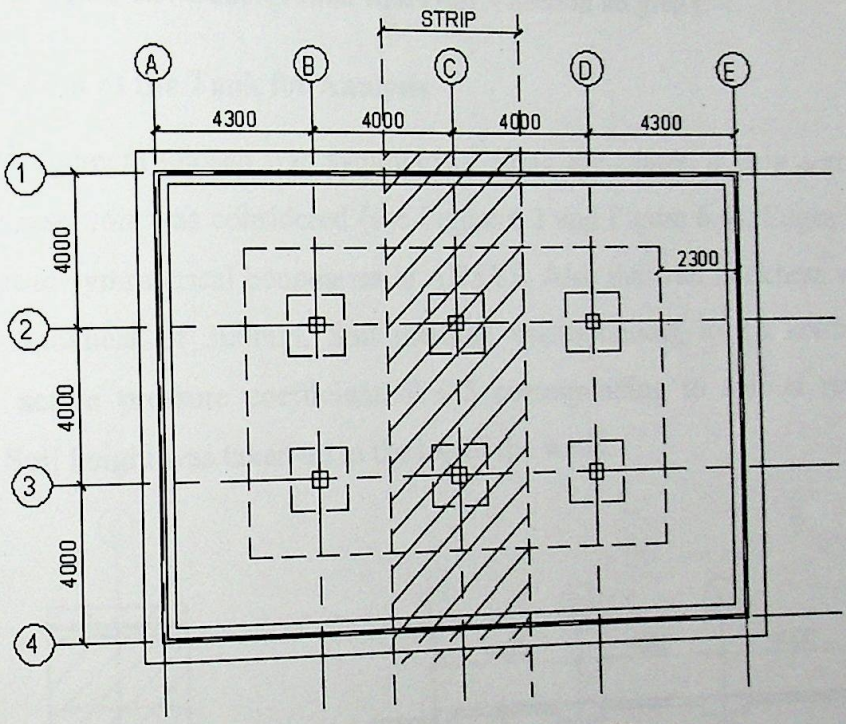

Figure 6.1: Underground Reservoir - Plan

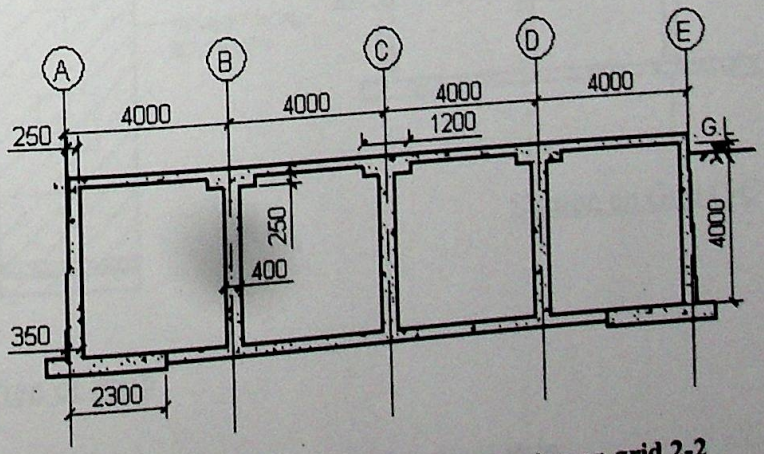

Figure 6.2: Underground Reservoir – Section on grid 2-2

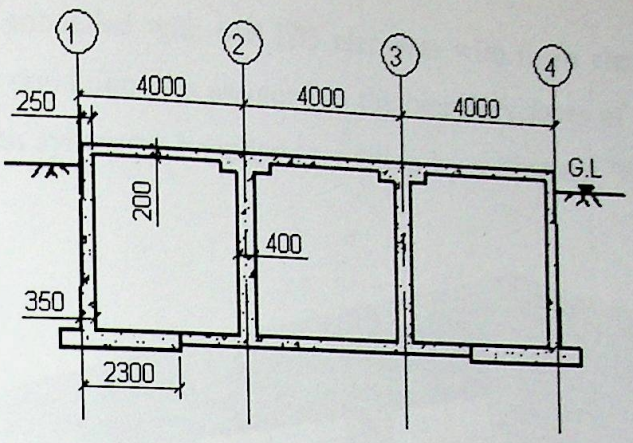

Figure 6.3: Underground Reservoir – Section on grid C-C

6.2 Idealization of the Tank for Analysis

Since the arrangement chosen was symmetrical along the centre, a strip across the width of the reservoir was considered (see Figure 6.2 and Figure 6.4). Edges of this strip were set to symmetrical boundaries in ANSYS. Also the wall thickness was set to constant thickness of 300mm. Soil pressure corresponding to 18 kN/m^3 unit weight and active pressure coefficient of 0.5 corresponding to soil at rest was considered. Soil height was taken up to the top of the walls.

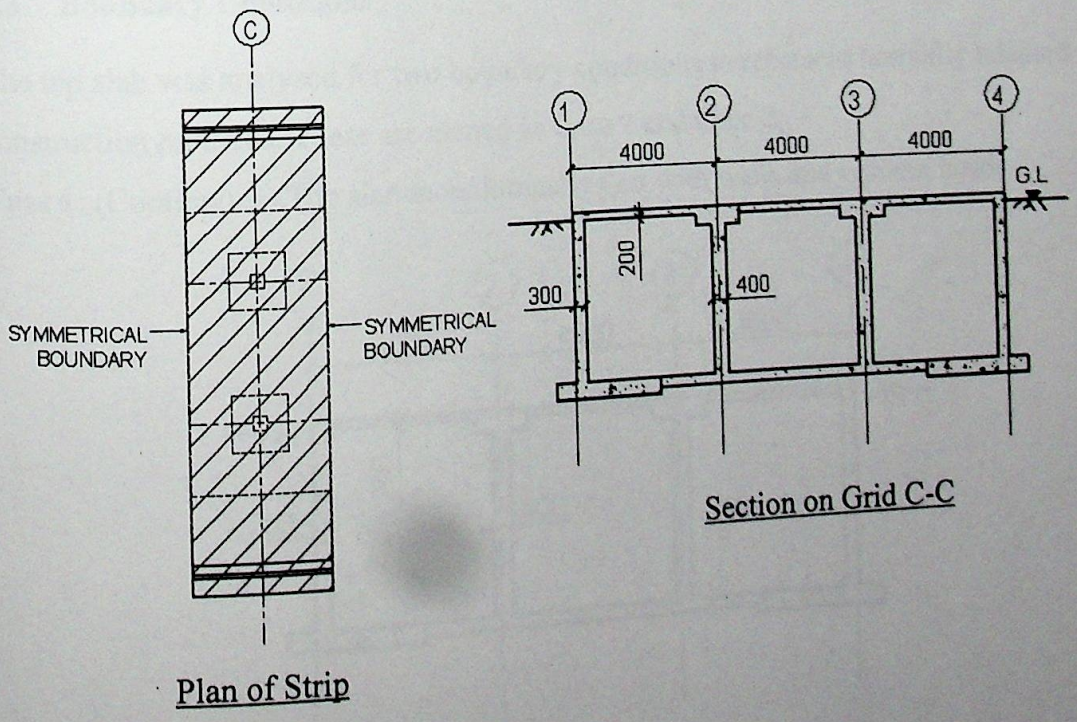

Figure 6.4: Idealized strip

UNIVERSITY OF MORATUWA
LIBRARY
SRI LANKA

The strip was modelled with SOLID5 elements with 0.1m element size. The symmetry boundary condition was assigned to the boundary faces of the strip using DOF constraints with symmetry boundary condition by setting the "SYMM" of the "DA" command.

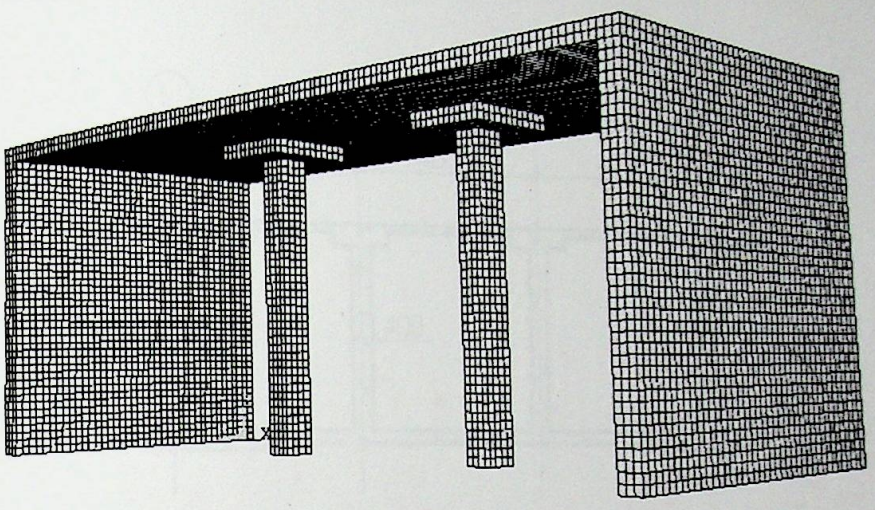

Figure 6.5: Finite element model (perspective view)

6.3 Boundary Conditions

The top slab was analysed for two boundary conditions to represent normally adapted construction methods. These are named as Case 1 and Case 2.

Case 1: (Continuous) Top slab monolithically cast with walls and column heads

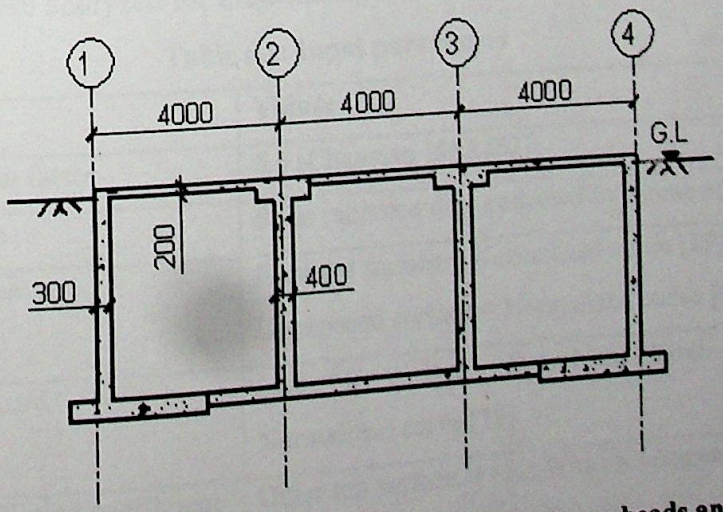

Figure 6.6: (Continuous) monolithically cast on column heads and walls

Case 2: (Sliding) Top slab frictionally sliding on walls and monolithic on column heads

For this case, the slab was positioned on a frictional arrangement on wall tops with a friction factor of 0.3. At column head the slab was monolithically connected to the column head.

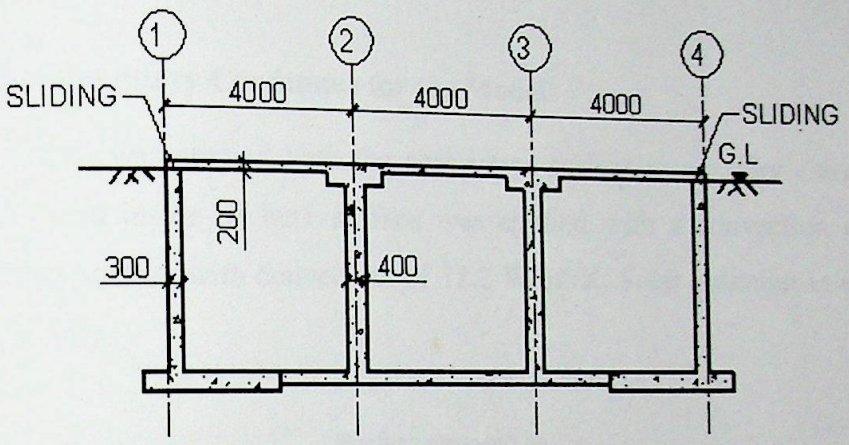

Figure 6.7: (Sliding) monolithically cast over columns but sliding on walls

To represent frictional surfaces, elements TARGE170 and CONTA173 were used. The contact elements were set on wall tops with its normal facing upwards and the Target elements were set to the slab soffit with its normal facing downwards.

6.4 Inputs for Analytical Model

The two cases were analyzed for the conditions as given in Table 6.1.

Table 6.1: Input parameters

Condition	Values
Solar absorption factor	0.6 (Chapman 1982 [32])
Solar Radiation	Solar radiation data collected by Aruna et al. [19]
Ambient temperature	Exposed surface = Normalized curve [19] Unexposed surface = Normalized curve [19]
Initial temperature	23.6 ^{0}C = start of ambient temp. based on Normalized curve [19]
Convection-radiation coefficient	Outer top surface. =11.2.W/m^2/K (Appendix A) Inside tank surface =100 W/m^2/K Outer walls in contact with soil = 100 W/m^2/K

Specific heat capacity	800 J/kg/K (Common value)
Thermal conductivity	1.4 W/m/K (Limestone aggregates)
Reference temperature for stresses	27.5 ^{0}C (considered as the "temperature of the reservoir at its completion")
Friction Factor	0.3 between wall top and slab

6.5 Thermal Boundary Conditions for the Model

The top 1m depth was applied with the convective surface to consider convection and radiation. The inside of tank surface was applied with a convection of 100 W/m^2/K and top surface with convection of 11.2 W/m^2/K. Solar radiation as applied to the top face only.

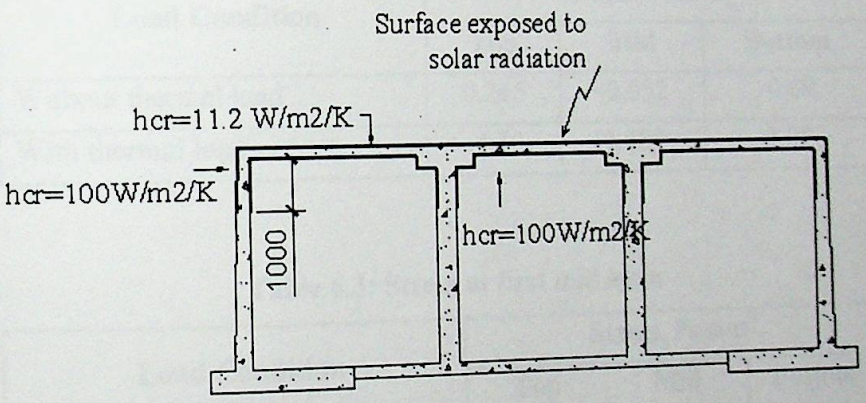

Figure 6.8: Region of Convective Surface

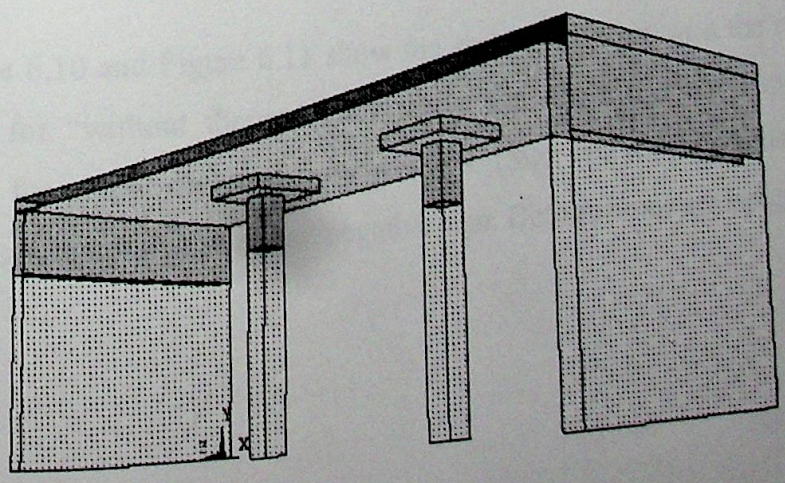

Figure 6.9: Convective surfaces indicated (Perspective view)

6.6 Results

6.6.1 Slab Monolithically Cast With Walls and Column Heads (Case 1)

For a position at the end of the column head the stress comparison is shown in Table 6.2. By comparing the stress increase due to the thermal effect, compared to that of the stress due to self-weight and soil pressure, it is seen that the stress increases from -0.69 N/mm^2 (compressive) to 4.03 N/mm^2 (tensile) at the underside of the slab near the column head. At the mid span (Table 6.3) the tensile stress increases from 0.121N/mm^2 to 2.57 N/mm^2. Therefore for this structural arrangement, the solar radiation increases the tensile stress in the concrete slab significantly.

Table 6.2: Stress at end of column head - Continuously Cast Slab (Case 1)

Load Condition	Stress, N/mm^2		
	Top	Mid	Bottom
Without thermal load	0.265	-0.052	-0.69
With thermal load	-4.30	0.480	4.03

Table 6.3: Stress at first mid span

Load Condition	Stress, N/mm^2		
	Top	Mid	Bottom
Without thermal load	-0.301	-0.090	0.121
With thermal load	-3.839	0.611	2.573

Figure 6.10 and Figure 6.11 show the stresses together with the exaggerated deformation for "without thermal load" and "with thermal load" condition. See Appendix C for output obtained from ANSYS. (Sign convention: Tensile stresses positive sign; compressive stresses: negative sign. Deformations are exaggerated.)

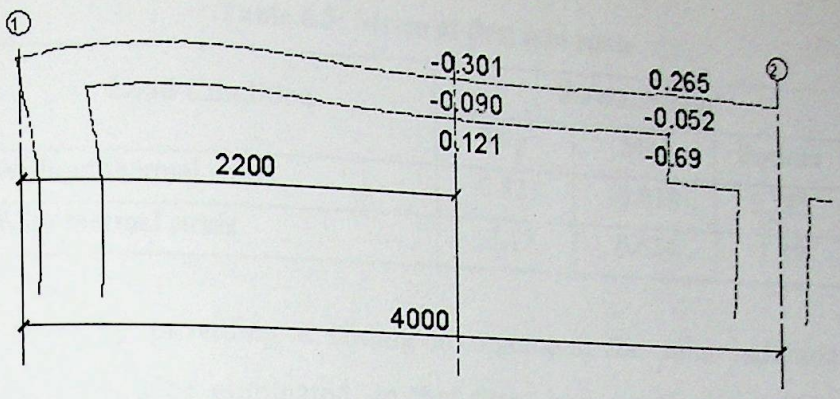

Figure 6.10: Stresses due to Selfweight + Soil pressure (Case 1)

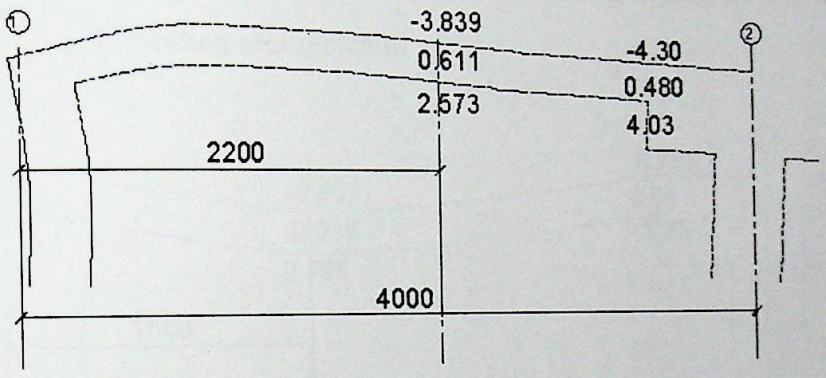

Figure 6.11: Stresses due to Selfweight + Soil pressure + Thermal Load (Case 1)

6.6.2 Frictional Sliding on Walls and Monolithic at Column Heads (Case 2)

For this case, at a position near the column head the stress comparison is shown in Table 6.4. By comparing the stress increase due to the thermal effect, compared to that of the stress due to self-weight and soil pressure only, it is seen that the stress increases from -1.23 N/mm2 (compressive) to 4.26 N/mm^2 (Tensile) at the underside of the slab. At the mid span Table 6.5, for the slab soffit the tensile stress increases from 0.78N/mm^2 to 1.89 N/mm^2.

Table 6.4: Stress near column head

Load Condition	Stress, N/mm^2		
	Top	Mid	Bottom
Without thermal stress	0.783	0.04	-1.23
With thermal stress	-4.36	0.429	4.26

Table 6.5: Stress at first mid span

Load Condition	Stress, N/mm^2		
	Top	Mid	Bottom
Without thermal stress	-0.821	-0.018	0.785
With thermal stress	-3.13	0.624	1.89

Therefore even by providing a sliding arrangement, the solar radiation induced tensile stress cannot be eliminated. In fact there is a marginal increase in tensile stress when a sliding arrangement is provided. One reason could be that the compressive stress induced by the side wall (loaded with soil pressure), is not being transferred due to the sliding arrangement.

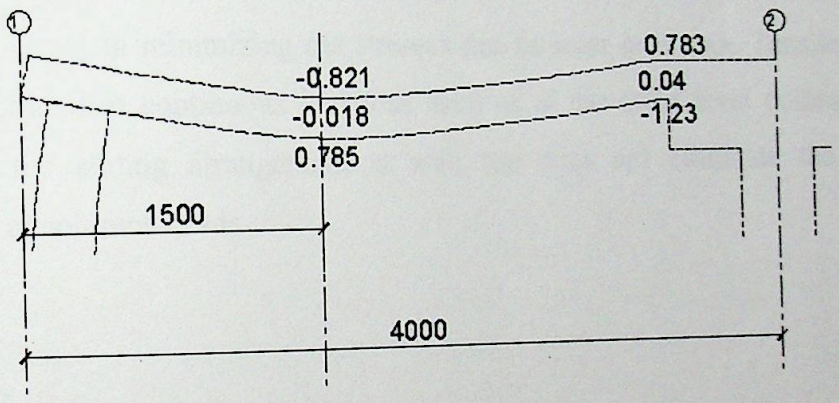

Figure 6.12: Stresses due to Selfweight + Soil pressure (Case 2)

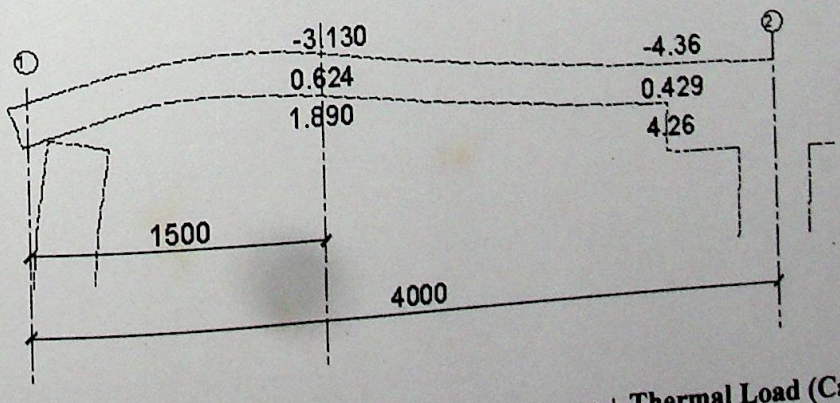

Figure 6.13: Stresses due to Selfweight + Soil pressure + Thermal Load (Case 2)

7 Chapter 6 – Conclusions and Recommendations

A finite element model was defined to incorporate the solar heat flux, convection and conduction. Using standard numerical equations, the model was verified for temperature variation and structural stresses.

Sensitivity analysis was carried out and it was found that solar radiation, solar absorption factor, coefficient of convection, radiation and ambient temperature variation had a significant impact on the peak surface temperature.

Based on the verified finite element modeling approach, an underground reservoir was analyzed with top roof slab exposed to solar radiation. Results show that the sliding and fixity conditions between the roof slab and wall does not have a significant effect in minimizing the stresses due to solar heat gain. Tensile stresses are concentrated at continuous locations such as at the soffit level column heads. Providing the sliding arrangement at wall top does not eliminate the stresses developed at columns heads.

UNIVERSITY OF MORATUWA
LIBRARY
SRI LANKA

8 Bibliography

[1] *Design of concrete structures for retaining aqueous liquids*. BS 8007, 1987.

[2] British Standard Institution, *Eurocode 1: Actions on structures, Part 1-5: General actions — Thermal actions*. BS EN 1991-1-5, 2003.

[3] F. J. Vecchio and J. A. Sato, "Thermal Gradient Effects in Reinforced Concrete Frame Strucuters," *ACI Structural Journal*, vol. 87, no. 3, pp. 262-275, May 1990.

[4] M. J. S. Hirst, "Measuring the temperature of concrete structures," University of Adelaide, 1984.

[5] Michael Boxwell. (2009-2013) Solar Electricity Handbook. [Online]. http://solarelectricityhandbook.com/solar-irradiance.html

[6] M. J. S. Hirst, "Thermal Loading of Concrete Bridges," *Canadian Journal of Civil Engineering*, vol. 11, no. 3, pp. 423-429, 1984.

[7] F. A. Branco and P. Mendes, "Thermal actions for concrete bridge design," *J. Struct. Eng.*, vol. 119, no. 8, p. 2313–2331, Aug. 1993.

[8] R. Faria, M. Azenha, and J. A. Figueiras, "Modelling of concrete at early ages: Application to an externally restrained slab," *Cement & Concrete Composites 28*, no. 28, p. 572–585, May 2006.

[9] C. P. Kothandaraman, *Fundamentals of Heat and Mass transfer*, 3rd ed. New Delhi, India: New Age International Publishers, 2006.

[10] A. Ghali, R. Ravre, and M. Elbadry, *Concrete Structures : Stresses and Deformations*, 3rd ed. London: Chapman and Hall, 2002.

[11] J. F. Lamond and J. H. Pielert, Eds., *Significance of Tests and Properties of Concrete and Concrete-Making Materials*. West Conshohocken, PA: ASTM International, 2006.

[12] P. Mitchell, *Central Heating, Installation, Maintenance and Repair*. Great Britain: WritersPrintShop, 2008.

[13] A. D. Kovalenko, *Thermoelasticity: Basic theory and applications. [By] A. D. Kovalenko. Translated from the Russian by D. B. Macvean. With an appendix on Thermoelastic stability by J. B. Alblas*. Wolters-Noordhoff Publishing, Groningen, 1969.

[14] B. A. Boley and J. H. Weiner, *Theory of Thermal Stresses*. Robert E. Krieger Publishing

Company, Malabar, Florida., 1985.

[15] A. Saetta, R. Scotta, and R. Vitaliani, "Stress analysis of concrete structures subjected to variable thermal loads," *J. Struct. Eng.*, vol. 121, no. 3, pp. 446-457, Mar. 1995.

[16] *ANSYSV12.0, Release 12.0 documentation for ANSYS*. ANSYS, Inc..

[17] L. Dahmani, A. Khennane, and S. Kaci, "Crack identification in reinforced concrete beams using ANSYS," *Strength of Materials*, vol. 42, no. 2, pp. 232-240, Mar. 2010.

[18] L. Dahmani and M. Kouane, "Thermal Cracking Respone of Reinforced Concrete Beam to Gradient Temperature," *World Academy of Science, Engineering & Technology*, no. 71, p. 1385, 2012.

[19] A. Karunarathne, W. Mampearachchi, and A. Nanayakkara, "Modelling of thermal effects due to solar radiation on concrete pavements," 2010.

[20] L. T. Wong and W. K. Chow, "Solar radiation model," *Applied Energy 69*, p. 191–224, 2001.

[21] Wikipedia. [Online]. http://en.wikipedia.org/wiki/Sunlight

[22] Z. Sen, *Solar Energy Fundamentals and Modeling Techniques*. Springer-Verlag London Limited, 2008.

[23] PV Education. [Online]. http://pveducation.org/pvcdrom/properties-of-sunlight/measurement-of-solar-radiation

[24] R. Levinson, H. Akbari, and P. Berdahl, "Measuring solar reflectance—Part I: Defining a metric that accurately predicts solar heat gain," *Solar Energy*, vol. 84, no. 9, pp. 1717-1744, 2010.

[25] Denis Lenardic. (2001 - 2012, Jun.) Solar Radiation. [Online]. http://www.pvresources.com/SiteAnalysis/SolarRadiation.aspx

[26] (2013) Daystar Solar Meter - Tecnhical Specifications. [Online]. http://www.daystarpv.com/solarmeter3.html

[27] (2013) Daystar Solar Meter - PV Sensor. [Online]. http://www.daystarpv.com/spectrum.html

[28] K. Perera and S. Jayasekara, "Fitting generalized lambda distribution to solar radiation in Colombo, Sri Lanka," in *2012 Int. Conf. Sustainable Built Environment*, Kandy, Sri

Lanka, 2012.

[29] T. S. G. Peiris and R. O. Thattil, "An "alternative"model to estimate solar radiation," *Cocos*, no. 10, pp. 26-34, 1994-1995.

[30] D. Renné, R. George, B. Marion, D. Heimiller, and C. Gueymard, "Solar resource assessment for Sri Lanka and Maldives," National Renewable Energy Laboratory, August 2003.

[31] Dennis A. Morian, "Characterization and analysis of early age concrete pavement behavior at the national airport pavement test facility (NAPTF)," Texas Transportation Institute, Texas, Research Report Report IPRF 01-G-002-04-2(s), 2007.

[32] A. J. Chapman, *Fundamentals of Heat Transfer*. New York: Macmillan Inc, 1982.

[33] B. Taljaston, "Temperature Development and Maturity Growth for Ordinary Swedish Portland Cement Type II," Technical University of Lulea Diploma Work , 1987.

[34] ACPA (2002), "Albedo: A Measure of Pavement Surface Reflectance," American Concrete Pavement Association, 2002.

[35] K. Boriboonsomsin and F. Reza, "Mix Design and Benefit Evaluation of High Solar Reflectance Concrete for Pavements," *Journal of the Transportation Research Board*, 2007.

[36] R. Levinson and H. Akbari, "Effects of composition and exposure on the solar reflectance of Portland cement concrete," *Cement and Concrete Research*, vol. 32, no. 11, p. 1679–1698, Nov. 2002.

[37] T. D. M. A. Samuel and R. Srikanthan, "Solar radiation estimation for Sri Lanka," in *1982 Proc. Ann. Conf. Institution of Engineers*, Sri Lanka, 1982.

APPENDIX A

A.1 Convection Radiation Coefficient

As per Faria et al (2006) [**8**], the convection coefficient and be combined with irradiation to be used as a convection-radiation coefficient.

According to Eq. 2.6,

$$h_c = \begin{cases} 5.6 + 3.95v, & v \leq 5 \text{ m/s} \\ 7.6v^{0.78}, & v > 5 \text{ m/s} \end{cases}$$

For still air, v= 0 m/s, then $h_c = 5.6\ W/m2/°C$

$$h_r = \varepsilon[4.8 + 0.075(T_{air} - 5)]$$

For 28.2°C average air temperature (based on reading of Ambient temperature variation)

$$h_r = 0.85[4.8 + 0.075(28.2 - 5)]$$

$$h_r = 5.56\ W/m2/°C$$

Therefore the convection-radiation coefficient, h_{cr}

$$h_{cr} = h_c + h_r$$

$$h_{cr} = 11.2\ W/m2/°C$$

Similarly for velocities of 2 m/s and 5 m/s the convection radiation coefficient was calculated as 19 and 30.9 W/m2/°C respectively.

A.2 Numerical Calculation on Conduction and Convection under Constant Heat Flux

$$(T_{x,t} - T_i) = \frac{2q(\frac{\alpha t}{\pi})^{\frac{1}{2}}}{k} \exp\left(\frac{-x^2}{4\alpha t}\right) - \frac{qx}{k}\left(1 - \text{erf}\left(\frac{x}{2\sqrt{\alpha t}}\right)\right) \quad ---- \text{Eq. 2.11}$$

k	1.6	W/m
alpha	8.33333E-07	
q	100	W/m2
Ti	25	°C
h	10	W/m2/°C
Tambient	25	°C

Time (S)	Surface Temperature (^{0}C)	qv(W/m2)	Σqv	avg. Convection
0	25.000	0.000	0.000	0.000
120	25.705	7.052	7.052	7.052
240	25.927	9.270	16.323	8.161
360	26.122	11.218	27.541	9.180
480	26.281	12.810	40.351	10.088
600	26.418	14.179	54.529	10.906
720	26.539	15.391	69.920	11.653
840	26.648	16.484	86.405	12.344
960	26.748	17.485	103.890	12.986
1080	26.841	18.410	122.299	13.589
1200	26.927	19.271	141.570	14.157
1320	27.008	20.079	161.649	14.695
1440	27.084	20.840	182.489	15.207
1560	27.156	21.561	204.050	15.696
1680	27.225	22.246	226.295	16.164
1800	27.290	22.899	249.194	16.613
1920	27.352	23.523	272.717	17.045
2040	27.412	24.121	296.839	17.461
2160	27.470	24.696	321.535	17.863
2280	27.525	25.249	346.784	18.252
2400	27.578	25.783	372.567	18.628
2520	27.630	26.298	398.865	18.994
2640	27.680	26.796	425.660	19.348
2760	27.728	27.278	452.938	19.693

2880	27.775	27.746	480.684	20.029
3000	27.820	28.199	508.883	20.355
3120	27.864	28.640	537.524	20.674
3240	27.907	29.069	566.593	20.985
3360	27.949	29.487	596.080	21.289
3480	27.989	29.893	625.973	21.585
3600	28.029	30.290	656.262	21.875
3720	28.068	30.676	686.939	22.159
3840	28.105	31.054	717.993	22.437
3960	28.142	31.423	749.415	22.710
4080	28.178	31.783	781.199	22.976
4200	28.214	32.136	813.335	23.238
4320	28.248	32.481	845.816	23.495
4440	28.282	32.819	878.635	23.747
4560	28.315	33.150	911.785	23.994
4680	28.347	33.474	945.260	24.237
4800	28.379	33.792	979.052	24.476
4920	28.410	34.104	1013.156	24.711
5040	28.441	34.410	1047.567	24.942
5160	28.471	34.711	1082.278	25.169
5280	28.501	35.006	1117.284	25.393
5400	28.530	35.296	1152.579	25.613
5520	28.558	35.580	1188.160	25.830
5640	28.586	35.860	1224.020	26.043
5760	28.614	36.136	1260.156	26.253
5880	28.641	36.406	1296.562	26.460
6000	28.667	36.673	1333.235	26.665
6120	28.693	36.935	1370.169	26.866
6240	28.719	37.193	1407.362	27.065
6360	28.745	37.446	1444.808	27.261
6480	28.770	37.697	1482.505	27.454
6600	28.794	37.943	1520.448	27.645
6720	28.819	38.186	1558.634	27.833
6840	28.842	38.425	1597.058	28.019
6960	28.866	38.661	1635.719	28.202
7080	28.889	38.893	1674.612	28.383
7200	28.912	39.122	1713.735	28.562
7320	28.935	39.348	1753.083	28.739
7440	28.957	39.571	1792.655	28.914
7560	28.979	39.792	1832.446	29.086
7680	29.001	40.009	1872.455	29.257
7800	29.022	40.223	1912.678	29.426

7920	29.043	40.435	1953.112	29.593
8040	29.064	40.643	1993.756	29.758
8160	29.085	40.850	2034.606	29.921
8280	29.105	41.053	2075.659	30.082
8400	29.125	41.255	2116.914	30.242
8520	29.145	41.453	2158.367	30.400
8640	29.165	41.650	2200.017	30.556
8760	29.184	41.844	2241.861	30.710
8880	29.204	42.036	2283.897	30.863
9000	29.223	42.225	2326.122	31.015
9120	29.241	42.413	2368.535	31.165
9240	29.260	42.598	2411.133	31.313
9360	29.278	42.781	2453.914	31.460
9480	29.296	42.963	2496.877	31.606
9600	29.314	43.142	2540.019	31.750
9720	29.332	43.319	2583.338	31.893
9840	29.349	43.494	2626.832	32.035
9960	29.367	43.668	2670.500	32.175
10080	29.384	43.840	2714.339	32.314
10200	29.401	44.009	2758.349	32.451
10320	29.418	44.178	2802.527	32.588
10440	29.434	44.344	2846.871	32.723
10560	29.451	44.509	2891.379	32.857
10680	29.467	44.672	2936.051	32.989
10800	29.483	44.833	2980.884	33.121

A.3. Temperature Variation Throughout Depth

$$(T_{x,t} - T_i) = \frac{2q(\frac{\alpha t}{\pi})^{\frac{1}{2}}}{k} \exp\left(\frac{-x^2}{4\alpha t}\right) - \frac{qx}{k}\left(1 - \text{erf}\left(\frac{x}{2\sqrt{\alpha t}}\right)\right) \quad \text{---- Eq. 2.11}$$

k	1.6
c	800
ρ	2400
alpha	8.3E-07
q (Const.)	500
Ti (^{0}C)	25

	Temperature at distance x from surface							
x	X=0	X=0.04	X=0.08	X=0.12	X=0.16	X=0.20	X=0.24	X=0.28
t	0	0.04	0.08	0.12	0.16	0.2	0.24	0.28
120	28.527	25.006	25.000	25.000	25.000	25.000	25.000	25.000
240	29.987	25.106	25.000	25.000	25.000	25.000	25.000	25.000
360	31.108	25.329	25.002	25.000	25.000	25.000	25.000	25.000
480	32.053	25.628	25.012	25.000	25.000	25.000	25.000	25.000
600	32.886	25.969	25.036	25.000	25.000	25.000	25.000	25.000
720	33.638	26.332	25.077	25.001	25.000	25.000	25.000	25.000
840	34.330	26.706	25.136	25.004	25.000	25.000	25.000	25.000
960	34.974	27.083	25.212	25.010	25.000	25.000	25.000	25.000
1080	35.580	27.461	25.304	25.018	25.001	25.000	25.000	25.000
1200	36.152	27.837	25.411	25.031	25.001	25.000	25.000	25.000
1320	36.696	28.208	25.529	25.049	25.002	25.000	25.000	25.000
1440	37.216	28.576	25.658	25.072	25.004	25.000	25.000	25.000
1560	37.715	28.938	25.797	25.100	25.007	25.000	25.000	25.000
1680	38.195	29.295	25.944	25.133	25.012	25.001	25.000	25.000
1800	38.658	29.646	26.097	25.172	25.017	25.001	25.000	25.000
1920	39.106	29.992	26.257	25.216	25.024	25.002	25.000	25.000
2040	39.540	30.333	26.421	25.265	25.033	25.003	25.000	25.000
2160	39.962	30.668	26.590	25.319	25.044	25.004	25.000	25.000
2280	40.372	30.998	26.763	25.377	25.057	25.006	25.000	25.000
2400	40.771	31.324	26.939	25.440	25.072	25.008	25.001	25.000
2520	41.161	31.644	27.117	25.507	25.089	25.011	25.001	25.000
2640	41.541	31.960	27.298	25.579	25.109	25.015	25.002	25.000
2760	41.913	32.271	27.481	25.654	25.130	25.019	25.002	25.000
2880	42.276	32.578	27.665	25.732	25.154	25.025	25.003	25.000
3000	42.633	32.880	27.850	25.814	25.181	25.031	25.004	25.000
3120	42.982	33.179	28.037	25.900	25.209	25.038	25.005	25.001

3240	43.324	33.473	28.224	25.988	25.240	25.045	25.007	25.001
3360	43.661	33.764	28.412	26.078	25.272	25.054	25.008	25.001
3480	43.991	34.051	28.600	26.172	25.307	25.064	25.011	25.001
3600	44.316	34.335	28.789	26.268	25.344	25.075	25.013	25.002
3720	44.635	34.615	28.978	26.366	25.384	25.087	25.016	25.002
3840	44.949	34.891	29.167	26.466	25.425	25.100	25.019	25.003
3960	45.258	35.165	29.356	26.568	25.468	25.115	25.023	25.004
4080	45.563	35.435	29.545	26.672	25.513	25.130	25.027	25.005
4200	45.863	35.703	29.734	26.778	25.560	25.147	25.032	25.006
4320	46.159	35.967	29.922	26.885	25.609	25.164	25.037	25.007
4440	46.451	36.229	30.111	26.994	25.659	25.183	25.042	25.008
4560	46.739	36.487	30.299	27.104	25.712	25.203	25.049	25.010
4680	47.023	36.744	30.486	27.216	25.766	25.224	25.055	25.011
4800	47.304	36.997	30.673	27.329	25.821	25.247	25.063	25.013
4920	47.581	37.248	30.860	27.443	25.878	25.270	25.071	25.016
5040	47.854	37.497	31.046	27.558	25.937	25.295	25.079	25.018
5160	48.125	37.743	31.232	27.674	25.997	25.320	25.088	25.021
5280	48.392	37.987	31.417	27.791	26.058	25.347	25.098	25.024
5400	48.657	38.228	31.601	27.908	26.121	25.375	25.108	25.027

RATUWA

A.4. Stress Calculation

Slab Depth	0.28	m
Slab width	1	m
Slab Length	3	m
E	2.50E+07	kN/m2
α	1.00E-05	
Reference temperature	25.000	°C
Second Moment of Area, w.r.t. top, I	0.01	m4
First Moment of Area, B	0.0392	m3
Area, A	0.28	m2

Depth		0	0.04	0.08	0.12	0.16	0.2	0.24	0.28
Temperature		44.32	34.33	28.79	26.27	25.34	25.08	25.01	25.00
Temperature Rise		19.32	9.33	3.79	1.27	0.34	0.08	0.01	0.00
εf		1.93E-04	9.33E-05	3.79 E-05	1.27 E-05	3.44 E-06	7.51 E-07	1.30 E-07	1.79 E-08
$\sigma_{estrained}$=-E. ε_f		-4828.88	-2333.68	-947.22	-316.91	-86.10	-18.78	-3.26	-0.45
ΔN	-235.062	-24.14	-23.34	-9.47	-3.17	-0.86	-0.19	-0.03	0.00
ΔM	-9.677	-0.06	-0.93	-0.76	-0.38	-0.14	-0.04	-0.01	0.00
Δε0	1.05E-04								
Δψ	-5.08E-04								
E(AI-B^2)	12805.33								
Δσ		2553.923425	2109.44513	1601.4699	1093.49	585.52	77.54434	-430.43	-938.41
		-2274.96	-224.24	654.25	776.58	499.42	58.77	-433.69	-938.85
Numerical Solution (N/mm2)		-2.27	-0.22	0.65	0.78	0.50	0.06	-0.43	-0.94

APPENDIX B

B.1. Command Code of Analysis of Underground Reservoir

```
finish
/clear
/title, Underground Reservoir - Sliding
/filnam,UGRSL
/prep7      ! Enter preprocessor

EMUNIT, MKS

Height=4
Width=12
StripWidth=4
SlabTK=0.2
WallTK=0.3
ColHTk=0.2  ! Column head thickness
ColHW=1.2 ! Column head width
Ncolumns=2
ColTk=0.4
ColumnSpacing = Width/(Ncolumns+1)


! walls
BLOCK,0,WallTK,0,Height,0,StripWidth
BLOCK,Width-WallTK,Width,0,Height,0,StripWidth

! Columns
BLOCK,ColumnSpacing-ColTk/2,ColumnSpacing+ColTk/2,0,Height-
ColHTk,StripWidth/2-ColTk/2,StripWidth/2+ColTk/2
BLOCK,ColumnSpacing*2-ColTk/2,ColumnSpacing*2+ColTk/2,0,Height-
ColHTk,StripWidth/2-ColTk/2,StripWidth/2+ColTk/2

! top slab
BLOCK,0,Width,Height,Height+SlabTk,0,StripWidth

!Column Head
BLOCK,ColumnSpacing-ColHW/2,ColumnSpacing+ColHW/2,Height-
ColHTk,Height,StripWidth/2-ColHW/2,StripWidth/2+ColHW/2
BLOCK,ColumnSpacing*2-ColHW/2,ColumnSpacing*2+ColHW/2,Height-
ColHTk,Height,StripWidth/2-ColHW/2,StripWidth/2+ColHW/2

ET,1,SOLID5,8        ! Concrete with thermal property only
ET,2,SHELL57         ! Super Imposed Surface for convection


! properties of Concrete
MP,EX,1, 25000000000
MP,EY,1, 25000000000
MP, EZ,1,25000000000
MP,NUXY,1, 0.18
MP,NUYZ,1,0.18
MP,NUXZ,1,0.18
MP,ALPX,1, 1.0e-5
```

```
MP,ALPY,1, 1.0e-5
MP,ALPZ,1,1.0e-5
MP,DENS,1,2400
MP,DAMP,1,0.05
MP,KXX,1,1.4 ! Thermal Conductivity
MP,KYY,1,1.4  ! Thermal Conductivity
MP,KZZ,1,1.4  ! Thermal Conductivity
MP,C,1,800


! properties of Concrete
MP,EX,2, 25000000000
MP,NUXY,2, 0.18
MP,NUYZ,2,0.18
MP,NUXZ,2,0.18
MP,ALPX,2, 1.0e-5
MP,ALPY,2, 1.0e-5
MP,ALPZ,2,1.0e-5
MP,DENS,2,2400
MP,DAMP,2,0.05
MP,KXX,2,1.4 ! Thermal Conductivity
MP,KYY,2,1.4   ! Thermal Conductivity
MP,KZZ,2,1.4   ! Thermal Conductivity
MP,C,2,800


esize,0.1     ! Element size
Type, 1
Mat, 1
VMESH,1,7,1   ! Mesh the model

surftk=0.00001
!Define Real parameters for super imposed Surface
R,1,surftk,surftk,surftk,surftk,0,

!*
sect,1,shell,,q
secdata, surftk,2,0.0,3    ! TK, MAT, THETA, NUMPT, LayerName
secoffset,MID
seccontrol,,,, , , ,

TYPE,2
MAT,2
REAL,1
ESYS,0
SECNUM,1
TSHAP,QUAD
!*

! Select and Merge nodes of columns and column head and slab
!
NSEL, S,LOC, x,WallTK+0.01,Width-WallTK-0.01
NSEL, R,LOC, Y,Height-ColHTk-0.01,Height+0.01
NUMMRG,ALL
```

UNIVERSITY OF MORATUWA LIBRARY SRI LANKA

```
/Com Select top faces and add the surface element
! Select Top surface
NSEL, S,LOC, Y, Height+SlabTk-0.05, Height+SlabTk+0.05
ESURF,0       ! Create surface on nodes
ESEL, S, Type,,2,,,
CM,SURF_TOP, ELEM

! Select Bottom inner surfaces
allsel,all
NSEL, S,LOC, x, WallTK, Width-WallTK
NSEL, R,LOC, Y, Height-1, Height+0.05
ESURF,0       ! Create surface on nodes
ESEL, S, Type,,2,,,
ESEL,U,,,SURF_TOP
CM,SURF_BOTTOM, ELEM


! Select outer sides
allsel,all
NSEL, S,LOC, x, 0,0
NSEL, A,LOC, x, Width, Width
NSEL, R,LOC, Y, Height-1, Height+SlabTk+0.05
ESURF,0       ! Create surface on nodes
ESEL, S, Type,,2,,,
ESEL,U,,,SURF_TOP
ESEL,U,,,SURF_BOTTOM
CM,SURF_SIDES, ELEM

allsel,all
CPINTF,ALL

!Save the physics Environment
physics,write,fileS
physics,write,fileT
finish

/solu     ! Enter the solution phase

/Com Normalized Solar Heat Flux on Horizontal Plane-Top Slab Radiation (IRH)
*DIM, HFH, TABLE , 25
HFH(1,0)=0,1800,3600,5400,7200,9000,10800,12600,14400,16200
HFH(11,0)=18000,19800,21600,23400,25200,27000,28800,30600,32400,34200,36000,
37800,39600,41400,43200
HFH(1,1)=0.0,9.1,35.7,78.1,133.3,197.6,266.7,335.7,400.0,455.2
HFH(11,1)=497.6,524.3,533.3,524.3,497.6,455.2,400.0,335.7,266.7,197.6,133.3,
78.1,35.7,9.1,0.0

/Com Ambient Temperature
*DIM, AM, TABLE , 25
AM(1,0)=0,1800,3600,5400,7200,9000,10800,12600,14400,16200
AM(11,0)=18000,19800,21600,23400,25200,27000,28800,30600,32400,34200,36000,3
7800,39600,41400,43200
AM(1,1)=23.6,23.7,24.1,24.8,25.6,26.4,27.3,28.2,29.0,29.8
AM(11,1)=30.4,30.8,31.1,31.2,31.1,30.9,30.5,29.9,29.3,28.5,27.7,26.8,26.0,25
.3,24.8
```

```
!Heat Flux.
SFA,28,1,HFLUX,%HFH%  !Head Flux on Top Slab


! Outer  Top and Bottom Surface exposed to Normal Ambient Temp
SFE,SURF_TOP,1,CONV,2,%AM%,%AM%,%AM%,%AM%
SFE,SURF_TOP,1,CONV,1,11.2,11.2,11.2,11.2

SFE,SURF_BOTTOM,1,CONV,2,%AM%,%AM%,%AM%,%AM%
SFE,SURF_BOTTOM,1,CONV,1,100,100,100,100

SFE,SURF_SIDES,1,CONV,2,%AM%,%AM%,%AM%,%AM%
SFE,SURF_SIDES,1,CONV,1,100,100,100,100

! apply symmetric
DA,25,SYMM
DA,26,SYMM
DA,1,SYMM
DA,2,SYMM
DA,7,SYMM
DA,8,SYMM


allsel,all
antype,4              ! Transient analysis
SOLCONTROL, OFF       ! Solution Control OFF

toffst,273            ! temperature offset from absolute zero to zero.
TUNIF, 23.6           ! Set to Ambient start temp

CNVTOL, TEMP,, 0.001, 2,-1        ! Set Convergence Tolerance
OUTRES,NSOL,ALL       ! Write nodal solution for all steps
AUTOTS,ON     ! Auto Time stepping on.

Ftime=40000
TIME, Ftime

DELTIM, 1, 1,1800, ON
KBC, 1                !Loads are step changed (stepped) at the first substep
of this load step to the values of this load step
allsel,all
solve


! To solve for Stresses
/prep7
physics,read,fileS

ET,1,SOLID5

/COM, CONTACT PAIR CREATION - START
CM,A_NODECM,NODE
CM,A_ELEMCM,ELEM
CM,A_KPCM,KP
CM,A_LINECM,LINE
CM,A_AREACM,AREA
```

```
CM,A_VOLUCM,VOLU

Frictionfac=0.3
MP,MU,1,Frictionfac
MAT,1
!MP,EMIS,1,
R,3
REAL,3

ET,3,170
ET,4,173,0  ! limit to UX,UY and UZ DOF only

R,3,,,1.0,0.1,0,
RMORE,,,1.0E10,0.0,1.0,0.1
RMORE,0.0,0,1.0,,1.0,0.5
RMORE,0,1.0,1.0,0.0,,1.0
KEYOPT,4,4,0
KEYOPT,4,5,0
NROPT,UNSYM
KEYOPT,4,7,0
KEYOPT,4,8,0
KEYOPT,4,9,0
KEYOPT,4,10,2
KEYOPT,4,11,0
KEYOPT,4,12,0
KEYOPT,4,2,0
KEYOPT,3,5,0
KEYOPT,4,1,1

! Generate the target surface
ASEL,S,,,4
ASEL,A,,,10
CM,A_TARGET,AREA

TYPE,3
NSLA,S,1
ESLN,S,0
ESLL,U
ESEL,U,ENAME,,188,189
ESURF
CMSEL,S,A_ELEMCM

! Generate the contact surface
ASEL,S,,,27
CM,A_CONTACT,AREA
TYPE,4
NSLA,S,1
ESLN,S,0
ESURF
ALLSEL
ESEL,ALL
ESEL,S,TYPE,,3
ESEL,A,TYPE,,4
ESEL,R,REAL,,3

allsel,all
```

```
/solu
allsel,all

! Set structural boundary conditions
DA,9, UX,0
DA,9, UY,0
DA,9, UZ,0

DA,3, UY,0
DA,3, UX,0
DA,3, UZ,0

DA,15, UY,0
DA,15, UX,0
DA,15, UZ,0

DA,21, UY,0
DA,21, UX,0
DA,21, UZ,0


! apply symmetric
DA,25,SYMM
DA,26,SYMM
DA,1,SYMM
DA,2,SYMM
DA,7,SYMM
DA,8,SYMM

allsel,all
antype,0

SOLCONTROL, ON
NLGEOM, ON

OUTRES, all, all    ! Write all information
Ftime=27000
time, 1
ddele,all,temp
tref,27.5           ! reference temperature is set to mean ambient
ldread,temp,,,Ftime,1,,rth        ! temperature body loads at "Ftime"
(overwrites TUNIF with this temperature value)

ACEL, 0, 9.81, 0 ! Define Selfweight

SFGRAD, PRES, ,Y, 0, -9000
SFA, 12, , PRES,36000
SFA, 5, , PRES, 36000

Solve
```

APPENDIX C

C. 1. Fixed at Wall Top – Case 1

C.1.1 Temperature variation

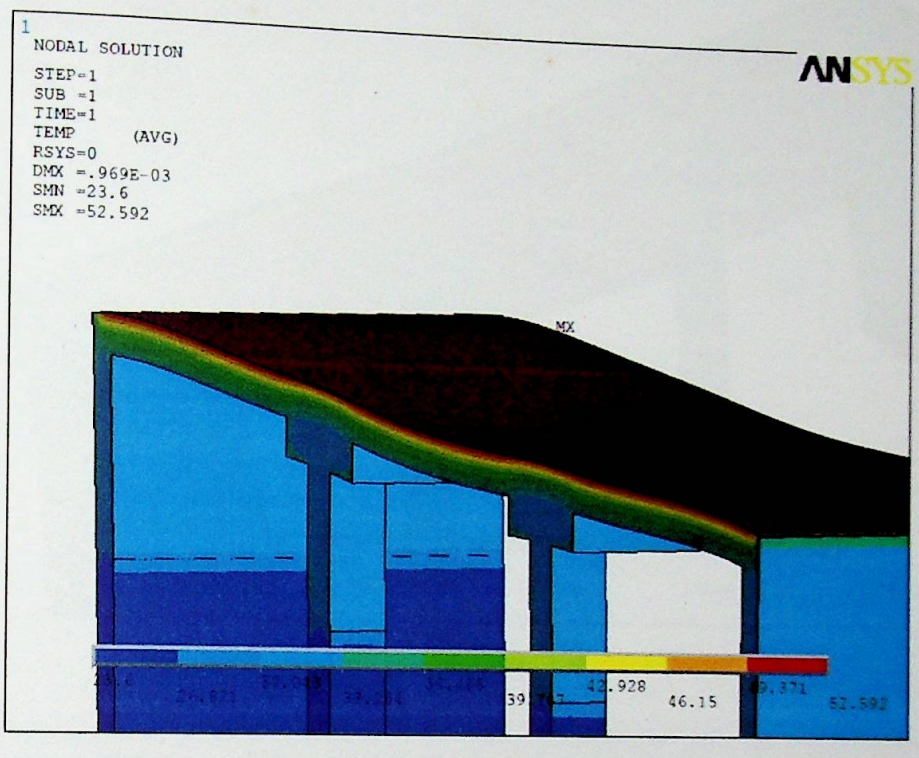

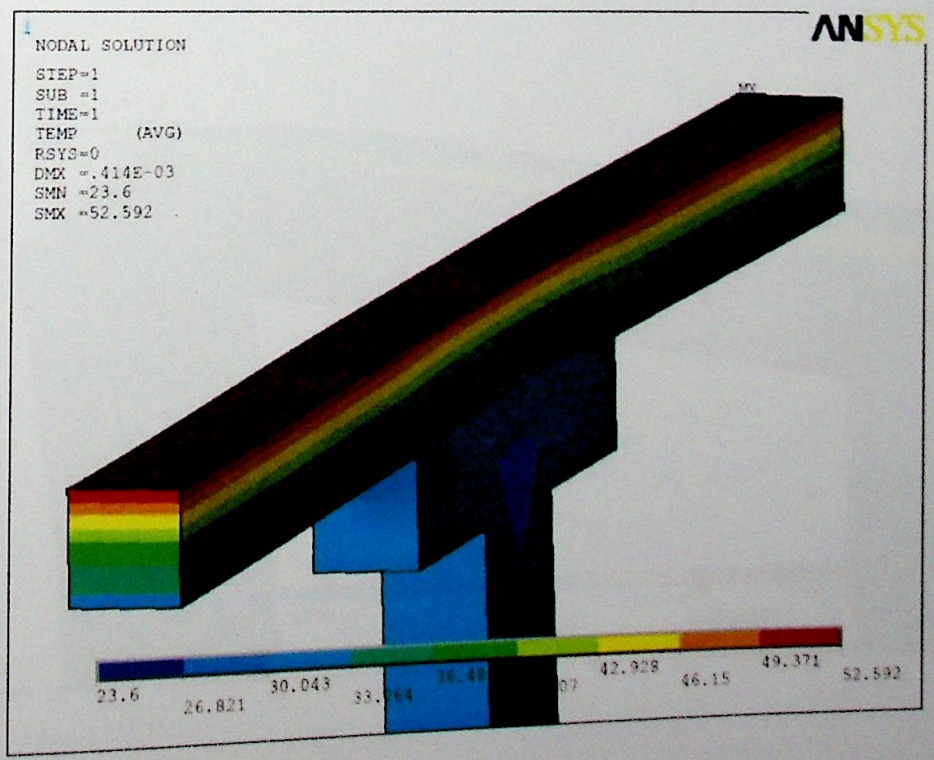

UNIVERSITY OF MORATUWA
LIBRARY

C.1.2 Stress Variation (Selfweight + Soil + Thermal) – Sx (Stress in Slab)

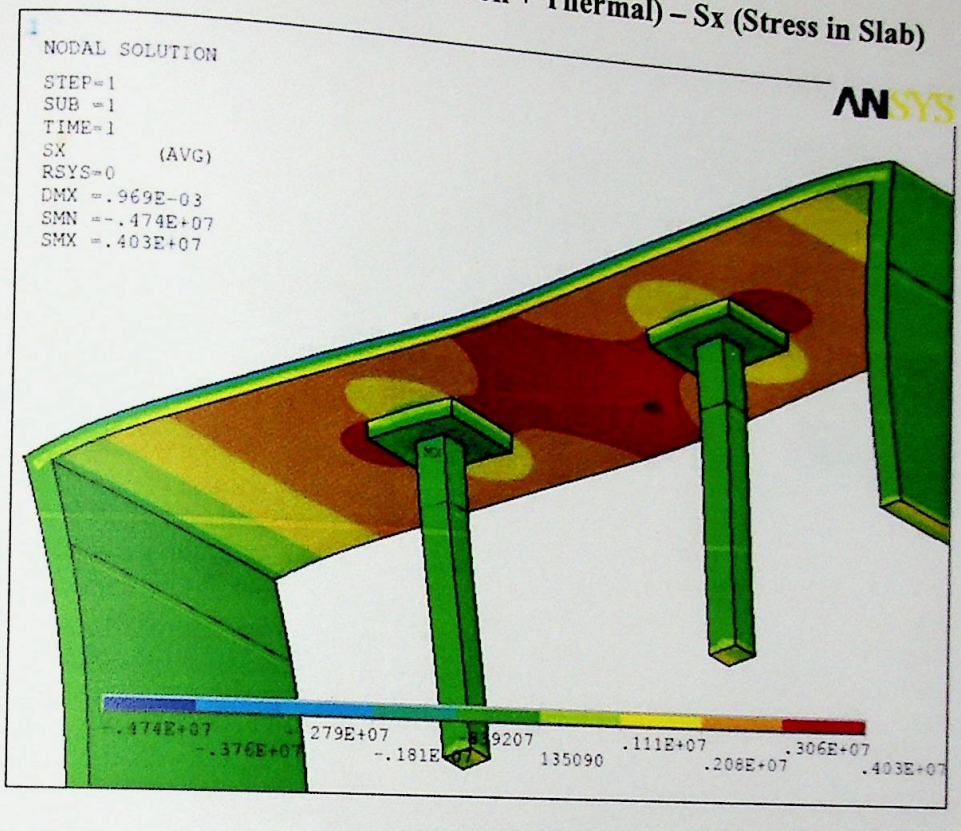

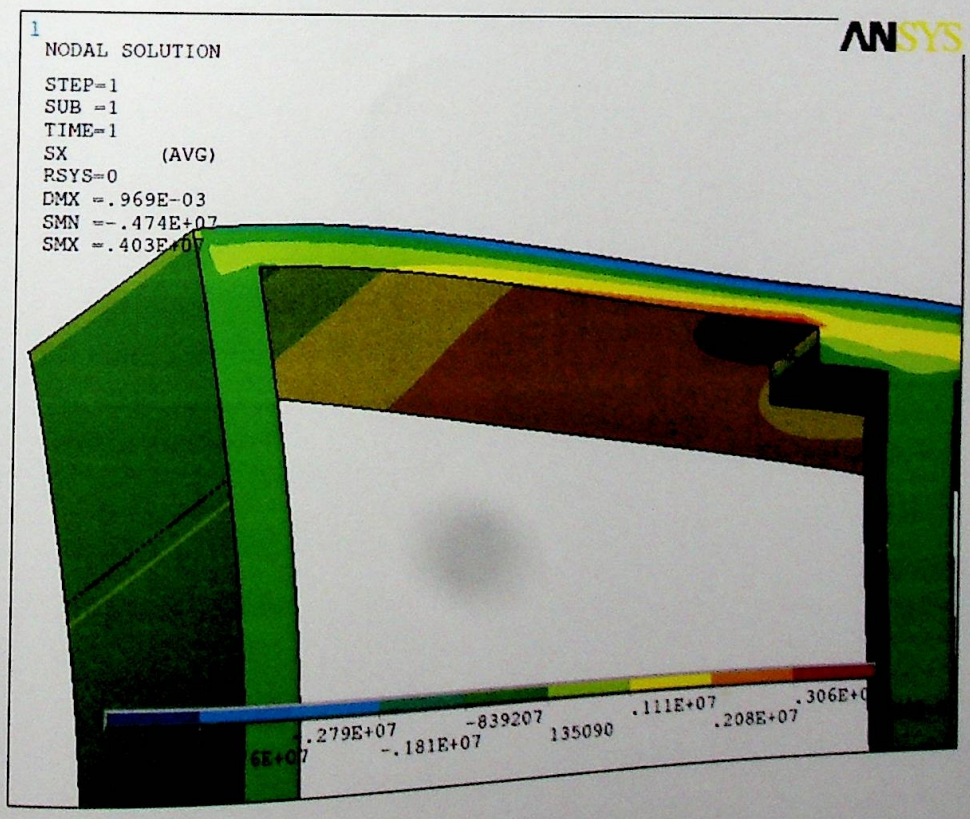

C.1.3 Stress Variation (Selfweight + Soli + Thermal) – Sy (Stress in Walls)

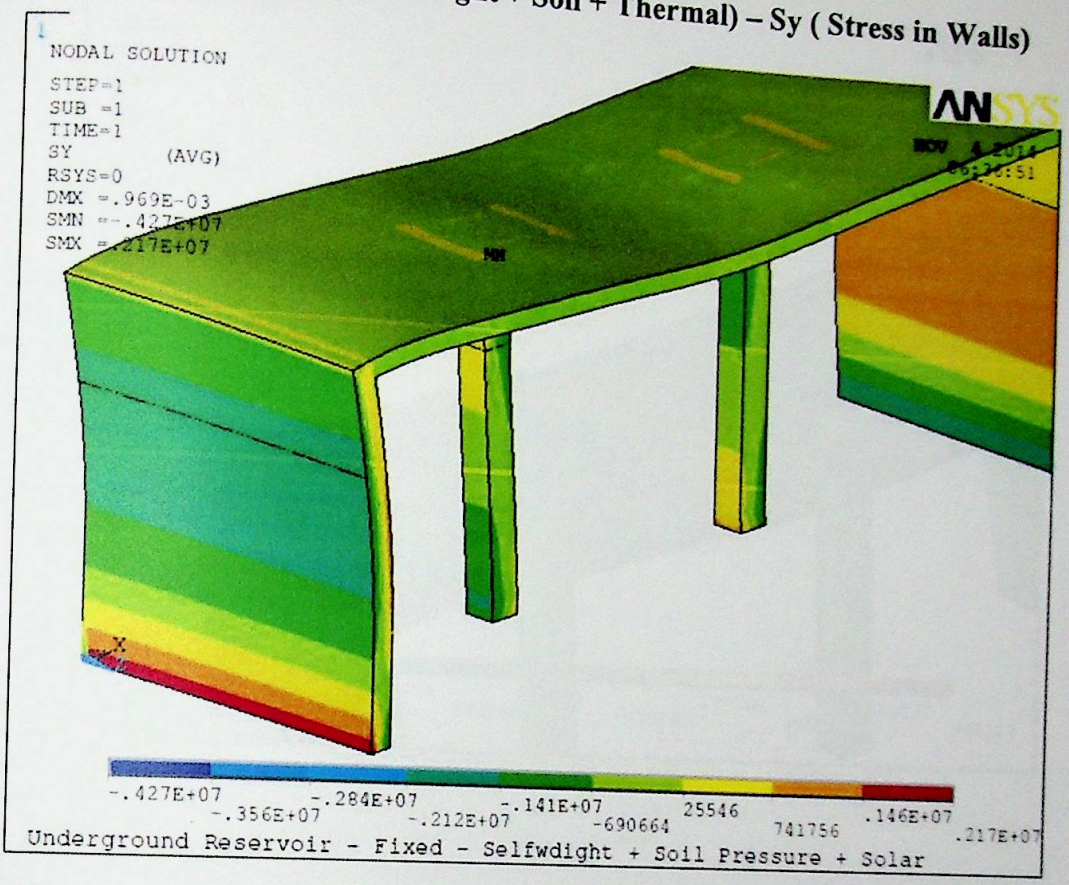

C.1.4 Stress Variation (Selfweight + Soil) – Sx (Stress in Slab)

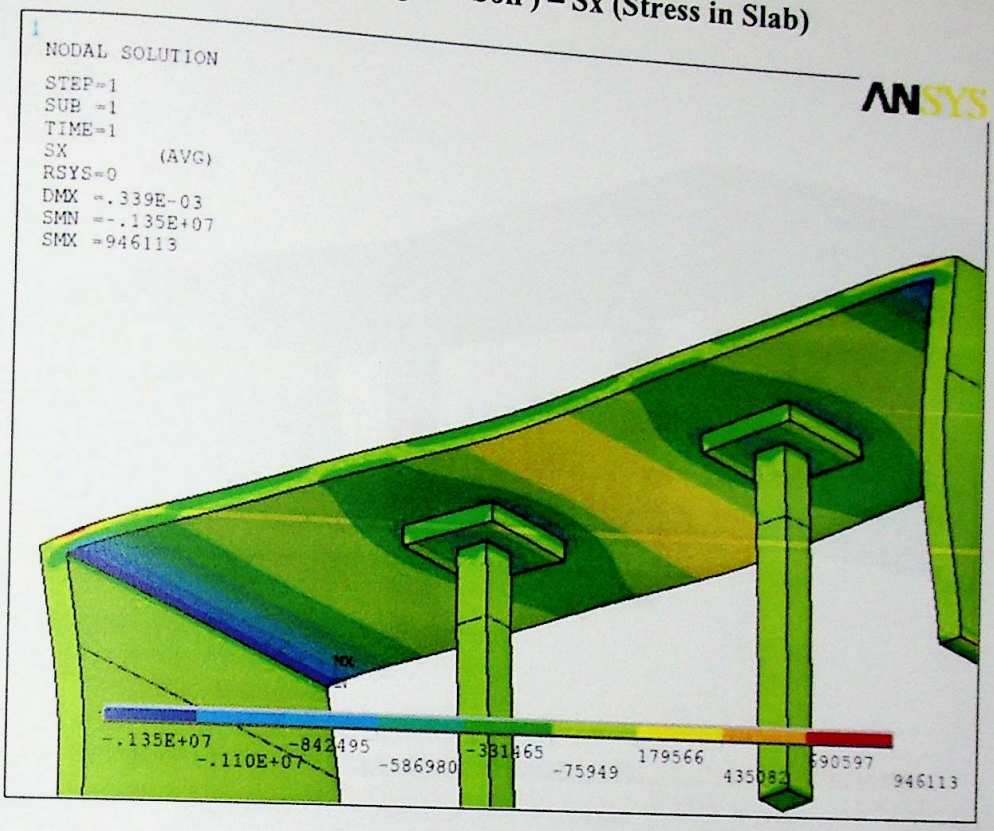

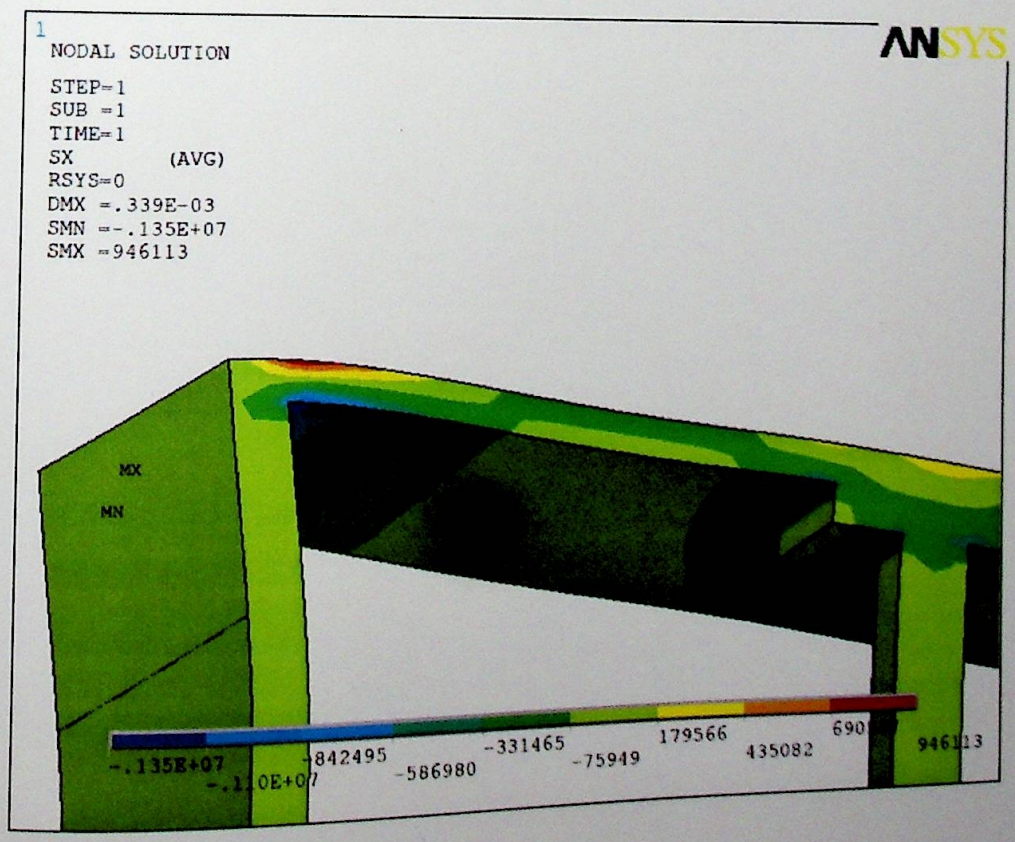

C.1.5 Stress Variation (Selfweight + Soil) – Sy (Stress in Walls)

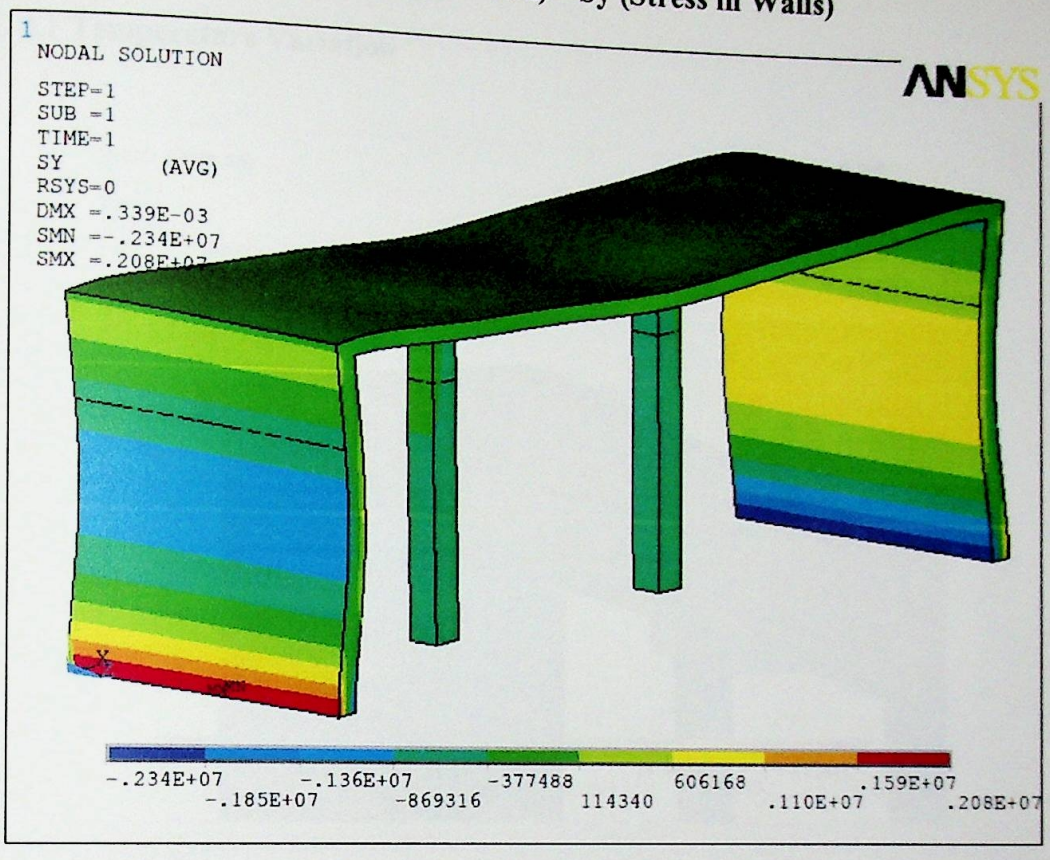

C.2. Sliding Over Wall Top

C.2.1 Temperature Variation

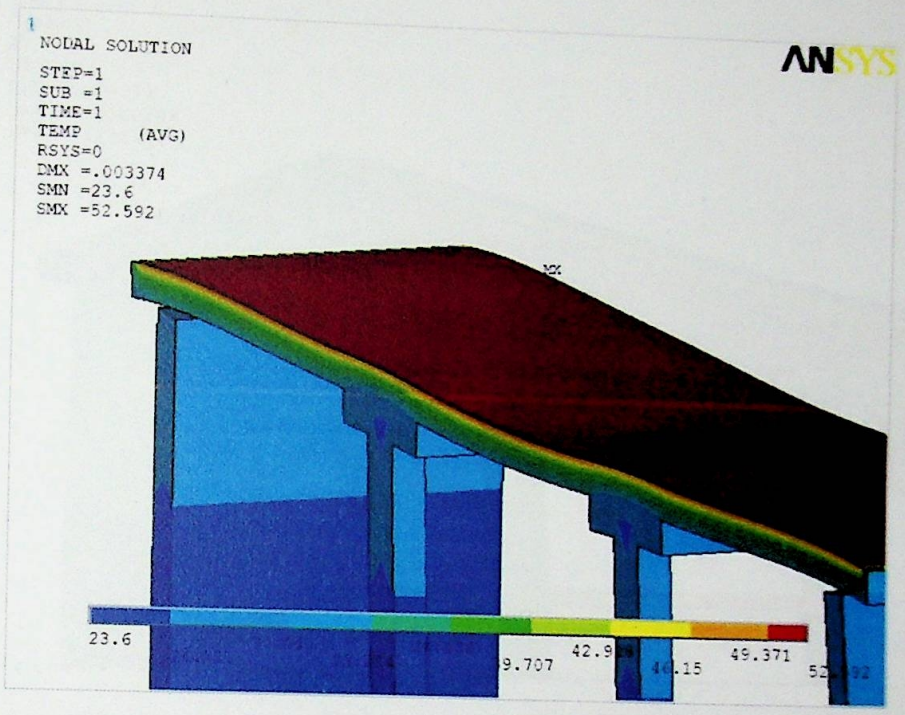

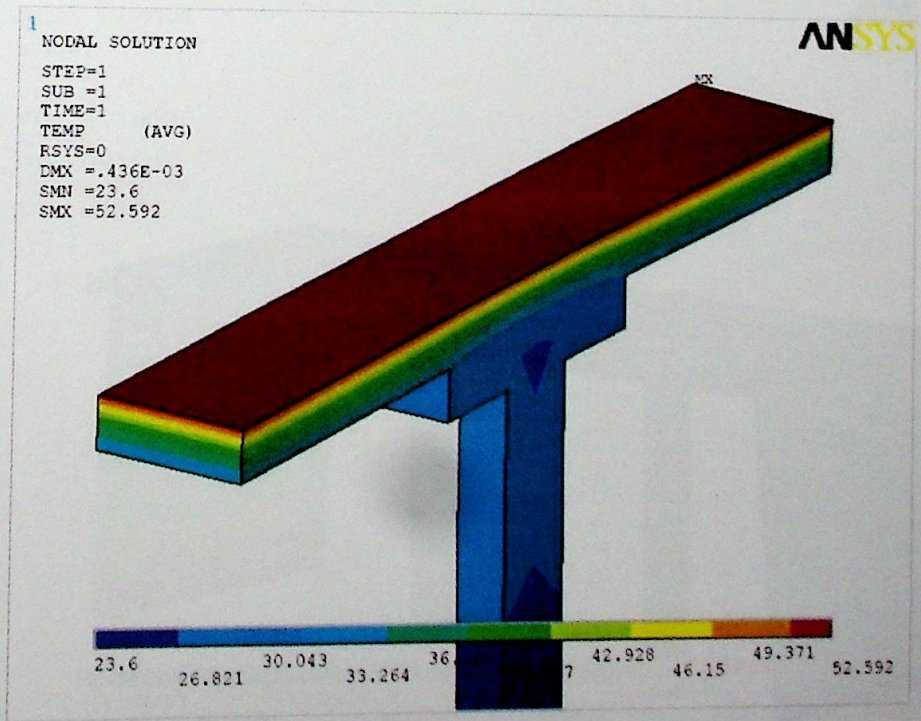

C.2.2. Stress Variation (Selfweight + Soil + Thermal) – Sx (Stress in Slab)

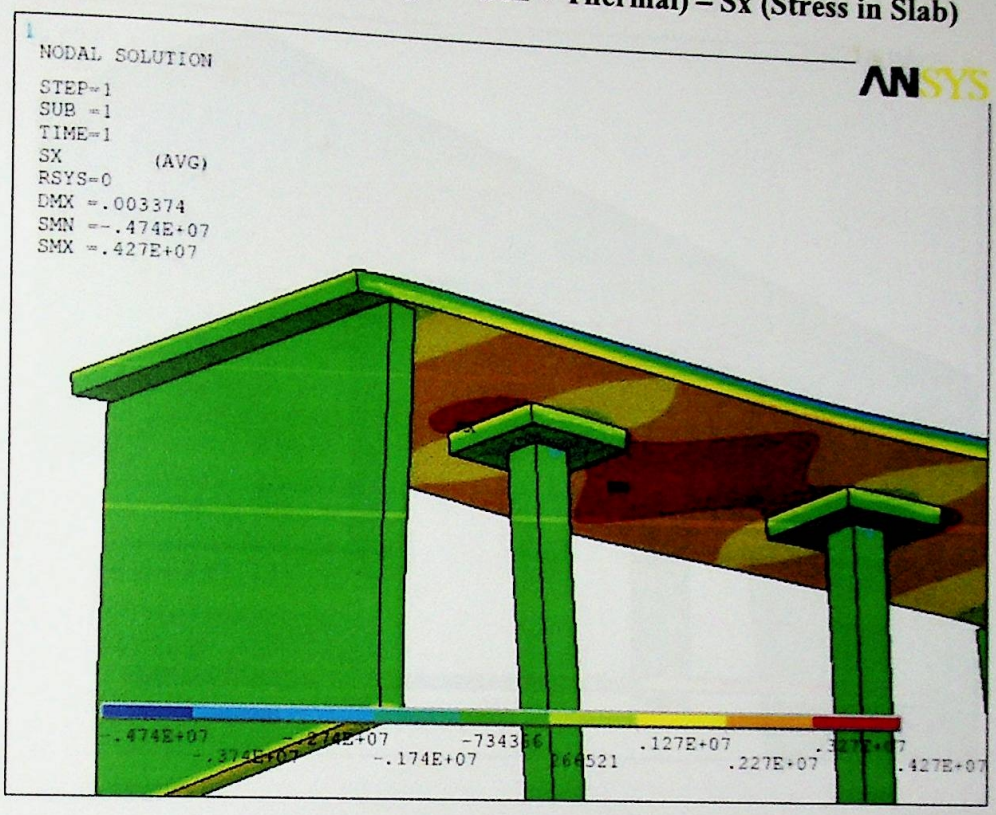

C.2.3. Stress Variation (Selfweight + Soil + Thermal), Sy (Stresses in Wall)

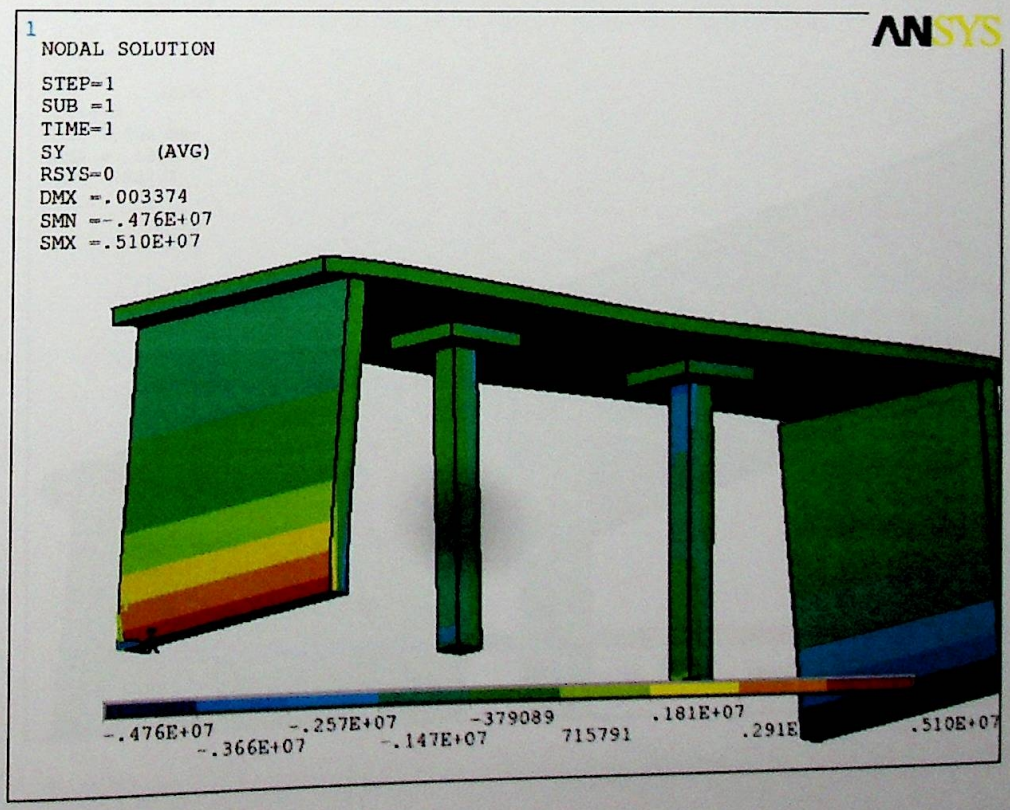

C.2.4. Stress Variation (Selfweight + Soil), Sx (Stresses in Slab)

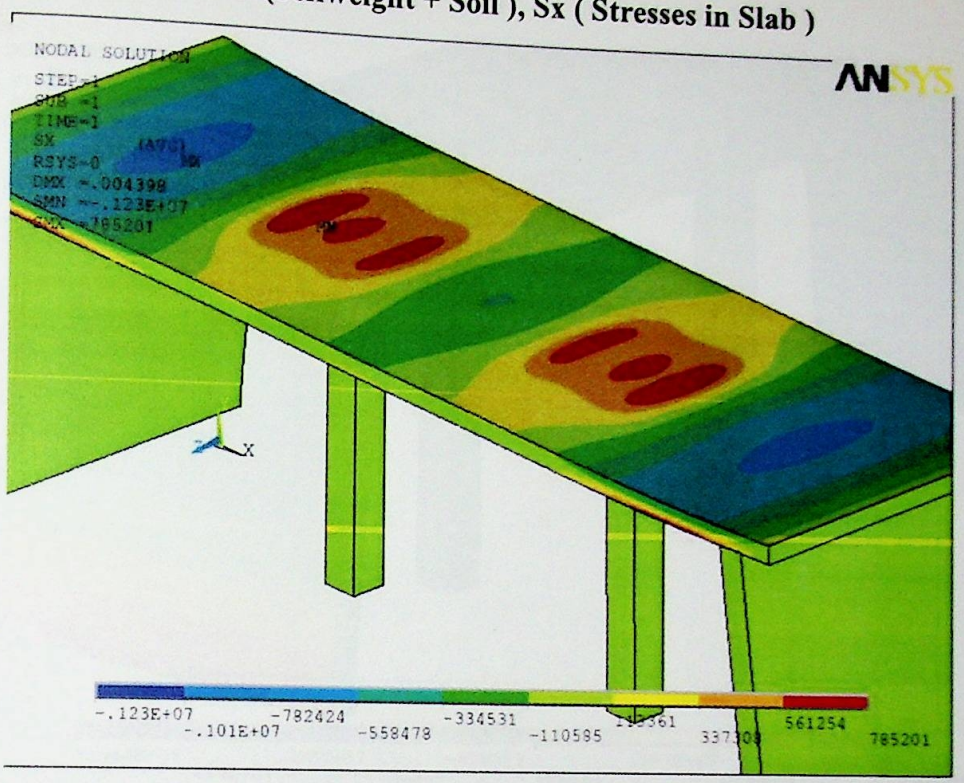

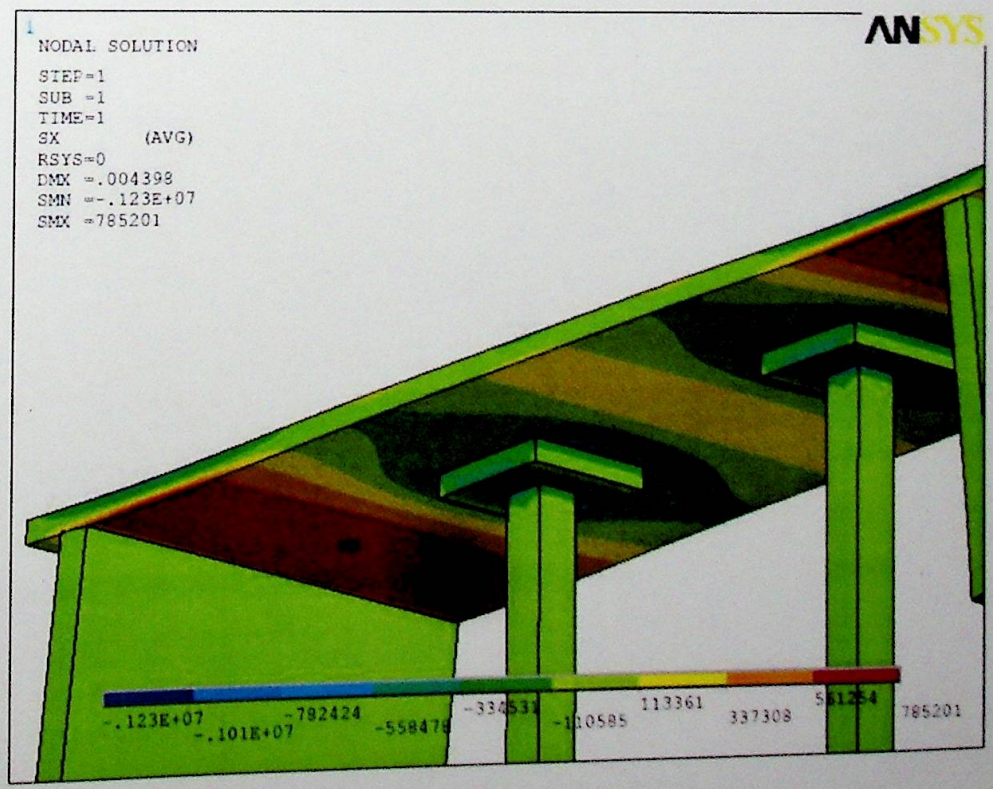

C.2.5. Stress Variation (Selfweight + Soil), Sy (Stresses in Wall)

